DEGRADATION OF METHYLENE BLUE DYE AND RIFAMPICIN ANTIBIOTIC USING *Parthenium hysterophorus*- MEDIATED GREEN ZINC OXIDE AND COPPER OXIDE NANOPARTICLES

DENNIS MWANZA NZILU

MASTER OF SCIENCE

(Analytical and Environmental Chemistry)

JOMO KENYATTA UNIVERSITY

OF

AGRICULTURE AND TECHNOLOGY

2025

Degradation of Methylene Blue Dye and Rifampicin Antibiotic Using *Parthenium hysterophorus*- Mediated Green Zinc Oxide and Copper Oxide Nanoparticles

Dennis Mwanza Nzilu

A Thesis Submitted in Partial Fulfilment of the Requirements for the Degree of Master of Science in Analytical and Environmental Chemistry of the Jomo Kenyatta University of Agriculture and Technology

2025

DECLARATION

This thesis is my original work and has not been presented for a degree in any other University

Signature....…….....Date……...……

Dennis Mwanza Nzilu

This thesis has been submitted for examination with our approval as the University Supervisors

Signature....…….....Date……...……

Dr. Edwin Shigwenya Madivoli, PhD

JKUAT, Kenya

Signature....…….....Date……...……

Dr. David Sujee Makhanu, PhD

Karatina University, Kenya

Signature....…….....Date……...……

Prof. Patrick Gachoki Kareru, PhD

JKUAT, Kenya

DEDICATION

I dedicate this research work to my beloved parents, Boniface Nzilu and Freda Nzilu, for the endless support and encouragement they offered me throughout my education journey. This achievement will fulfill the education dream they envisioned for me.

ACKNOWLEDGEMENT

I am thankful to Almighty God for giving me the strength to pursue my studies and to complete this research study. I am grateful to my supervisors, Dr. Edwin Shigwenya Madivoli, JKUAT, Dr. David Sujee Makhanu, Karatina University, and Prof. Patrick Gachoki Kareru, JKUAT, for their overwhelming support, guidance, and positive criticism during the period I was working on this study. I also wish to thank the Chemistry Department, JKUAT for the support they accorded me throughout my Master's journey and its staff for assisting me as I prepared and worked on this research. In addition, I express my gratitude to the Chemistry Department, University of Fribourg, Switzerland for their support to access characterization instruments at Prof. Katharina Fromm's Laboratory.

I also express my sincere gratitude to my colleagues at GoK Chemistry Laboratory, Mr. Sammy Wanakai, Ms. Joyline Gichuki, Mr. Brian Otenda, Mr. Vincent Ngunjiri, Mr. Samuel Irungu, Mr. John Kamau (Botany), and all the technicians at GoK Chemistry Laboratory for creating conducive environment during my research.

I want to thank my parents, Boniface Nzilu and Freda Nzilu, and friends Mwanzia Makau, Thomas Kimanga, Rachael Mwanzia, Alex Mavuti, Vincent Mbugua, and Joy Hollela for their support during my studies. I am grateful to my siblings Tabitha and Gilbert for your endless support. With your support, I accomplished this milestone.

May Almighty God bless you all abundantly.

TABLE OF CONTENTS

LIST OF TABLES

LIST OF FIGURES

LIST OF PLATES

LIST OF APPENDICES

ACRYONYMS AND ABBREVIATIONS

CuO NPs	Copper Oxide Nanoparticles
FTIR	Fourier Transform Infrared
MB	Methylene Blue
MNPs	Metallic nanoparticles
SEM	Scanning Electron Microscope
TEM	Transmission Electron Microscope
UV-VIS	Ultra Violet- Visible Spectroscopy
XRD	X-Ray Diffraction
WHO	World Health Organization
ZnO NPs	Zinc Oxide Nanoparticles

ABSTRACT

Contamination of water with antibiotics and organic dyes is causing a serious threat to human health and ecosystems. Wastewater treatment technologies such as membrane filtration, advanced oxidation processes, and resin ion exchange have been in use over time; however, they are associated with limited removal capacity of pollutants and are reported to be cost-intensive. Recently, decontamination with green metallic nanoparticles has been found to be promising. This study aimed to synthesize green copper oxide nanoparticles (CuO NPs) and zinc oxide nanoparticles (ZnO NPs) from *Parthenium hysterophorus* aqueous extract and determine their degradation ability against the rifampicin antibiotic and the methylene blue (MB) dye. The formation of green CuO NPs and ZnO NPs was confirmed by several characterization techniques: UV-Vis spectroscopy (UV-Vis), Fourier Transform Infrared spectroscopy (FTIR), Scanning Electron Microscope (SEM), Transmission Electron Microscope (TEM), Powder X-Ray Diffraction (XRD), and Dynamic Light Scattering (DLS). The percentage degradation of rifampicin antibiotic and MB dye using green CuO NPs and ZnO NPs was affected by the nanoparticle amount, rifampicin and MB concentration, pH, reaction time, and temperature. The highest percentage degradation (>99%) was obtained for the rifampicin antibiotic using 10 mg/L of rifampicin solution and 50 mg of green CuO NPs within 210 minutes. In contrast, the highest percentage of degradation (>58%) was obtained for MB dye using 5 mg/L of MB solution and 10 mg of green ZnO NPs within 360 minutes. The percentage degradation was determined to increase when the parameters were combined at their optimal conditions, with over 99% degradation of rifampicin and 59% degradation of MB reported within 8 and 32 minutes, respectively. Additionally, green CuO NPs and ZnO NPs were demonstrated to retain their degradation ability even after multiple cycles of use. According to the study's findings, *P. hysterophorus*-mediated green CuO NPs and ZnO NPs exhibited degradation properties that enabled them to break down the studied pollutants, indicating potential use in the decontamination of other aquatic pollutants.

CHAPTER ONE

INTRODUCTION

1.1 Background Information

Majority of the world's population experiences severe water scarcity. Statistics show that about 2 billion people (26% of the world's population) do not have access to safe drinking water (UNESCO, 2023). The challenges of water shortage worldwide have escalated primarily due to climate change, and more than half of the population globally is expected to lack sufficient freshwater in the future (Naddaf, 2023). A recent report by the Africa Health Agenda International Conference (AHAIC2023) held in Kigali, Rwanda, in March 2023, showed that climate change has exacerbated water scarcity issues in Africa (Ongaji, 2023). Amidst the global water scarcity issue, environmental pollution of existing waters by untreated industrial effluents continues to rise, threatening people's daily lives (Fayiga *et al*., 2018; Manisalidis *et al*., 2020).

Pharmaceuticals and organic dyes are some of the contaminants of greatest concern when they enter water bodies because of their adverse effect on the ecosystem and human health (Fagier, 2021; Kairigo *et al.*, 2020). These contaminants exhibit high persistence, and their occurrence in water systems must be addressed by devising strategies to remediate them. A concern about pharmaceuticals, such as antibiotics, is that they contribute to the development of antimicrobial resistance, which makes it more difficult for conventional antibiotics to treat, thereby increasing the disease burden (Kairigo *et al.*, 2020; WHO, 2023). The ubiquitous nature of organic dyes emanates from their uncontrolled release into water bodies from the textile, pharmaceutical, polymer, and paper industries (Katheresan *et al*., 2018; Slama *et al*., 2021). The dyes are reported to possess carcinogenic and mutagenic properties, demonstrating that they cause serious health concerns (Lellis *et al*., 2019). The release of antibiotics and dyes into water systems compromises the quality of this valuable and limited resource required for human livelihood (Lellis *et al*., 2019; Polianciuc *et al*., 2020).

Physical, biological, and chemical methods are regarded as conventional methods used in wastewater treatment plants. However, these methods have limitations in decontaminating organic dyes and antibiotics, especially at low concentrations (Kamaz *et al.,* 2019; Nam *et al.,* 2017). Conventional wastewater treatment methods are also limited due to their expensive nature, use of toxic reagents, high power consumption, and ineffectiveness in removing the target pollutants completely (Derakhshan *et al*., 2016; Kamaz *et al*., 2019). The potential pathways for the release of these pollutants into water bodies are via infiltration from the wastewater treatment plants and from the domestic discharge of human excreta (De Ilurdoz *et al.,* 2022; Hanna *et al*., 2023; Polianciuc *et al*., 2020).

Recently, researchers have embraced green nanotechnology to develop nanomaterials for use in removing emerging pollutants of concern (Anjum *et al.,* 2019; Kokkinos *et al.,* 2020).

Nanomaterials can have multiple uses as catalysts, gas sensors, organic converters, and waste treatment (Maruthupandy *et al.*, 2017; Patil *et al*., 2021). Research has proven that plant-mediated metallic nanoparticles are effective in the environmental remediation of contaminants because the synthesis process is cost-effective, requires simple preparation steps, does not produce toxic byproducts, and the developed nanoparticles can find multiple applications (Narasaiah *et al.,* 2017; Shafey, 2020). The resultant metallic nanoparticles are characterized by a high surface area-to-volume ratio and improved chemical and mechanical stability, which make them suitable for the remediation of aquatic pollutants (Khan *et al*., 2020; Nayeri and Mousavi, 2020). Therefore, green synthesized metallic nanoparticles are promising candidates for remediating aquatic pollution and promoting environmentally friendly chemistry.

This study utilized aqueous *P. hysterophorus* extract as a reducing, capping, and stabilizing agent to synthesize green CuO NPs and ZnO NPs and investigated their degradation ability against rifampicin antibiotic and methylene blue dye.

1.2 Statement of the Problem

Water shortage remains an issue of global concern as many people worldwide lack access to safe drinking water (Ngumba *et al*., 2020). Despite issues of water scarcity being experienced, water pollution from untreated industrial effluents, including antibiotics and organic dyes, continues to be reported in water bodies, further exacerbating the water shortage crisis (Fayiga *et al*., 2018; Manisalidis *et al*., 2020). Furthermore, with the increasing environmental contamination and climatic changes, water scarcity is becoming a significant challenge in developing nations. Common emerging pollutants of concern are antibiotics, and with increasing disease prevalence worldwide, antibiotic prescriptions are expected to increase (Kairigo *et al*., 2020). Organic dyes have multiple applications in different industries, and their release into water bodies remains evident. These pollutants persist in the environment and, therefore, harm humans and the ecosystem. The existing conventional methods utilized in wastewater treatment have proven ineffective in completely removing pollutants and are regarded as cost-intensive and time-consuming (Kumari *et al.,* 2019; Rogowska *et al.,* 2020).

1.3 Justification

Many research endeavors have tried to find solutions for removing residual antibiotics and dyes from our water systems. However, more attention still needs to be paid to the effectiveness of the methods used to address water pollution from these contaminants. Some of the methods for remediating water pollution, such as reverse osmosis, distillation, ion exchange, and electrodialysis, which have been in use, are regarded to be financially intensive and most developing countries, such as Kenya, cannot afford them due to cost implications, hence the need to find simple, cost-effective ways in which these pollutants can be removed. If action is not taken, antimicrobial resistance, propagated by antibiotics and the toxicity properties of dyes, will continue to affect humanity. To this end, developing a novel approach to safeguard our water system from contamination by antibiotics and dyes is required. The use of green metallic nanoparticles is proving to be fruitful in the remediation of antibiotics and dyes from the water systems by countering

the limitations exhibited by conventional wastewater treatment methods (Mekconewi *et al.*, 2016; Roy *et al.*, 2021).

Therefore, incorporating green nanotechnology in solving environmental pollution challenges can be an appropriate approach to address water pollution issues arising from antibiotics and dyes.

Metallic nanoparticles have also been reported to possess enhanced properties compared to their large particles because they exhibit a greater surface area to volume ratio, improved mechanical and chemical stability, and potential for reusability. These nanoparticles can be prepared using chemical, physical, and biological methods, with each method having its benefits and drawbacks. Specifically, biological methods that rely on secondary metabolites from plants as reducing, capping, and stabilizing agents are known to promote a cost-friendly and greener approach to preparing metallic nanoparticles. To this end, researchers are embracing greener approaches in the synthesis of metallic nanoparticles by exploiting the sustainability nature of plant-based sources of secondary metabolites. Simultaneously, the researchers are investigating the effectiveness of these nanoparticles in the removal of antibiotics and dyes from aquatic systems, as the method involves simple steps, non-toxic products, is affordable, and promotes environmentally green chemistry.

1.4 Hypothesis

P. hysterophorus-mediated green zinc oxide and copper oxide nanoparticles cannot degrade rifampicin antibiotic and methylene blue dye.

1.5 Objectives

1.5.1 General Objective

To degrade methylene blue dye and rifampicin antibiotic using *P. hysterophorus*-mediated green zinc oxide and copper oxide nanoparticles.

1.5.2 Specific Objectives

i. To screen phytochemicals in *P. hysterophorus* aqueous extract.

ii. To characterize *P. hysterophorus*-mediated green ZnO NPs and CuO NPs using UV-Vis, FTIR, SEM, TEM, XRD, and DLS techniques.

iii. To determine the degradation percentage of rifampicin antibiotic and methylene blue dye using green zinc oxide and copper oxide nanoparticles by optimizing parameters such as nanoparticle amount, pollutant concentration, pH, reaction time, and temperature, and subsequently assess the degradation percentage under optimal parameter conditions.

iv. To determine the reusability potential of green ZnO NPs and CuO NPs in degrading fresh methylene blue dye and rifampicin antibiotic in multiple cycles.

CHAPTER TWO

LITERATURE REVIEW

2.1 *Parthenium hysterophorus* (Parthenium Weed)

P. hysterophorus (Plate 2.1) is an invasive weed growing in agricultural and cultivated lands and along roadsides (Wabuyele *et al*., 2015). It is a much-branched, short-lived (annual), upright herbaceous plant that forms a basal rosette of leaves during the early stage of growth. In addition, it grows between 0.5 and 1.5 m tall and occasionally can reach 2 m or more in height (Bashar *et al*., 2022).

Plate 2.1: *P. hysterophorus* Plant Growing in the Field

In Kenya, the weed is reported to grow in coffee plantations in Kiambu, Kajiado, and Naivasha (Wabuyele *et al*., 2015). *P. hysterophorus* belongs to the Asteraceae

(Compositae) family (Kaur *et al.,* 2021). It is known by other names such as Parthenium weed, false chamomile, parthenium, whitehead, whitetop, congress grass, feverfew, carrot grass, false ragweed, and bitter weed (Ahsan *et al.*, 2020). However, no specific local name for parthenium has been recognized in Kenya.

Traditionally, parthenium has been used as a therapeutic remedy in the treatment of ailments such as herpes, diarrhoea, heart issues, and fever, among others (Kaur *et al*., 2021; Saini *et al.,* 2014) and in the formulation of bioherbicides in the management of weed growth (Motmainna *et al.,* 2021; Pati and Chowdhury, 2015). Recently, researchers have shown that the plant has potential benefits in the removal of heavy metals and dyes from aquatic systems (Bashar *et al*., 2022). Phytochemical screening of *P. hysterophorus* plant extract indicates the presence of terpenoids (5, 6), phenolic acids (3, 4), flavonoids (1, 2), trace oils (7, 8), major oils (9, 10), pseudoguaianolides (11, 12), and allelochemicals (13, 14) (Bezuneh, 2015) as shown in Figure 2.1.

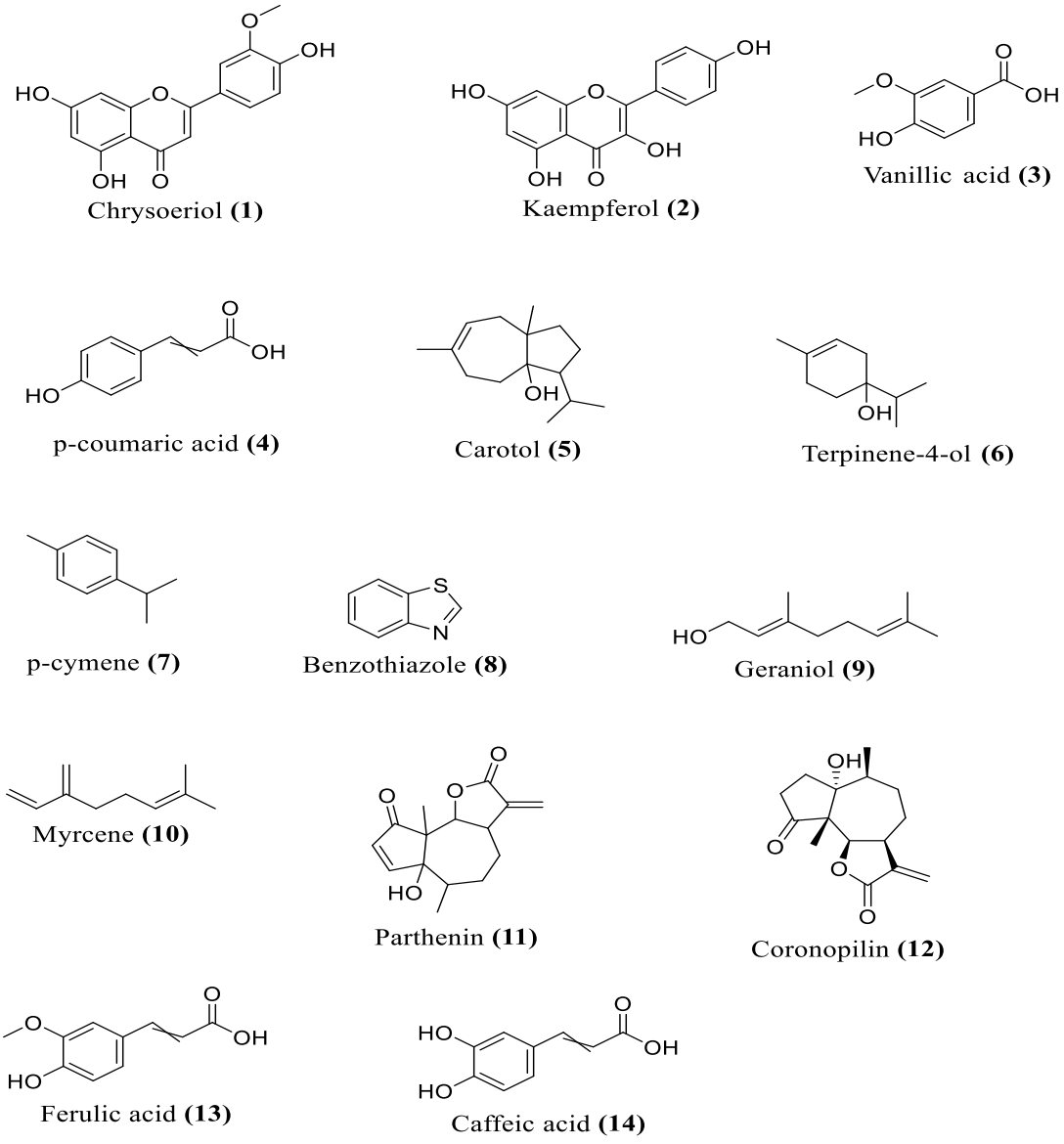

Figure 2.1: Compounds (1-14) Isolated from *P. hysterophorus* Plant

2.2 Occurrence of Organic Dyes

Organic dyes are among the common industrial pollutants contaminating water systems. Industries such as textiles, cosmetics, paper, pharmaceuticals, and plastics use organic dyes in large quantities as colorants (Choudhary *et al*., 2023; Katheresan *et al*., 2018). These dyes enter water bodies through discharge from industries or from wastewater

treatment plants, where they are released in low concentrations. As a result, the organic dyes compromise water quality, making it unfit for human consumption and agriculture. Additionally, organic dyes have high water solubility, which increases their prevalence in water systems (Fagier, 2021).

The occurrence of organic dyes in water bodies leads to the escalation of chemical oxygen demand and biological oxygen demand levels, affecting photosynthesis rate and plant growth (Bhatia *et al*., 2018). Another problem with textile dyes in water is that they react with chlorine disinfectants to form carcinogenic compounds that threaten human health (Saini, 2018). Studies show that organic dyes have mutagenic and carcinogenic properties, which continue to threaten human health (Berradi *et al.*, 2019; Lellis *et al*., 2019). Consequently, contamination of available water by organic dyes amidst the water shortage crisis exacerbates problems humanity faces today. Figure 2.2 depicts structures of common organic dyes present in water systems, including rhodamine B (15), methyl orange (16), orange G (17), methylene blue (18), Carbol Fuschin (19), and Congo red (20) (Patil *et al*., 2021).

A recent study reveals that organic dyes in surface waters remain prevalent in East African countries, such as Kenya, with concentrations ranging from 9.1247 to 1682.9 mg/L being reported (Kapanga *et al*., 2024). The study attributed pollution in surface waters to textile industries.

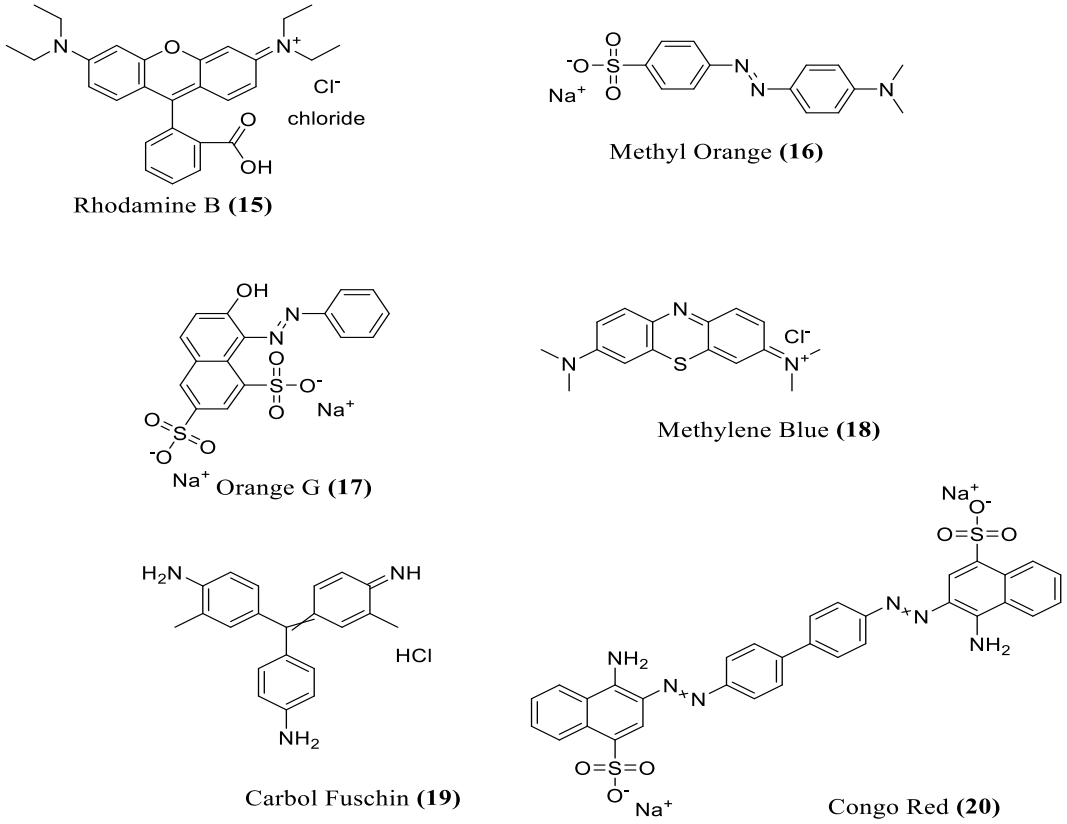

Figure 2.2: Some Organic dyes (15-20) Isolated from Aquatic Systems

2.3 Occurrence of Antibiotics

Active Pharmaceutical Ingredients (APIs) have been classified as emerging pollutants of concern. Specifically, APIs, for instance, antibiotics have increasingly been detected in various environmental compartments, especially in aquatic systems where their threat to human and aquatic ecosystems remains significant (Wilkinson *et al*., 2022). Antibiotics find their way into water bodies as either actual antibiotics or their metabolized form from patients taking them via human excretion (Carvalho and Santos, 2016). Antibiotics can also find their way into water systems due to discharge from wastewater treatment plants, which are currently limited to removing antibiotics at trace concentrations (Kulkarni *et al*., 2017). The occurrence of antibiotics in water systems increases proportionally to the increasing population and improper disposal, and with escalating global disease burden increased prescription of antibiotics would worsen the situation (Kairigo *et al*., 2020). The

presence of antibiotics in water bodies propagates antimicrobial resistance, which the WHO declared a public health threat (Kairigo *et al*., 2020).

With increasing antibiotic resistance, the available antibiotics would not be able to treat the ever-emerging diseases. Furthermore, the presence of antibiotic traces in the environment disrupts physiological processes and triggers ecotoxicological effects (Polianciuc *et al*., 2020).

In Kenya, for instance, some common examples of antibiotics detected in the Nairobi River Basin and other aquatic environment include tetracycline (21), ofloxacin (22), ciprofloxacin (23) (129 ng/L), trimethoprim (24) (327 ng/L), amoxicillin (25) (0.3 μg/L), sulfamethoxazole (26) (1800 ng/L), oxytetracycline (27), and erythromycin (28) as illustrated in Figure 2.3 (De Ilurdoz *et al.*, 2022; Kairigo *et al.*, 2020; Ngumba *et al.*, 2016).

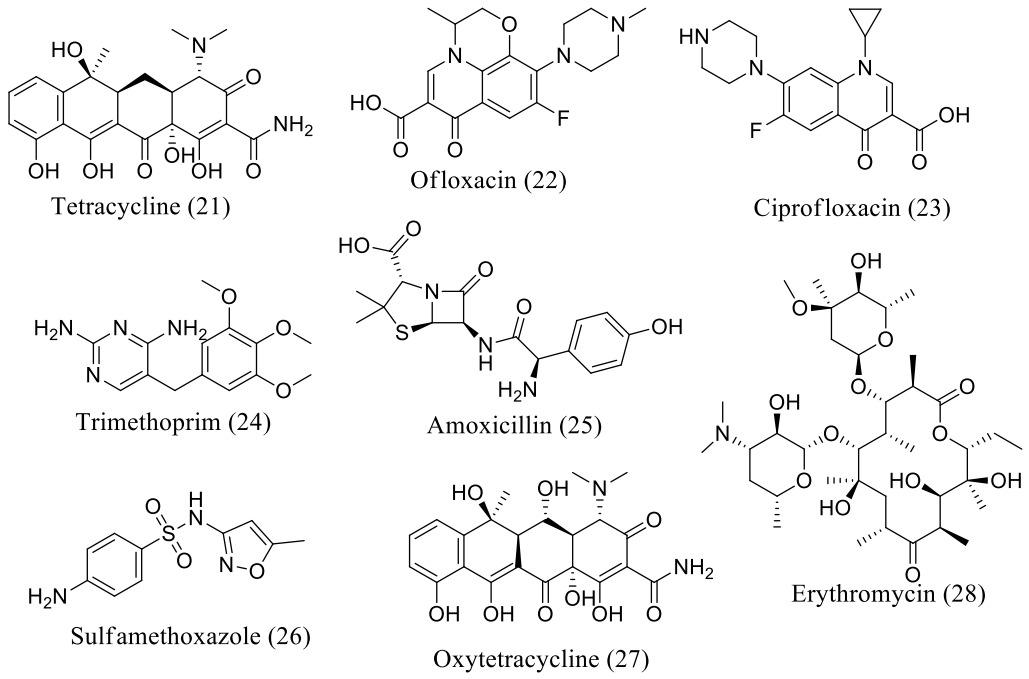

Figure 2.3: Some Antibiotics (21-28) Isolated from Aquatic in Aquatic Systems

2.3.1 The Case of Rifampicin Antibiotic

Rifampicin (Figure 2.4) is an anti-tubercular drug used in the management of all stages of Tuberculosis infection.

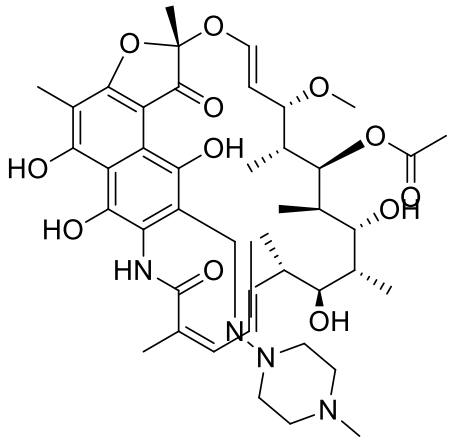

Rifampicin

Figure 2.4: Structure of Rifampicin

The fight against TB continues to show improvements, with the Ministry of Health citing remarkable progress in achieving a 41% decline from the projected 50% in 2025 (MOH, 2025). However, despite the efforts to manage TB, the incidences remain high (124,000 cases) recorded in Kenya as of 2024, according to the country's Ministry of Health (2025) and prescription of conventional anti-tubercular agents such as rifampicin, remains prevalent. As with common antimicrobial agents, anti-tubercular drugs such as rifampicin are not completely metabolized in the patient's body, and portions are excreted in urine or in fecal matter in their original or metabolized forms, finding their way into water bodies (Magwira *et al*., 2019). A recent study by Mtetwa *et al*. (2024) indicates that 4.27 ng/mL rifampicin was detected in treated wastewater samples, which proves the gap in removing the antibiotics at trace levels. TB treatment involves a combination of drug regimens such as Isoniazid, pyrazinamide, and ethambutol, as TB patients are susceptible to developing other infections, including HIV, posing environmental risks of the antibiotics in water (Mtetwa *et al*., 2024; Magwira *et al*., 2019). As noted earlier, the conventional wastewater treatment plants are not designed to remove these antibiotic metabolites at trace levels; these antimicrobial agents find their way into water bodies eventually (Magwira *et al*., 2019; Ngumba *et al.*, 2016).

2.4 Remediation Techniques for Antibiotics and Organic Dyes

Physical, chemical, and biological treatment methods are conventional methods used to remove antibiotics and organic dyes in wastewater treatment plants (Piaskowski *et al*., 2018). The physical methods involve ionic resin, membrane filtration, and physical adsorption (Huang *et al*., 2022). The removal of pollutants by physical methods is achieved through electrostatic interaction, hydrophobic interactions, and anionic exchange (Huang *et al*., 2022). For instance, Ajala *et al.*

(2023) reports removal of antibiotics from wastewater by adsorptive processes employing biochar-based adsorbents. On the other hand, chemical methods involve strong oxidation methods and advanced oxidation processes that react with antibiotics in a redox manner (Huang *et al*., 2022). Compared to physical methods, chemical methods destroy antibiotics and dyes to less harmful compounds (Huang *et al*., 2022). The biological methods used in the treatment of pollutants involve the use of enzymes, microorganisms, plants, and fungi, which react with pollutants and decompose them into stable and less-toxic substances (Ardila-Leal *et al.*, 2021; Huang *et al*., 2022; Narasaiah *et al.*, 2017).

However, these conventional methods used in treating antibiotics and organic dyes are faced with limitations. For instance, physical methods are reported to be expensive and do not result in the complete removal of the pollutants (Ismail *et al*., 2019). Chemical and physical methods are also associated with the production of sludge, which proves difficult to remove and requires large remediation spaces (Ardila-Leal *et al*., 2021). In comparison, biological methods are reported to be cost-effective and environmentally friendly.

Magnetic manganese catalysts have been employed to remove organic dyes in water (Hu *et al*., 2019). Biodegradation using microorganisms (Huang *et al*., 2021), use of adsorbents (Eniola *et al*., 2019), membrane technologies (Nasrollahi *et al*., 2022), coagulation-flocculation (Ho *et al*., 2019), and advanced oxidation processes (De Ilurdoz *et al.*, 2022) are some of the approaches which have been employed in remediation of antibiotics from the aquatic system.

2.5 Approaches for Nanoparticle Synthesis

Due to scientists' curiosity to explore this exigent research area, two approaches to synthesizing nanomaterials were adopted: top-down and bottom-up (Parveen *et al*., 2016). In the top-down approach, bulk materials are broken down into nano-sized materials while in the bottom-up approach, molecules or atoms are assembled to create nanometer-sized materials (Parveen *et al*., 2016). Figure 2.5 summarizes methods used in top-down and bottom-up approaches for nanoparticle synthesis.

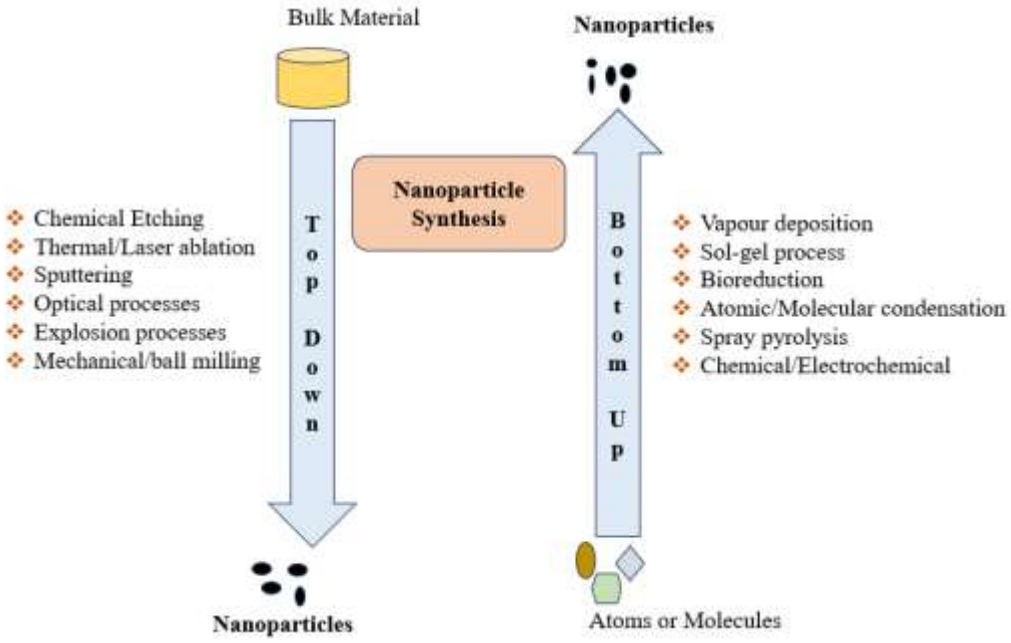

Figure 2.5: A Simplified Illustration of Top-Down and Bottom-Up Approach for Nanoparticle Synthesis

From the top-down and bottom-up approaches, three methods for synthesizing nanoparticle exist, which include chemical, physical, and biological, each with advantages and disadvantages depending on the field of application.

2.5.1 Methods of Nanoparticle Synthesis

2.5.1.1 Physical Methods

The physical methods for nanoparticle synthesis involve high-energy radiations, mechanical pressure, or thermal energy, which cause materials to disintegrate to form nanoparticles (Dhand *et al*., 2015). For instance, copper nanoparticles were synthesized using two ball mills of different sizes employing a planetary ball mill in which a crystal size of 21 nm was obtained after 40 hours (Yadav, 2016). In another study, Copper/Copper (I) oxide (Cu/Cu_2O) nanoparticles were produced by ball milling incorporated with organic additives (Musza *et al*., 2018). In addition, induced laser ablation was used to synthesize copper oxide colloidal and silver nanoparticles (Khashan *et al.*, 2015; Iravani *et al.*, 2014). Another study synthesized chitosan-coated iron oxide nanoparticles using a laser pyrolysis technique (Criveanu *et al*., 2023).

Although the physical method for synthesizing metallic nanoparticles with uniform and controlled-sized particles is employed, it is limited due to its expensive nature and the need for huge amounts of energy and power (Almatroudi, 2020; Wu *et al.*, 2019). Physical methods for nanoparticle synthesis are also associated with the production of huge wastes, and thus it is not economical for the large-scale production of nanoparticles (Dhand *et al*., 2015).

2.5.1.2 Chemical Methods

This method involves using chemical reagents to reduce metal salts into nanoparticles. Some chemical methods include hydrothermal synthesis, chemical vapor synthesis, microemulsion technique, plasma-enhanced chemical vapor deposition, and sol-gel method (Dhand *et al*., 2015). Co-precipitation methods have been used to prepare copper oxide nanoparticles (Rangel *et al*., 2020). Synthesis of pure CuO NPs and nano clay-supported CuO NPs using chemical reduction was reported (Khan *et al*., 2020). The

synthesis of titanium oxide nanoparticles was achieved using the sol-gel method by dissolving titanium chloride using distilled water (Madivoli *et al.,* 2020).

Microemulsions (water-in-oil) are a common method for synthesizing superparamagnetic nanoparticles. In one study, Cetyl Trimethyl Ammonium Bromide and 1-butanol were used to synthesize superparamagnetic magnetite nanoparticles (Salvador *et al*., 2021). Moreover, hydrothermal techniques were used to synthesize ZnO NPs for the production of nanoflowers and nanorods for optical applications (Mohan *et al*., 2020). While the chemical method is an appropriate strategy that can be employed to synthesize metallic nanoparticles, it has a host of drawbacks. For instance, it generates toxic byproducts, which were reported to be more toxic than the intended target for removing aquatic pollutants, threatening the ecosystem (Rahimi and Doostmohammadi, 2019). Transfer of pollutants between the phases has also been evident in chemical methods for synthesis of nanoparticles (Gudikandula and Charya, 2016; Ngumba *et al.,* 2020). These drawbacks make the chemical method expensive to operate.

2.5.1.3 Biological Methods

Biological methods for nanoparticle synthesis involve using biological organisms as reducing agents for metallic precursors to form the nanoparticles (Abdullah *et al*., 2023). For this reason, a biological method for nanoparticle synthesis is divided into three categories, namely, the use of microorganisms, the use of biomolecules as templates, and the use of plant extracts (Dhand *et al*., 2015). Biological nanoparticle synthesis methods are greener than chemical and physical methods since they are energy-efficient, cost-effective, and self-sustaining (Parveen *et al*., 2016). In addition, biological methods possess other advantages, such as the ability to be used in large-scale production of nanoparticles due to their cost effectiveness (Keat *et al.,* 2015).

The use of microorganisms such as bacteria and fungi provides a greener approach to synthesizing nanoparticles as these organisms release chemicals responsible for reducing, capping, and stabilizing metal ions into their nanometer size (Bao *et al.,* 2021; Singh *et*

al., 2019; Singh *et al.,* 2018). For instance, Faisal *et al*. (2023) synthesized silver nanoparticles using the *Paraclostridium benzoelyticum* strain for investigation as an anti-aging agent. The use of bacteria is advantageous because of rapid reproduction, which is suitable for the large-scale production of nanoparticles. Moreover, the bacterial cells can be frozen and regrown cheaply, making the method friendly and sustainable (Gebre and Sendeku, 2019). On the contrary, microorganisms based methods exhibit challenges in separating the biomass mixed with the nanoparticles (Sridevi *et al*., 2023; Zikalala *et al*., 2022).

As a result of the aforementioned limitations, researchers are opting to plant-mediated methods for preparing nanoparticles attributing the method to be a greener alternative for nanoparticle synthesis. Plant parts such as seeds, fruits, stems, leaves, roots, and flowers have been used to synthesize nanoparticles. In nanoparticle synthesis, plant extracts from these plant parts are mixed with metallic precursors, forming nanoparticles (Parveen *et al*., 2016). The plant contains secondary metabolites such as flavonoids, tannins, alkaloids, and terpenoids, which act as reducing agents, and amine, carbonyl, and carboxyl groups, which act as stabilizing agents in the formation of nanoparticles (Dhand *et al*., 2015; Jan *et al.*, 2021). Plant-mediated nanoparticles have been proven safe and effective, making them suitable for biomedical applications. In addition, plant-mediated nanoparticles promote an environmentally friendly chemistry compared to chemical methods for nanoparticle synthesis (Gebre and Sendeku, 2019). The use of plant parts in nanoparticle synthesis is also sustainable as plants can be replanted, and different plants can be used to prepare the same type of nanoparticles (Dhand *et al*., 2015). Biological agents are recognized as low-toxic, cost-effective, and environmentally friendly methods for synthesizing metallic nanoparticles (Dhand *et al*., 2015). Green synthesis using plant extracts has excited researchers to investigate the effectiveness of green nanoparticles in photocatalytic degradation of dyes (Muthukumar *et al*., 2022) and antibiotics from aquatic surfaces (De Ilurdoz *et al.,* 2022; Jadoun *et al.,* 2020; Narasaiah *et al.,* 2017; Pal *et al.,* 2019).

For instance, Abdullah *et al*. (2023) synthesized barium oxide nanoparticles (BaONPs) using *Spirogyra hyalin*a extracts. The formed nanoparticles exhibited anti-inflammatory activities and demonstrated a potential for use in the medical field. Faisal *et al*. (2021) used *Myristica fragrans* fruit extracts to synthesize ZnO NPs for use as a photocatalyst in environmental contaminant removal. In addition, ZnO NPs were formed using aqueous leaf extracts of *Aquilegia pubiflora* for investigation for medical treatment of cancer and diabetes (Jan *et al*., 2021). Figure 2.6 shows a simplified summary of nanoparticle producing methods.

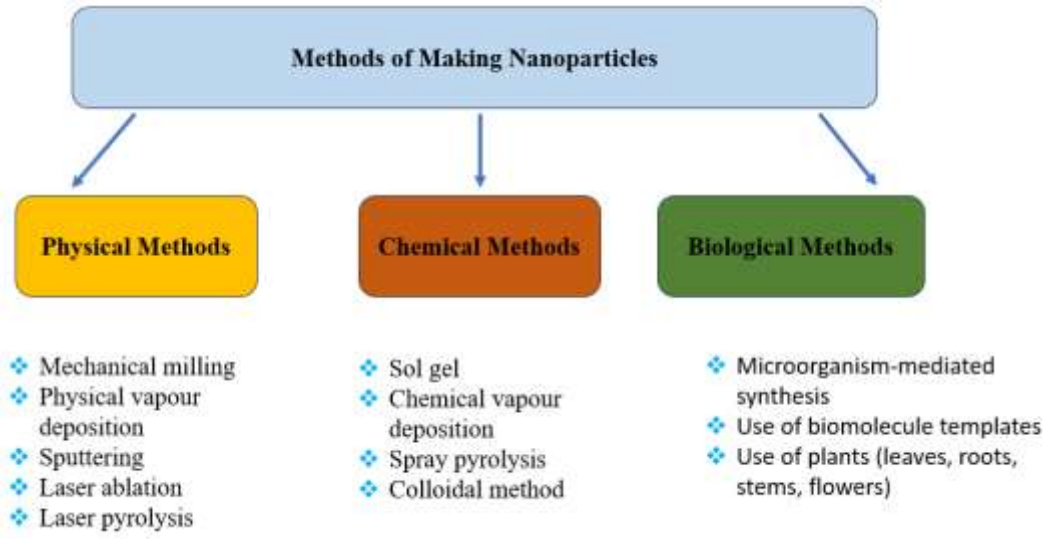

Figure 2.6: A Simplified Illustration of Physical, Biological, and Chemical Techniques for Making Nanoparticles

2.6 Nanoparticles in Environmental Remediation

As an exigent research area, researchers are developing nanoparticles for environmental remediation of pollutants of concern. These endeavors support the United Nations' Sustainable Development Goals on clean water and sanitation, and promoting human well-being by using nanotechnology to develop nano adsorbents that are cheap, environmentally friendly, and sustainable. Examples of nanomaterials commonly used to remediate water, soil, and air contaminants include metallic nanoparticles,

nanocomposites, carbonaceous nanomaterials, and polymeric-supported nanoparticles (El-Ramady *et al*., 2023). These nanomaterials have promising applications because of their enhanced characteristics in comparison to their large materials, including improved surface area to volume ratio, improved stability, and potential for recycling and reusability (El-Ramady *et al*., 2023; Khan *et al*., 2020; Nayeri and Mousavi, 2020). Nanoparticles can be prepared using chemical, physical, or biological methods (Ijaz e*t al.,* 2020; Iravani *et al.,* 2014). To promote sustainable and an environmentally-friendly chemistry, the use of plant extracts is showing to be fruitful in the synthesis of nanoparticles for environmental pollution remediation.

2.6.1 Synthesis of Nanoparticles Using Plant Extracts

Secondary metabolites in the plant extracts mediate the nanoparticle synthesis process. As previously mentioned, plant extracts contain phytochemicals such as tannins, flavonoids, terpenoids, phenols, and saponins, which have functional groups capable of reducing metallic ions from high oxidation states to zero valent ions (Jan *et al*., 2021; Letchmanan *et al*., 2021; Patil *et al.,* 2021). This process results in the formation of the nanoparticles. Specifically, the secondary metabolites perform the capping and stabilizing roles, which leads to formation of the nanoparticles (Narasaiah *et al.,* 2017; Singh *et al.,* 2018). Figure 2.7 illustrates a generalized schematic representation of a step-by-step pathway of synthesizing nanoparticles using plant extracts in which metal nanoparticles can be formed from their respective metal salts.

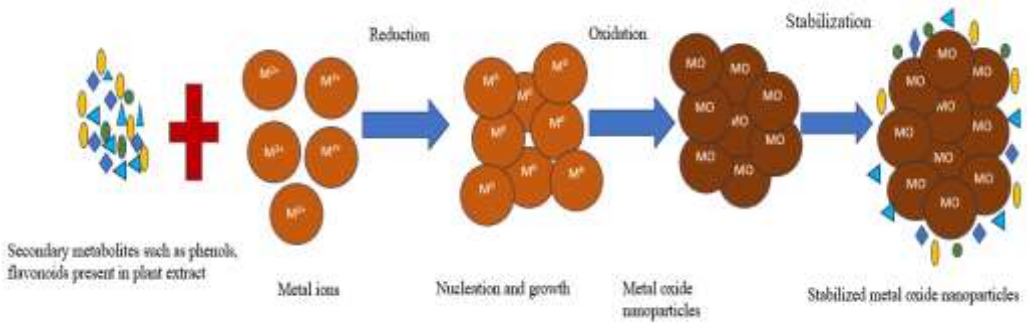

Figure 2.7: Pathway of Synthesizing of Nanoparticles by Reduction of Metal Ion Salt Using Plant Phytochemicals

2.6.2 Use of Metallic Nanoparticles

Metallic nanoparticles find wide application in numerous areas, such as in biomedicine, photocatalysis, soil stabilization, waste treatment cells, light emitting devices, and gas sensors (Maruthupandy *et al.,* 2017; Singh *et al.,* 2020; Yang *et al.,* 2021). The modification of usual metal oxides initially used as catalysts into a nanometer size range increases their effectiveness in the degradation of environmental pollutants due to an increase in their surface area to volume ratio (Anastopoulos *et al*., 2017; Danish *et al*., 2021).

With an increase in contamination of water systems, metallic nanoparticles' functionality as catalysts is widely exploited in this area. In this light, synthesizing nanoparticles to remove pollutants and curb the effect that the contaminants impose on the ecosystem and human health remains useful. To bring it into context, several metallic nanoparticles have been synthesized using green methods to remove antibiotics and organic dyes from aquatic systems to improve water and human safety. Selenium nanoparticles were reported to degrade industrial dyes compared to conventional catalysts utilized to degrade organic dyes (Menon *et al*., 2021). Carbon nitride-mediated metal oxide forms a recent class of nanocomposite being used in photocatalysis and degradation of dyes from effluent streams (Patil *et al*., 2021). Carbon nitride (C_3N_4) possesses essential characteristics which make

the material fit for catalysis. It exhibits good thermal stability with metal oxides and exists in a planar polymeric structure, similar to a graphite molecule (Patil *et al*., 2021). Malakootian *et al.* (2020) achieved degradation of ciprofloxacin antibiotics using titanium (IV) oxide nanoparticles. Carbon nitride-mediated metal oxide has also been reported to be useful in photocatalysis and degradation of Carbol Fuschin dye from effluent streams (Patil *et al*., 2021).

2.6.2.1 Mechanism of Degradation using Metallic Nanoparticles

The probable mechanism of degradation of antibiotics and organic dyes using metallic nanoparticles (MNPs) have been proposed in previous studies (El-Sayed *et al*., 2014; Faisal *et al*., 2021; Kulis-Kapuscinska *et al*., 2023; Kumar, 2017; Saeed *et al*., 2018; Nabilah Mohd Noor *et al*., 2022; Venkatesan *et al*., 2022; Zhou *et al*., 2018). A schematic representation of the degradation mechanism of antibiotics and dyes using green MNPs is depicted in Figure 2.8.

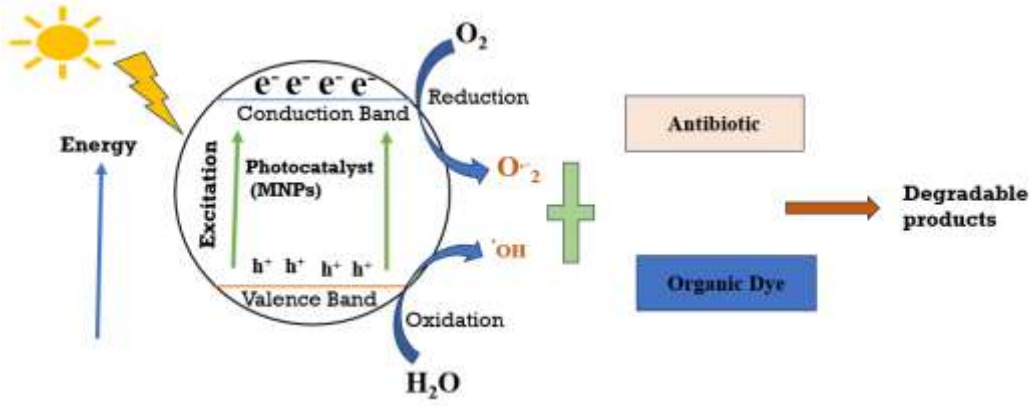

Figure 2.8: Generalized Probable Mechanism of Degradation of Antibiotic and Dye Using Green MNPs

From Figure 2.8, the incident light leads to the excitation of an electron from the valence band (VB) to the conduction band (CB) on the green MNPs surface, leading to the creation of a positive hole in the VB (h^{+}_{VB}) (Kulis-Kapuscinska *et al*., 2023; Saeed *et al*., 2018).

The electron on the CB (e^-_{CB}) is taken up by oxygen adsorbed onto the surface of green MNPs, leading to the generation of a superoxide anion radical ($O_2^{\cdot -}$). The ($O_2^{\cdot -}$) radical anion further reacts with hydrogen peroxide, a radical generator used in the degradation reaction, and produces an OH radical (Saeed *et al*., 2018). The generation OH radical reacts with the dye, leading to the generation of degradation products. The positive hole in the VB then moves onto the surface of green MNPs, releasing more oxygen that produces ($O_2^{\cdot -}$). A similar process repeats itself to produce OH radicals, which are involved in the degradation of antibiotic/dye. Consequently, the (h^+_{VB}) serves as the oxidizing agent and interacts with the OH^-which leads to the significant generation of OH radicals that react with antibiotic/dye adsorbed onto the surface of the green MNPs, enhancing oxidation of antibiotic/dye (Venkatesan *et al*., 2022).

2.6.2.2 Use of Zinc Oxide Nanoparticles

Zinc oxide nanoparticles have numerous uses. It is widely used in industries that produce cosmetics, rubber, and coating products (Jiang *et al*., 2018). These nanoparticles are also used in biological applications since they have good biocompatibility and less toxicity. Moreover, zinc oxide nanoparticles are useful as anticancer and antimicrobial agents, making them promising candidates for biomedicine applications (Jiang *et al*., 2018). ZnO NPs have feasibly been used in green agrochemicals, antimicrobial activity, antibacterial activity, photocatalytic degradation, and photocatalysis in environmental remediation (Fagier, 2021). Additionally, zinc oxide nanoparticles have been used to degrade 4-chlorophenol and Rhodamine B dye in water (Raj *et al.*, 2022). The ZnO NPs have high electron mobility, large surface area, and electrochemical stability, which makes them fit for photocatalysis (Basnet *et al*., 2019; Khan *et al*., 2022).

2.6.2.3 Use of Copper Oxide Nanoparticles

CuO NPs possess crucial properties that are fascinating to researchers. Specifically, CuO NPs have strong thermal, magnetic, electrical, and mechanical functionalities (Crisan *et al*., 2022). Because of these properties, CuO NPs find applications in diverse areas. They

exhibit high-temperature superconductivity, electron correlation effects, and spin dynamics (Ijaz *et al.,* 2017). The crystal morphologies and high surface area that CuO NPs possess prove to be a potential antimicrobial and antioxidant agent (Ijaz *et al.,* 2017). Singh *et al.* (2019) reported the degradation of Nile blue dye with a degradation efficiency of 93%. Ciprofloxacin was removed using a combination of copper oxide and UV irradiation with over 83% removal efficiency (Khoshnamvand *et al*., 2018).

2.7 Determination of Degradation Percentage

The degradation percentage of organic dyes and antibiotics using metallic nanoparticles is determined by recording the absorbance values of these compounds using a UV-Vis spectrophotometer at varying time intervals. The percentage degradation is then determined using equation 2.1 modified from previous studies (Ashwini *et al.*, 2021; Mali *et al.,* 2020; Patil *et al.,* 2021).

$$\%\ \mathrm{D(Degradation\ )} = \frac{(\mathrm{Ao} - \mathrm{At})}{\mathrm{Ao}} \times 100 \ldots\ldots\ldots\ldots\ldots\ldots\ldots (2.1)$$

Where;

A_o is the initial dye or antibiotic absorbance value

A_t is the absorbance value of the dye or antibiotic after time, t.

2.8 Kinetics of Degradation

Kinetics of degradation of pollutants using metallic nanoparticles are obtained by fitting kinetic data at different temperatures assuming a pseudo-first-order kinetic model (equation 2.2) and pseudo-second-order kinetic model (equation 2.3), which gives an idea of the order of reaction (Madivoli *et al.,* 2020). The order of the reaction is then obtained by comparing it to correlation coefficient (R^2) values for each kinetic model (Wang *et al*., 2014). Other thermodynamics parameters, such as change in heat and entropy, are obtained using the Van't Hoff plot using equation 2.4 (Wanakai *et al*., 2022).

$$\ln[A]t = -kT \ln[A]o \ldots\ldots\ldots\ldots\ldots\ldots\ldots\ldots\ldots\ldots\ldots\ldots (2.2)$$

$$\frac{1}{[A]t} = -kT + \frac{1}{[A]o} \ldots\ldots\ldots\ldots\ldots\ldots\ldots\ldots\ldots\ldots\ldots\ldots (2.3)$$

$$\ln Keq = \frac{\Delta H}{RT} + \frac{\Delta S}{R} \ldots\ldots\ldots\ldots\ldots\ldots\ldots\ldots\ldots\ldots\ldots\ldots (2.4)$$

Where;

$[A]_0$ is the initial concentration of the reactants

[A] is the change in concentration of a reactant after time t,

t is the reaction time

K is the rate constant

ΔH is a change in heat

ΔS is a change in entropy

T is the temperature in kelvin

R is the universal gas constant

CHAPTER THREE

MATERIALS AND METHODS

3.1 Sample Collection and Preparation

A Fresh *P. hysterophorus* whole plant sample was collected from Kalimoni, Juja town, Kiambu County, and transported to the GoK Chemistry Laboratory at Jomo Kenyatta University of Agriculture and Technology (JKUAT) for further preparation. It was identified and authenticated by Mr. John Kamau Muchuku, a Botanist from the Department of Botany, JKUAT, and a voucher specimen deposited in the JKUAT Botany Herbarium with the accession number DMN-JKUATBH/001/2023A-C (Appendix 1). The sample was then washed with running tap water, rinsed with distilled water, and dried under the shade for two weeks. The dry sample was ground to a fine powder using a milling machine (no model number, assembled locally).

3.2 Chemicals and Reagents

The following analytical grade chemicals and reagents were used in this study: Copper (II) sulfate ($CuSO_4$), Zinc nitrate hexahydrate ($Zn(NO_3)_2.6H_2O$), Sodium hydroxide (NaOH), Hydrochloric acid (HCl), Hydrogen peroxide (H_2O_2), Methylene blue, Rifampicin, 98% Methanol AR grade were purchased from Sigma-Aldrich through the Vision Scientific Ltd, Kenya. All chemicals and reagents were used without further purification.

3.3 Instrumentation

The following instruments were used in this study: Shimadzu UV-1800 spectrophotometer (Kyoto, Japan), Bruker Tensor II Fourier Transform Infrared Spectrophotometer (Bruker, Ettlingen, Germany), STOE STADIP P X-ray Powder Diffraction System (STOE and Cie, GmbH, Darmstadt, Germany), Tescan Mira3 LM FE Scanning Electron Microscope (TESCAN, Brno, Czechia), Tecnai G2 Spirit (Thermo

Fischer Scientific, Oregon USA), and Bechman Coulter DelsaMax pro dynamic light scattering analyzer (Beckman Coulter, Indianapolis, United States).

3.4 Extraction of Secondary Metabolites in the Sample

The aqueous extract of the *P. hysterophorus* sample was obtained following a previously established protocol by Marimuthu *et al*. (2015), with slight modification in which 20 g of fine plant powder was dissolved in 200 mL of distilled water. The mixture was heated at 40℃ on a hot plate while being stirred constantly for 20 minutes, and the resultant extract was filtered through a Whatman No. 1 filter paper (Marimuthu et al., 2015).

3.5 Phytochemical Screening Tests

The secondary metabolites in *P. hysterophorus* whole plant aqueous extract were screened using the procedures adopted by Marimuthu *et al*. (2015) and Marimuthu and Ravi (2014) as depicted in Table 3.1

Table 3.1: Phytochemical Screening Procedures

Phytochemical tests	Procedure
Flavonoids	To 2 mL of the extract, 5 mL of ammonia was added, followed by the addition of 1 mL of concentrated sulphuric acid, and a color change to yellow was indicative of the flavonoid's presence.
Tannins	A few drops of 1% neutral ferric chloride were added to 2 mL of extract, and the formation of greenish-black precipitate was indicative of the tannin's presence.
Alkaloids	Mayer's Test was used to test the presence of alkaloids, in which three drops of Mayer's reagent were added to 2 mL of the extract acidified with dilute hydrochloric acid. A creamy white precipitate indicated the presence of alkaloids.
Saponins	Foam Test was used to test the presence of saponins. In this procedure, 4 mL of the extract was added to a small amount of distilled water with thorough shaking. A form that persisted for 15 minutes indicated saponins' presence.
Steroids and Triterpenoids	In this test, a few drops of chloroform were added to 2 mL of the extract, after which a few drops of sulphuric acid were added and then shaken. The mixture was allowed to stand until the appearance of red color at the lower level of the test tube.

3.6 Synthesis of Zinc Oxide and Copper Oxide Nanoparticles

3.6.1 Synthesis of Zinc Oxide Nanoparticles

Using 0.01 M Zinc nitrate hexahydrate ($Zn(NO_3)_2.6H_2O$) solution and aqueous *P. hysterophorus* extract in the ratio of 1:4, ZnO NPs were prepared as guided by Datta *et al*. (2017) method. The mixture was hand-shaken and left for 45 minutes, and changes in color were noted. The mixture was centrifuged at 4000 rpm for 15 minutes, and the supernatant was poured out. The formation of ZnO NPs was monitored by measuring the surface plasmonic resonance (SPR) peak via a UV-Vis spectrophotometer. After the formation of ZnO NPs was ascertained, the nanoparticles were dried at 80℃ in an oven for 6 hours. A portion of the nanoparticles was also added to 1 mL of distilled water before being taken for characterization (Datta *et al*., 2017).

3.6.2 Synthesis of Copper Oxide Nanoparticles

Using Copper (II) sulfate ($CuSO_4$) (0.01 M) solution and aqueous *P. hysterophorus* extract in the ratio of 1:4, CuO NPs were prepared as described by Datta *et al*. (2017). The color change of the mixture was noted, and the SPR peak associated with the formation of CuO NPs was measured using a UV-Vis spectrophotometer. After the formation of CuO NPs was ascertained by its SPR band, the nanoparticles were then dried at 80℃ in an oven for 6 hours, and a portion was added to 1 mL of distilled water before being taken for characterization (Datta *et al*., 2017).

3.7 Characterization of Zinc Oxide and Copper Oxide Nanoparticles

3.7.1 Determination of Surface Plasmon Resonance

The UV-Vis profiles for *P. hysterophorus* extract, ZnO NPs, and CuO NPs were obtained in the wavelength range between 280 and 800 nm using a UV-Vis spectrophotometer (Kolahalam *et al*., 2022).

3.7.2 Identification of Functional Groups

The functional groups in the *P. hysterophorus* extract, ZnO NPs, and CuO NPs were identified using an FTIR spectrophotometer. The samples were directly placed on the sample holder, pressed, and scanned at a resolution of 4 cm^{-1}, and the spectra were recorded between 4000-400 cm^{-1} (Asamoah *et al*., 2020).

3.7.3 Determination of Crystallinity

The crystallinity of ZnO NPs and CuO NPs was determined using a STOE STADIP P X-ray Powder Diffraction System. The X-ray generator was equipped with a copper tube operating at 40 kV and 40 mA, irradiating the sample with a monochromatic CuKα radiation with a wavelength of 0.1545 nm. The XRD spectra were obtained at room temperature over the 2θ range of 10 – 90° at 0.05° intervals with a measurement time of 1 second per 2θ intervals (Madivoli *et al.,* 2016).

3.7.4 Determination of Surface Morphology

The ZnO NPs and CuO NPs were chemically fixed, dehydrated through an acetone series, and dried to a critical point. The dried sample was mounted on a stub of metal with adhesive, and surface morphology was observed using Tescan Mira3 LM FE scanning electron microscope operated at an accelerating voltage of 20 kV at an aperture size of 30 μm (Chaudhary *et al*., 2019).

3.7.5 Determination of Crystal Lattice Morphology

A smaller number of nanoparticles was dispersed in a small volume of ethanol. A smaller droplet of chemical solution was directed at one or both surfaces of a thin disk. The mixture was deposited on the TEM grid and left for the solvent to evaporate (Umamaheswari *et al.*, 2021). Tecnai G2 Spirit operated at 120 kV equipped with a Veleta 2048 x 2048 wide angle detector and an Eagle 4096 x 4096 bottom mount detectors was used to visualize the crystal lattice morphology of the prepared ZnO NPs and CuO NPs.

3.7.6 Determination of Polydispersity Index and Particle Size Distribution

ZnO NPs and CuO NPs were resuspended in ultrapure water (18 MΩ.cm Barnstead Genpure UV-TOC, Thermoscientific, Germany) and ultrasonicated to obtain a solution of suspended nanoparticles. The solutions were filtered through 0.25 µM PTFE syringes into glass vials, and 45 µL of each solution was transferred onto quartz cuvettes before analysis. The particle size distribution and polydispersity index were then measured using a Bechman Coulter DelsaMax pro dynamic light scattering analyzer (Beckman Coulter, Indianapolis, United States) (Madivoli *et al*., 2016; Madivoli e*t al*., 2022).

3.8 Degradation Studies Using CuO NPs and ZnO NPs

3.8.1 Degradation of Rifampicin Antibiotic

Rifampicin solution (10 mg/L) was prepared by dissolving 0.0025 g of rifampicin in 1 mL of methanol and adding 10 mL of distilled water, and transferring the contents into a 250 mL volumetric flask using a previously established protocol (Wanakai *et al*., 2022). The UV-Vis spectral scan of 2 mL rifampicin solution alone, 2 mL rifampicin spiked with 1 mL H_2O_2, 2 mL rifampicin sprinkled with 10 mg ZnO NPs and CuO NPs and 2 mL rifampicin spiked with 1 mL H_2O_2 and 10 mg of ZnO NPs and CuO NPs sprinkled in separate reaction vessels for 1 h was recorded. The rifampicin solution alone and the rifampicin solution spiked with H_2O_2 were used as control experiments. The degradation progression of rifampicin was then monitored by measuring the changes in absorption intensity of rifampicin at λ_{max} = 480 nm using a UV-Vis spectrophotometer. FTIR analysis was performed for ZnO NPs and CuO NPs after the degradation process and compared with the FTIR spectra before degradation to observe any shifts in the functional groups' frequencies.

3.8.2 Degradation of MB Dye

The degradation of MB dye by ZnO NPs and CuO NPs was established using a previously established protocol with slight modifications (Wanakai *et al*., 2019). A 5 mg/L MB

solution was prepared using distilled water, and 2 mL of the solution was scanned in a UV-Vis spectrophotometer to obtain the MB dye spectral profile. 1 mL of H_2O_2 was added to the 2 mL MB solution, and a UV-Vis spectral scan was obtained in the same wavelength range. In addition, 10 mg of ZnO NPs and CuO NPs were added to 2 mL MB solution spiked with 1 mL of H_2O_2 in a separate reacting vessel, allowed a 1 h reaction time, and a UV-Vis spectral scan recorded. The degradation was then monitored by measuring the changes in the absorption intensity of MB dye at λ_{max} = 664 nm in the UV-Vis spectrophotometer. The MB solution alone and the MB solution spiked with H_2O_2 were used as control experiments for the degradation. FTIR analysis was performed for ZnO NPs and CuO NPs after the degradation process and compared with the FTIR spectra before degradation to observe any shifts in the functional groups' frequencies.

3.9 Optimization of Degradation Conditions

3.9.1 Optimization of Nanoparticle Amount

The effect of CuO NPs and ZnO NPs amount was investigated using 10 mg, 20 mg, 30 mg, 40 mg, and 50 mg of each of the nanoparticles with 10 mg/L rifampicin solution, 5 mg/L MB dye solution, all spiked with 1 mL H_2O_2. The mixture was allowed to react, and the UV-Vis spectrophotometric measurements were recorded at a constant time for all varied nanoparticle amounts to monitor the degradation progression of rifampicin and MB dye. The degradation percentage of the rifampicin antibiotic and MB dye for each amount of CuO NPs and ZnO NPs was calculated using equation 2.1 (Khan *et al*., 2020).

3.9.3 Optimization of pH

The effect of pH on the degradation of rifampicin and MB dye was investigated using 10 mg/L rifampicin, 5 mg/L MB dye solutions, and 10 mg of ZnO NPs and CuO NPs spiked with 1 mL H_2O_2. The pH was varied from 2, 4, 5, 8, 9, to 12 using 0.1 M HCl and 0.1 M NaOH for acidic and basic conditions, respectively. The change in absorbance values for the rifampicin and MB was recorded using a UV-Vis spectrophotometer, and equation 2.1

was used to calculate the degradation percentage at each pH value at a constant time (Khan *et al*., 2020).

3.9.2 Optimization of Rifampicin and MB Concentration

The effect of rifampicin and MB concentration on degradation percentage was studied using 10 mg CuO NPs and ZnO NPs, and 1 mL H_2O_2. The concentration for rifampicin was varied from 10, 15, 20, 25, to 30 mg/L while that of MB was varied from 2.5, 5, 7.5, 10, to 12.5 mg/L. The absorbance values for rifampicin and MB were recorded using a UV-Vis spectrophotometer at a constant time, and the degradation percentage was calculated using equation 2.1 (Khan *et al*., 2020).

3.9.4 Optimization of Reaction Time

The effect of reaction time on the degradation ability was investigated using 10 mg/L rifampicin, 5 mg/L MB dye, 10 mg of CuO NPs and ZnO NPs, 1 mL H_2O_2, and changes in absorption intensity were recorded via a UV-Vis spectrophotometer at specific minute intervals (Ahmadi and Adaobi, 2021). The degradation percentage at each time interval was calculated using equation 2.1.

3.9.5 Optimization of Temperature

The effect of temperature on degradation was studied using 10 mg of CuO NPs and ZnO NPs, 10 mg/L rifampicin and 5 mg/L MB solutions, and 1 mL H_2O_2. The temperature was varied from 25, 35, 45, 55, to 65°C. The absorbance values for the MB and rifampicin at each temperature condition were recorded using a UV-Vis spectrophotometer at a constant time, and the degradation percentage was calculated using equation 2.1 (Khan *et al*., 2020).

3.10 Degradation Studies at Optimal Conditions

For this study, CuO NPs and ZnO NPs amount, rifampicin and MB concentration, pH, reaction time, and temperature parameters that yielded the highest degradation percentage were taken as the optimal conditions for that parameter. These optimal conditions were combined, absorbance values for the rifampicin and MB were recorded using a UV-Vis spectrophotometer, and the degradation percentage was calculated using equation 2.1 (Khan *et al*., 2020).

3.11 Reusability Potential of CuO NPs and ZnO NPs

The ability to reuse CuO NPs and ZnO NPs in the degradation of rifampicin and MB was investigated in four cycles at a constant time in which 20 mg of CuO NPs and ZnO NPs, 10 mg/L rifampicin, 5 mg/L MB dye, and 1 mL H_2O_2 were used. After each use, the nanoparticles were decanted, washed with distilled water, and dried in an oven at 80°C for 6 hours (Chowdhury *et al*., 2020; Zainuri *et al*., 2018). The dry nanoparticles were then used in the subsequent degradation cycle with fresh rifampicin and MB solution. After each cycle, the degradation percentage was calculated using equation 2.1, and the results were plotted in a bar graph.

3.12 Data Analysis

All experiments were performed in triplicate, and the data were averaged and reported as mean $\pm$ SD. The results were represented using line and bar graphs plotted using OriginPro software (version 8.5). In addition, the correlation coefficients (R^2) values of the kinetic models were determined by statistical functions of OriginPro (version 8.5).

CHAPTER FOUR

RESULTS AND DISCUSSION

4.1 Phytochemical Test Results

The phytochemicals in *P. hysterophorus* whole plant aqueous extract, responsible for reducing, capping, and stabilizing metallic nanoparticles, were screened and the results tabulated in Table 4.1.

Table 4.1: Phytochemical Test Results

Phytochemical Test	Presence/Absence
Flavonoids	+
Tannins	+
Alkaloids	+
Saponins	+
Terpenoids	+
Steroids	-

Key: + = presence, **-** = absence

The screening results showed that flavonoids, tannins, alkaloids, saponins, and terpenoids were present in the *P. hysterophorus* aqueous extract, while steroids were absent. The confirmation of the presence of these phytochemicals in the plant extract demonstrated their role in reducing copper ion and zinc ion salts from their 2^+ oxidation states to 0-valent species, leading to the formation of their respective metal oxide nanoparticles (Andualem *et al*., 2020; Marslin *et al*., 2018). Previous studies have attributed these secondary metabolites to also perform the function of capping and stabilizing the formed nanoparticles (Gebre and Sendeku, 2019; Marslin *et al*., 2018).

4.2 Characterization of Zinc Oxide and Copper Oxide Nanoparticles

4.2.1 UV-Vis Spectroscopy Profiles

Figure 4.1 represents the UV-Vis absorption profiles of *P. hysterophorus* extract and CuO NPs.

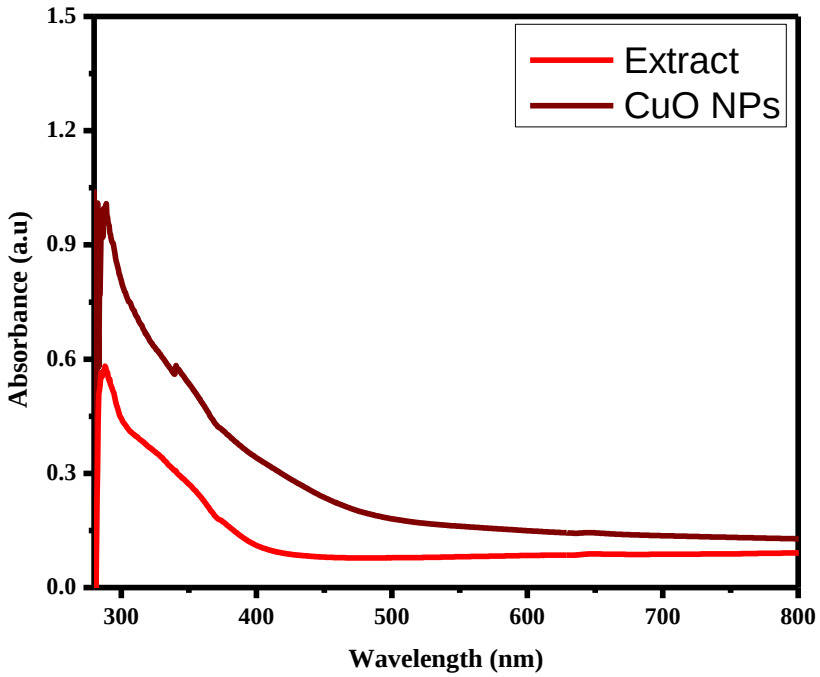

Figure 4.1: UV-Vis Profile of *P. hysterophorus* Extract and CuO NPs

The absorption spectrum associated with *P. hysterophorus* extract was recorded in the range of 280-800 nm and appearance of a peak at 287 nm revealed the presence of electron-rich secondary metabolites (Figure 4.1). The absorption peak associated with CuO NPs was recorded to occur at 340 nm. The CuO NPs absorption peak at 340 nm was indicative of the surface plasmonic resonance peak of the CuO NPs, a wavelength at which CuO NPs absorbed the UV-Vis light. The SPR peak associated with CuO NPs obtained in this study agreed to results reported in previous studies, indicating the peak occurs in the range of 200 to 350 nm (Akintelu *et al*., 2020).

The UV-Vis absorption profile associated with ZnO NPs and *P. hysterophorus* extract is represented in Figure 4.2.

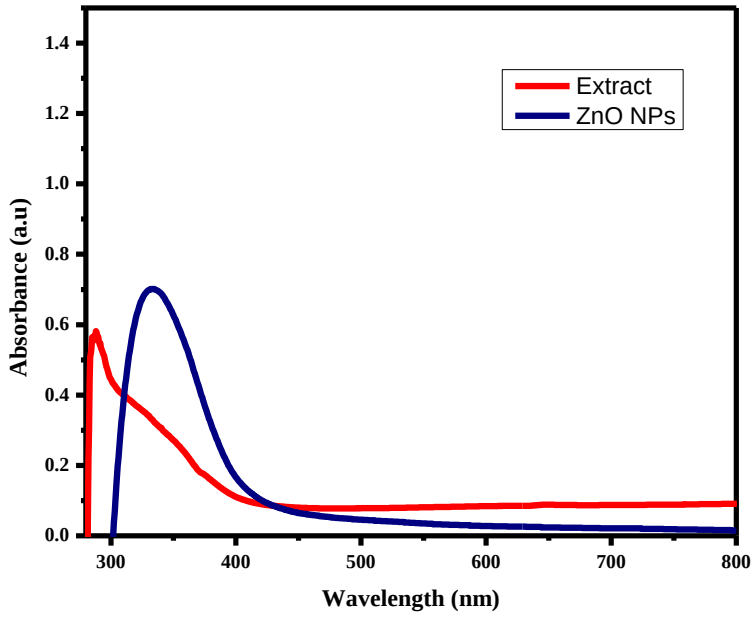

Figure 4.2: UV-Vis Profile of ZnO NPs and *P. hysterophorus* Extract

The formation of ZnO NPs was confirmed by appearance of surface plasmonic resonance (SPR) peak centered at 337 nm (Figure 4.2). The appearance of ZnO NPs SPR peak at 337 nm was in agreement with previous studies employing plant extract to form green ZnO NPs. For instance, Iqbal and colleagues (2021) prepared ZnO NPs using *Elaeagnus angustifolia* leaf extract and obtained an SPR band at 399 nm. Wang *et al*. (2022) reported ZnO NPs synthesized from coffee extract had an SPR peak at 376 nm. Naseer *et al*. (2020) also reported ZnO NPs prepared using *Cassia fistula* and *Melia azedarach* extracts had SPR peaks at 320 and 324 nm, respectively. Moreover, the formation of ZnO NPs was confirmed by a UV absorption peak at 320 nm in which plant extract of *Cayratia pedata* was used as a reducing agent (Jayachandran *et al*., 2021). For ZnO NPs, the absorption peaks are reported to occur between 310 nm to 380 nm and 310 to 360 nm, as pointed out by Jayachandran *et al*. (2021) and Wang *et al*. (2022) research findings, respectively. These wavelengths confirm the formation of ZnO NPs obtained using *P. hysterophorus* whole plant extract.

4.2.2 FTIR Spectroscopy Analysis

The functional groups present in the *P. hysterophorus* extract and green CuO NPs are depicted in Figure 4.3.

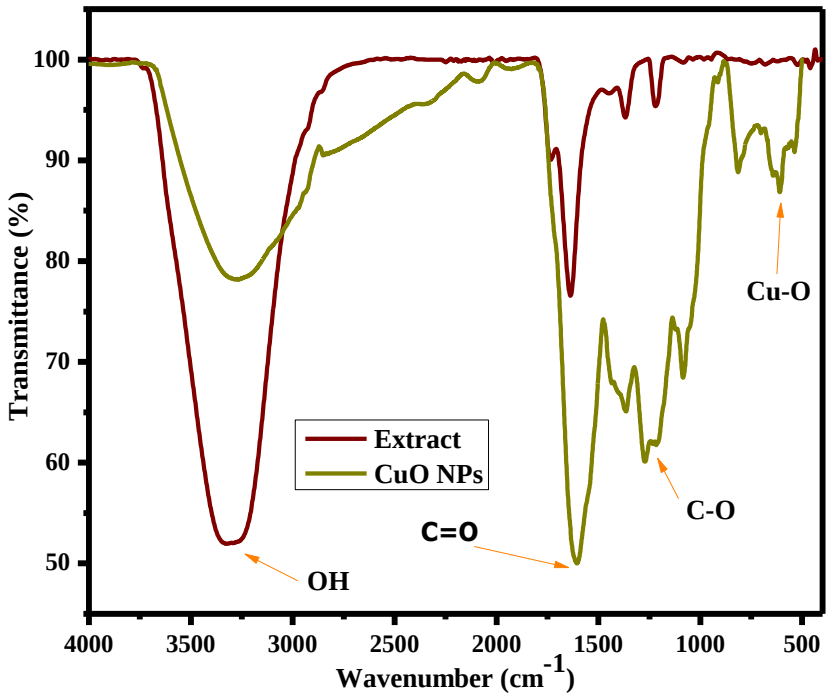

Figure 4.3: IR Spectra of *P. hysterophorus* Extract and CuO NPs

The IR spectrum for CuO NPs showed that functional groups appeared at wavenumbers of 3284, 1600, 1368, 1278, 1084, 820, 522, and 590 cm^{-1}. The peak in the range of 3371-3212 cm^{-1} indicated the presence of the O-H functional group typical of water in the extract. These findings are consistent with previously reported results on CuO NPs (Faisal *et al*., 2021). A C=O stretching vibration at 1630 cm^{-1} and 1600 cm^{-1} is present in both the extract and CuO NPs (Renuga *et al*., 2020). In addition, the spectra show the appearance of a peak at 1368 cm^{1} representing the C-N bending vibration of secondary metabolites, typically amines in the extract (Andualem *et al*., 2020). A C-O bending vibration associated with flavonoids in the extract appears 1084 cm^{-1} (Andualem *et al*., 2020). The Cu-O vibration band is confirmed by the peaks at 522 cm^{-1} and 590 cm^{-1}, which previous

studies report to be characteristic of the formation of green CuO NPs (Alhalili, 2022; Andualem *et al*., 2020). From the IR profile, the formation of green CuO NPs is confirmed.

In addition, the functional groups in the *P. hysterophorus* extract and green ZnO NPs are depicted in IR spectra in Figure 4.4.

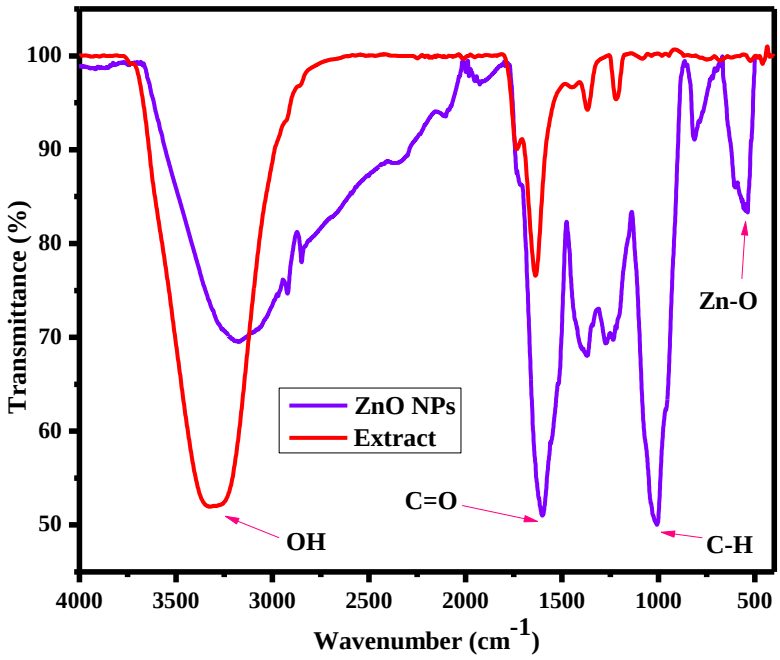

Figure 4.4: IR Spectra of *P. hysterophorus* Extract and ZnO NPs

From the IR profiles, *P. hysterophorus* extract shows presence of several absorption peaks. The peaks appear at 3299 cm^{-1}, 1632 cm^{-1}, 1362 cm^{-1}, and 1222 cm^{-1}. These peaks are attributable to broad O-H, C=O, and C-N stretching bands characterized by phenols, flavonoids, and amine metabolites in the plant extract (Datta *et al*., 2017). It was noticed that there was a shift in the peaks' position in the extract and after ZnO NPs were formed. The shift indicated the bonding and capping of the nanoparticles by the secondary metabolites in the extract (Alamdari *et al*., 2020). Observable vibration bands in ZnO NPs spectra were at 3173 cm^{-1}, 2923 cm^{-1}, 1591 cm^{-1}, 1375 cm^{-1}, 1259 cm^{-1}, 1001 cm^{-1}, 809 cm^{-1}, and 543 cm^{-1}. A characteristic peak attributed to the Zn-O bond appeared at 543 cm^{-}

[1] with previous studies using *Cayratia pedata*, *Cassia fistula,* and *Melia azedarach* plant extract, reporting the Zn-O vibration band to occur between 435 and 683 cm^{-1} (Jayachandran *et al*., 2021; Naseer *et al*., 2020). In addition, ZnO NPs formation was confirmed by the Zn-O band at 560 cm^{-1} (Umamaheswari *et al*., 2021). Hence, the formation of green ZnO NPs using *P. hysterophorus* extract was confirmed.

4.2.3 Scanning Electron Microscopy Analysis

The SEM micrographs of green CuO NPs (a) and ZnO NPs (b) are shown in Figure 4.5.

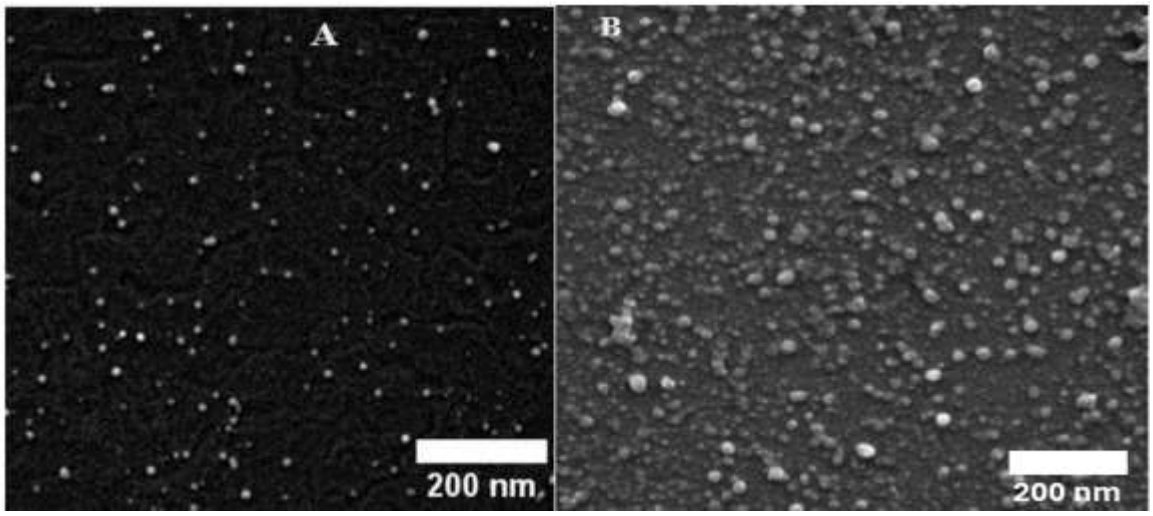

Figure 4.5: SEM Micrographs of (a) CuO NPs and (b) ZnO NPs

From Figure 4.5 (a) CuO NPs were nearly spherical with some evidence of agglomeration. ZnO NPs were also nearly spherical with more pronounced agglomeration evidence (Figure 4.5 (b)). The nearly spherical morphology of CuO NPs and ZnO NPs obtained in this study was in agreement with previous studies on CuO NPs and ZnO NPs' shape obtained using plant extracts (Altikatoglu *et al*., 2017; Amjad *et al*., 2021; Iqbal *et al*., 2021; Wang *et al*., 2022). The less agglomeration evidence illustrated that the synthesis process yielded more homogeneous particles (Alamdari *et al*., 2020; Datta *et al*., 2017; Faisal *et al*., 2021).

The particle size distribution of green CuO NPs and ZnO NPs was also determined using ImageJ software, and the distribution was plotted using a histogram as represented in Figure 4. 6.

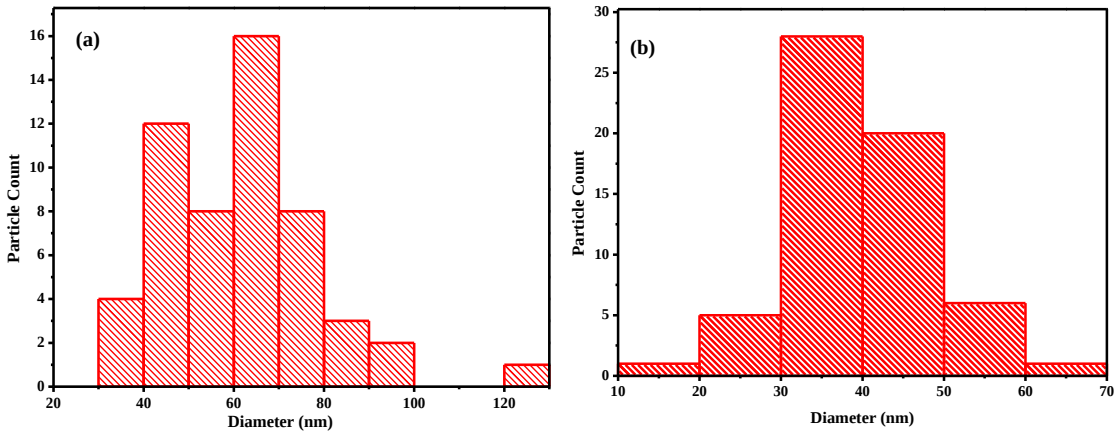

Figure 4.6: Average Particle Size Distribution of (a) CuO NPs and (b) ZnO NPs

As shown in Figure 4.6, most of the sizes of the nanoparticles were below 100 nm, with the average particle sizes for CuO NPs (a) and ZnO NPs (b) calculated to be 59.99 nm and 38.47 nm, respectively. The size distribution obtained in this study for green CuO NPs and ZnO NPs was in agreement with findings reported in previous studies (Altikatoglu *et al*., 2017; Amin *et al*., 2021). A study by Faisal *et al*. (2021) obtained ZnO NPs in the range of 43.3 to 83.1 nm. In another study, ZnO NPs were prepared from green algae, and SEM results revealed that the particle size ranged from 50 nm to 80 nm (Hameed *et al*., 2023).

4.2.4 Transmission Electron Microscopy Analysis

TEM micrographs of CuO NPs (A) and ZnO NPs (B) are depicted in Figure 4.7 below.

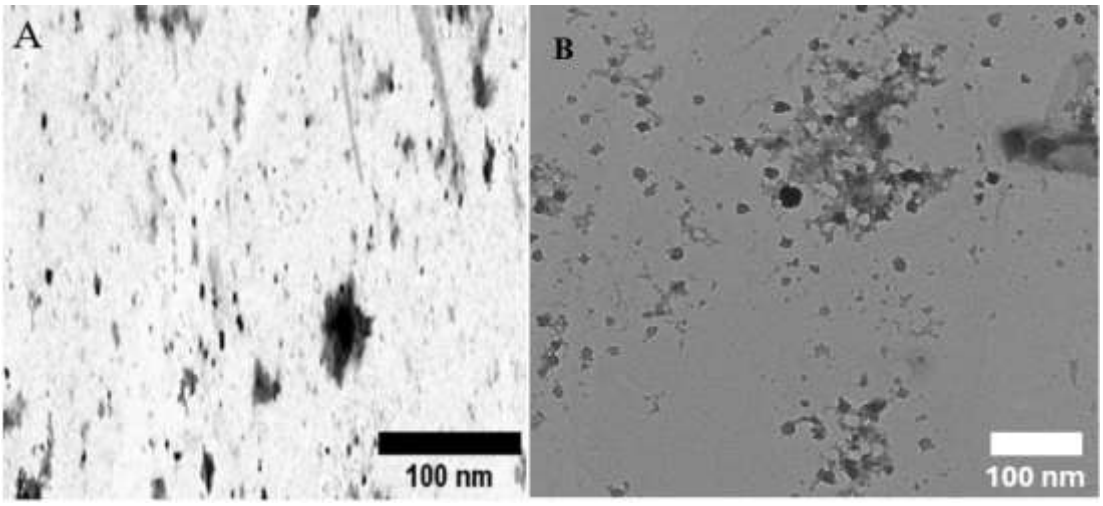

Figure 4.7: TEM Micrographs of (a) CuO NPs and (b) ZnO NPs

The TEM images showed that the nanoparticles were spherical and smaller than those observed under SEM visualization (Figure 4.6). The agglomeration of green CuO NPs was more pronounced than what was observed for green ZnO NPs. Figure 4.8 represents the size distribution of green CuO NPs and ZnO NPs determined using ImageJ software.

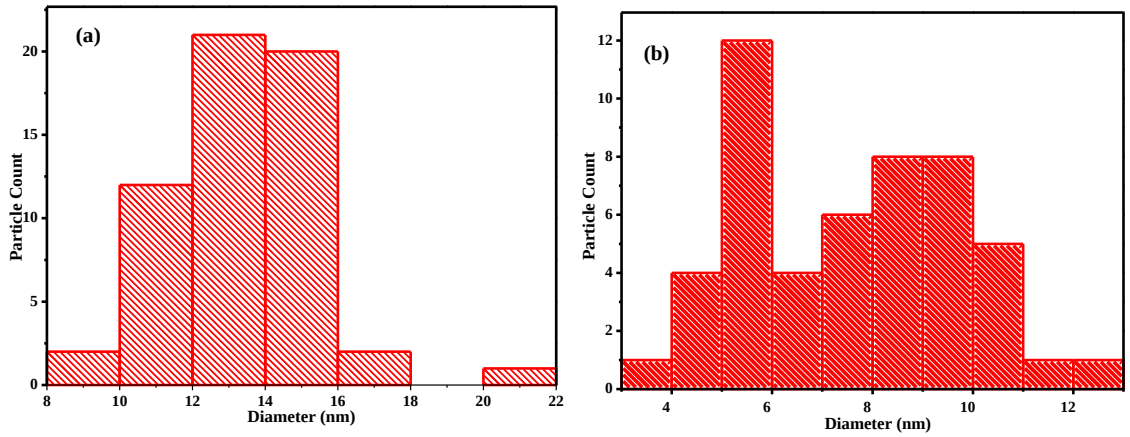

Figure 4.8: Particle Size Distribution of (a) CuO NPs and (b) ZnO NPs Determined Using TEM

From Figure 4.8, it can be shown that the size distribution for CuO NPs (a) ranged from 8 to 22 nm, while those of ZnO NPs (b) ranged from 1 to 13 nm, with the average particle

size for CuO NPs and ZnO NPs being 12.43 and 7.54 nm, respectively. The particle size range obtained in this study was consistent with previously reported studies in terms of the spherical morphology and size distribution (Bhatnagar *et al*., 2019; Chand Mali *et al*., 2019; Wang *et al*., 2022).

4.2.5 XRD Analysis

The crystallinity of the green CuO NPs was determined using the XRD diffractometer and the obtained diffractogram is represented in Figure 4.9.

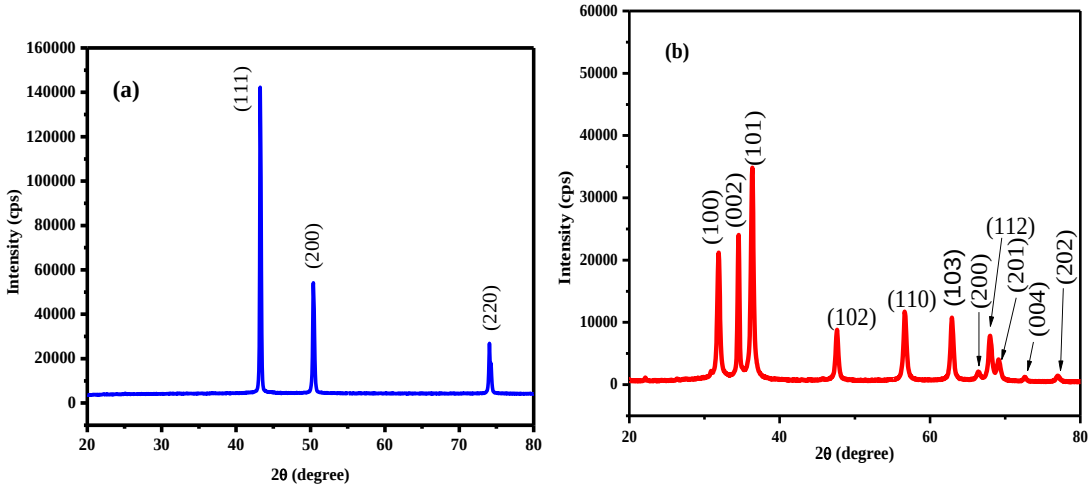

Figure 4.9: XRD Diffractogram of (a) CuO NPs and (b) ZnO NPs

The X-ray diffraction patterns for CuO NPs (a) revealed the presence of three prominent peaks at 2θ angles in the range of 20° to 80° at 43.6°, 50.8°, and 73.5°. These 2θ angles represent Miller indices (111), (200), and (220). According to the International Centre for Diffraction Data (ICDD) database, CuO NPs with such Miller indices are indexed to be highly crystalline with a monoclinic structure (Andualem *et al*., 2020; Alhalili, 2022; Amin *et al*., 2021; Raja *et al*., 2008). In addition, the XRD diffractogram for ZnO NPs revealed 11 peaks at 31.74°, 34.40°, 36.4°, 47.56°, 56.73°, 62.88°, 66.55°, 68.05°, 69.22°, 72.54°, and 77.05° (Figure 4.9 (b)). These 2θ values correspond to (100), (002), (101), (102), (110), (103), (200), (112), (201), (004), and (202) crystallographic planes, respectively, which correspond to International Center for Diffraction Data (ICDD)

database indexed for ZnO NPs (Alamdari *et al*., 2020; Iqbal *et al*., 2021; Wang *et al*., 2022). Based on these crystallographic planes ZnO NPs are indexed to possess a hexagonal wurtzite structure (Alamdari *et al*., 2020; Faisal *et al*., 2021a; Wang *et al*., 2022). Therefore, the XRD data confirmed the formation of green CuO NPs and ZnO NPs prepared using *P. hysterophorus* extract.were identified at

4.2.6 DLS Analysis

The particle size distribution for green CuO NPs and ZnO NPs was obtained using DLS and results depicted in Figure 4.10.

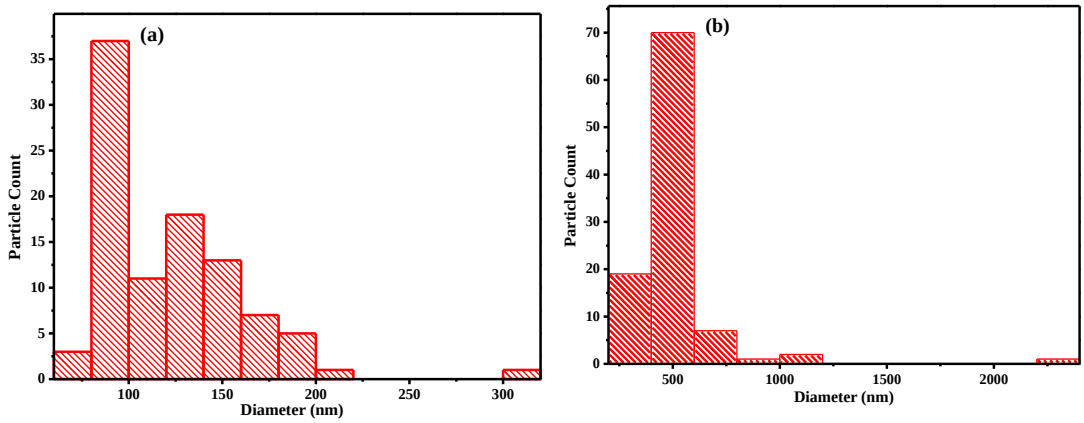

Figure 4.10: Particle Size Distribution of Green (a) CuO NPs and (b) ZnO NPs Obtained by DLS

From Figure 4.10 (a), most CuO NPs ranged between 1 to 200 nm with smaller group of particles with 300 nm size distribution. The size distribution for ZnO NPs ranged upto to 500 nm (Figure 4.10 (b)). The distribution of the nanoparticles from DLS analysis indicated that the particles were large and polydisperse. In both CuO NPs and ZnO NPs, the polydispersity index (PDI) was determined to be ≤0.3, which proved that the particles were polydisperse while individual groups of particles were monodisperse, which supported possible agglomeration of the particles (Alamdari *et al*., 2020; Carvalho *et al*., 2018; Jain *et al*., 2020). The individual monodispersity can be associated to the

agglomeration or aggregation during the nanoparticle synthesis process as seen in SEM and TEM micrographs above (Raval *et al.*, 2019). The monodispersity of the particles shows that the particles were homogenous, which is desired in the activity of the nanoparticles.

4.3 Degradation Studies Using CuO NPs and ZnO NPs

4.3.1 Degradation Studies of Rifampicin Antibiotic

The degradation progression of rifampicin antibiotic using green CuO NPs and ZnO NPs was monitored by a UV-Vis spectrophotometer, and the results are depicted in Figure 4.11.

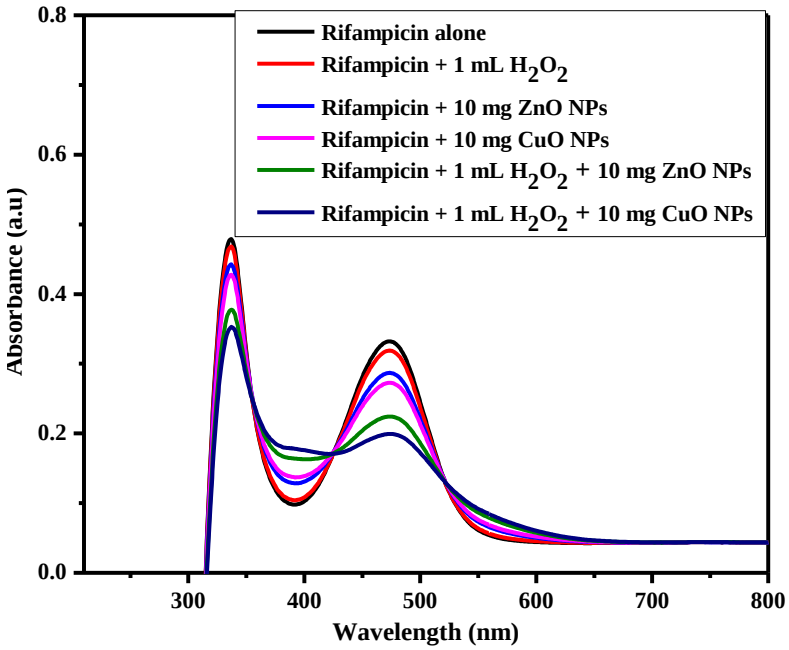

Figure 4.11: Degradation of Rifampicin Using ZnO NPs and CuO NPs

From Figure 4.11, no observable change in the rifampicin solution when it was left alone for 1 hour. However, spiking the rifampicin solution with 1 mL of H_2O_2 yielded a small change in the absorption intensity at 480 nm. Related smaller changes in the absorption intensity were recorded when rifampicin was reacted with 10 mg of ZnO NPs and CuO

NPs. Further spiking rifampicin and 10 mg of ZnO NPs and CuO NPs with 1 mL H_2O_2 recorded a remarkable decrease in the absorption intensity of rifampicin at 480 nm. This decline showed there was degradation of the antibiotic by the nanoparticles, and the presence of H_2O_2 led to the generation of reactive radicals, which necessitate the degradation process (Aksu Demirezen *et al*., 2019; Wanakai *et al*., 2022).

The degradation studies were conducted by varying conditions of green ZnO NPs and CuO NPs amount, rifampicin concentration, pH, reaction time, and temperature and at combined optimal conditions.

4.3.1.1 Effect of CuO NPs and ZnO NPs Amount on Percentage Degradation

The effect of green (a) CuO NPs and (b) ZnO NPs amount on the degradation of rifampicin was investigated using 10, 20, 30, 40, and 50 mg. The results are depicted in Figure 4.12.

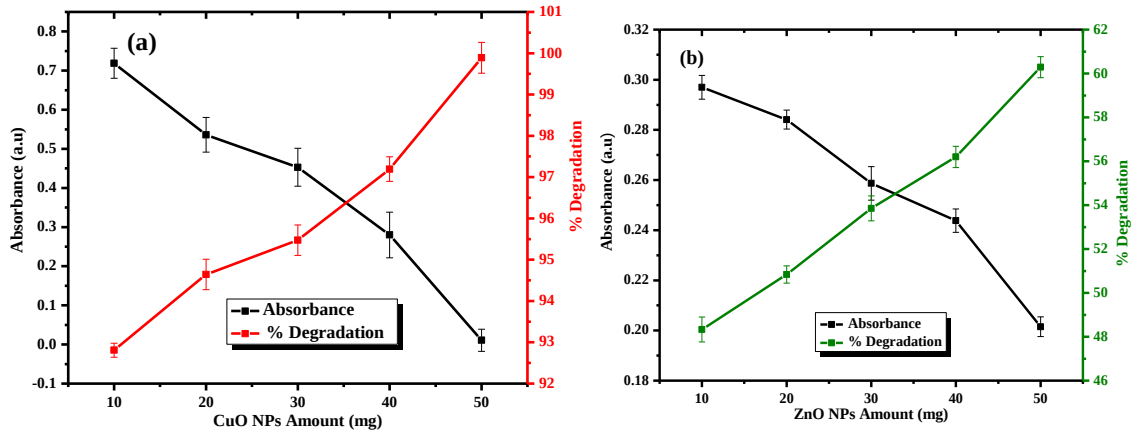

Figure 4.12: Effect of (a) CuO NPs and (b) ZnO NPs Amount on Percentage Degradation

As shown in Figure 4.12 (a), the rifampicin degradation percentage increased from 92.81% at a 10 mg amount to 99.89% at a 50 mg amount within 210 minutes using CuO NPs. It was observed that at 10 mg of green ZnO NPs, the degradation percentage was 48.33% but increased to 60.29% using 50 mg of green ZnO NPs within 180 minutes (Figure 4.12 (b)). The increase in degradation percentage upon increasing the amount of green CuO NPs and ZnO NPs was attributed to the increase in the number of active sites

on the surface of the nanoparticles that adsorbed the rifampicin antibiotic (Aksu Demirezen *et al*., 2019; Kutuzova *et al*., 2021). In this regard, the higher amount of green CuO NPs and ZnO NPs meant that there was a presence of a large total surface area to volume ratio, making the number of active sites increase as the amount of green CuO NPs and ZnO NPs was increased, enhancing the catalytic potential of the nanoparticle against the rifampicin antibiotic, similar to what is reported in previous studies (El-Sayed *et al*., 2014; Kutuzova *et al*., 2021).

Another observation in this investigation that supports the increase in degradation efficiency with increased nanoparticle amount was a decrease in absorbance intensity of rifampicin antibiotic as measured using a UV-Vis spectrophotometer. Absorbance is directly related to concentration according to Beer-Lambert Law; therefore, it can be concluded that the concentration of rifampicin antibiotic decreased as the amount of CuO NPs and ZnO NPs was increased. Hence, rifampicin molecules were adsorbed into the active sites at higher CuO NPs and ZnO NPs amounts, destroying the molecules faster and faster due to more active sites at higher nanoparticle amounts.

4.3.1.2 Effect of Rifampicin Concentration on Percentage Degradation

The effect of rifampicin concentration on the degradation percentage of green (a) CuO NPs and ZnO NPs (b) was determined by varying the concentration of rifampicin from 10, 15, 20, 25, to 30 mg/L using 10 mg of CuO NPs and ZnO NPs, and spiked with 1 mL H_2O_2. The results are represented in Figure 4.13.

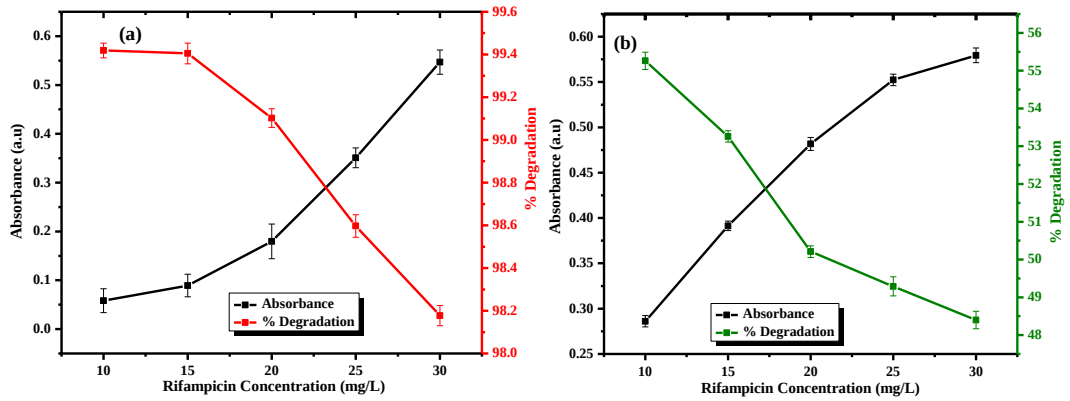

Figure 4.13: Effect of Rifampicin Concentration on Degradation Percentage

From Figure 4.13, the percentage of degradation of rifampicin solution decreased as its concentration was increased from 10 mg/L to 30 mg/L in both CuO NPs and ZnO NPs. The degradation efficiency decreased from 99.42% at 10 mg/L to 97.78% at 30 mg/L within 12 minutes of reaction while using CuO NPs (a). In addition, the degradation percentage of rifampicin using green ZnO NPs (b) decreased as the solution concentration was increased from 10 mg/L to 30 mg/L, from 55.26% to 48.4%, respectively. The decrease in degradation percentage of rifampicin at higher concentrations is attributed to the saturation of active sites on the surface of the green CuO NPs and ZnO NPs, making it difficult for degradation to occur (El-Sayed *et al*., 2014; Kutuzova *et al*., 2021). Another probable reason for the decrease in degradation efficiency upon increasing rifampicin solution concentration relates to the generation of intermediates or degradation products that compete with actual rifampicin molecules for the limited number of available active sites on the surface of the green CuO NPs and ZnO NPs. It is also possible that the generation of reactive radicals from the H_2O_2 becomes limited at a higher rifampicin solution, affecting the antibiotic's degradation (Kutuzova *et al*., 2021). The UV-Vis spectrum revealed that the absorption intensity of rifampicin remained higher at its higher concentrations, implying minimal antibiotic degradation occurred at higher concentrations using the same amount of green CuO NPs and ZnO NPs.

4.3.1.3 Effect of pH on Percentage Degradation

The effect of pH on degradation percentage on rifampicin antibiotic was determined from pH 2, 4, 5, 8, to 12 using 10 mg of green CuO NPs (a) and ZnO NPs (b) spiked with 1 mL H_2O_2. The results are presented in Figure 4.14.

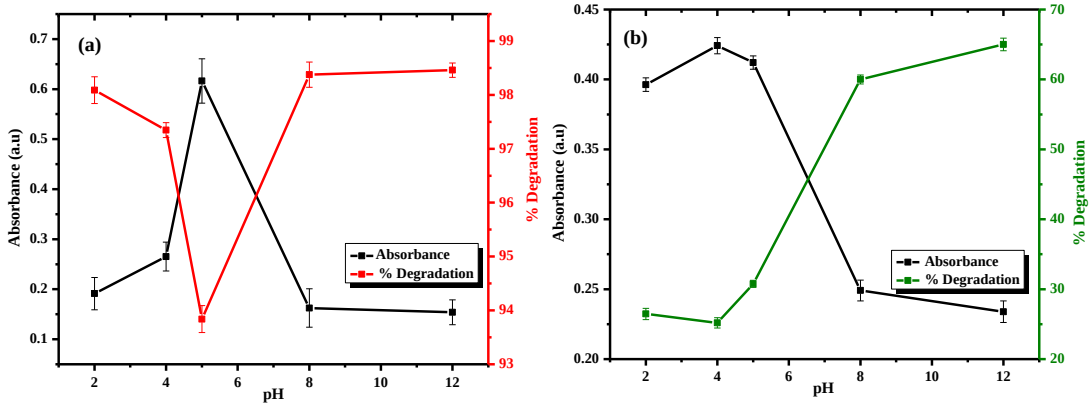

Figure 4.14: Effect of pH of Rifampicin Solution on Degradation Percentage

From Figure 4.14, the degradation percentage of rifampicin antibiotic using CuO NPs and ZnO NPs depended on the pH of the solution. The normal rifampicin solution was determined to have a pH of 5, and upon reaction with CuO NPs, the degradation percentage was calculated to be 93.84%. The pH was adjusted to acidic solutions, pH 2 and 4, with the degradation percentage calculated to be 98.09% and 97.35%, respectively. In basic pH 8 and 12, a degradation percentage of 98.38% and 98.46% was recorded, respectively. In addition, degradation of rifampicin using ZnO NPs at pH 2, 4, and 5, the degradation percentage was 26.46%, 25.19%, and 30.76%, respectively. On the other hand, at pH 8 and 12, the degradation percentage was 60% and 65%, respectively. The variation of rifampicin solution pH affects the concentration of H^+ and OH^- ions, which generate reactive radicals for the degradation process. The increase in the percentage of degradation in acidic media can be attributed to the generation of hydrogen radicals upon the interaction of H_2O_2 with green CuO NPs and ZnO NPs (Usman *et al.*, 2020). Simultaneously, in acidic media, the nanoparticles become positively charged, which

increases the rate of interaction of H_2O_2 with green CuO NPs and ZnO NPs, resulting in the generation of more H^+ ions and increasing the degradation of rifampicin (Aksu Demirezen *et al.*, 2019; Wanakai *et al.*, 2022). In basic conditions, a higher percentage of degradation of rifampicin can be attributed to increased generation of OH radicals, which activate the active sites of green CuO NPs and ZnO NPs, enhancing their catalytic potential. Compared to rifampicin at pH 5, it was observed that the acidic and basic pH media remarkably improved the degradation efficiency of green CuO NPs and ZnO NPs on rifampicin antibiotic, which shows that the degradation of rifampicin is pH-dependent. Its alteration impacts the surface charge of the green CuO NPs and ZnO NPs, resulting in varying percentages of degradation (Cai *et al.*, 2019). In both acidic and basic conditions, a remarkable decrease in absorption intensity of rifampicin was observed compared to rifampicin at its normal pH, which could support possible formation of intermediates or degradation products.

4.3.1.4 Effect of Reaction Time on Percentage Degradation

The effect of reaction time on degradation percentage of rifampicin antibiotic was studied in 30-minute intervals using 10 mg using green (a) CuO NPs and (b) ZnO NPs, 10 mg/L rifampicin solution spiked with 1 mL H_2O_2. The results are presented in Figure 4.15.

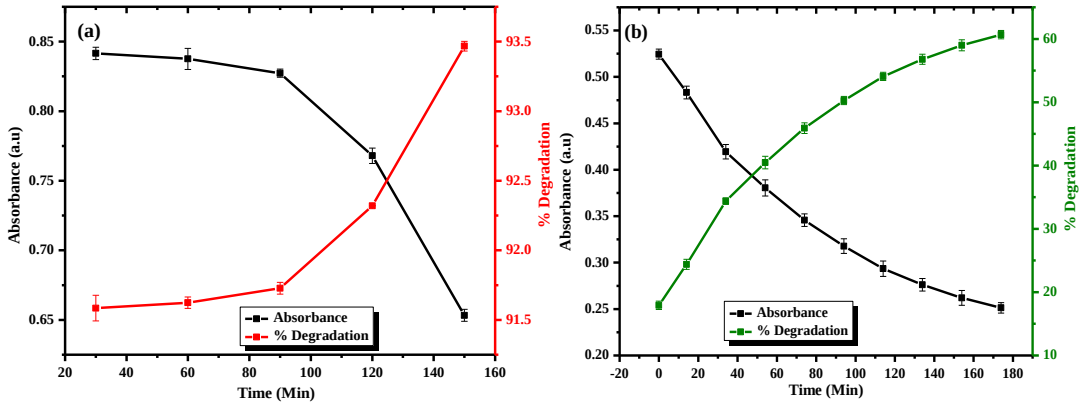

Figure 4.15: Effect of Reaction Time on Degradation Percentage of Rifampicin

The degradation percentage of rifampicin antibiotic using green CuO NPs increased as the reaction time was increased from 91% to 92% in 150 minutes (Figure 4.15 (a)). Using ZnO NPs the degradation percentage of rifampicin increased from 17% at the start of the reaction to 64% within 254 minutes (Figure 4.15 (b)). The decrease in absorbance intensity of rifampicin at λ_{max} = 480 nm was an indication of the degradation of rifampicin antibiotic by green CuO NPs and ZnO NPs, which shows that the concentration of the rifampicin decreased with time (Kansal *et al.*, 2014). Previous studies have reported an increase in the degradation efficiency of antibiotics using nanoparticles with increased contact time. Hamad and El-Sesy (2023) reported improved removal efficiency of levofloxacin antibiotic using green CuO NPs from 27% in 15 minutes to 71% within 120 minutes. It was therefore noted that reaction time had an influence on the interaction of the rifampicin antibiotic with the green CuO NPs and thus increase in degradation efficiency with reaction time.

4.3.1.5 Effect of Temperature on Percentage Degradation

The effect of temperature on degradation percentage of rifampicin antibiotic using green CuO NPs and ZnO NPs was studied at 25℃, 35℃, 45℃, 55℃, and 65℃ and the obtained results are represented in Figure 4.16.

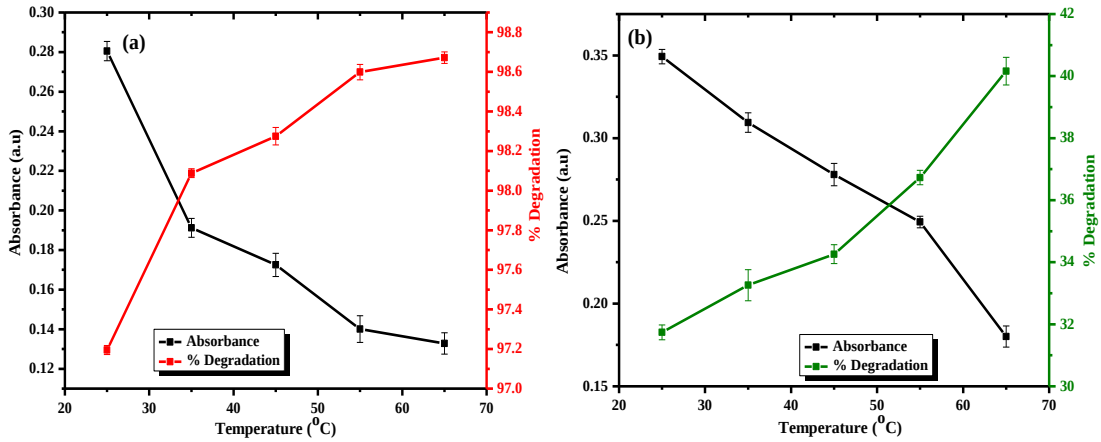

Figure 4.16: Effect of Temperature on Degradation Percentage

The percentage of degradation of rifampicin increased as the temperature increased from 25℃ to 65℃ from 97.19% to 98.76%, respectively, within 24 minutes using CuO NPs (Figure 4.16 (a)). While for ZnO NPs, the degradation percentage increased to 40.16% from 31.84% within 60 minutes (Figure 4.16 (b)). The increase in the percentage of degradation with temperature can be attributed to an increase in Brownian motion, which improves the kinetics of the rifampicin molecules (Aksu Demirezen *et al*., 2019; Wanakai *et al*., 2022; Xu *et al*., 2020). Simultaneously, the absorption intensity of the rifampicin antibiotic was observed to decrease exponentially as the temperature was increased from 25℃ to 65℃, meaning temperature increate the rate of degradation of antibiotic (Wanakai *et al*., 2022).

4.3.1.6 Kinetics of Degradation of Rifampicin Using CuO NPs and ZnO NPs

The kinetics of degradation of rifampicin using green CuO NPs and ZnO NPs were determined by fitting experimental data by assuming pseudo-first-order and pseudo-second-order at 298, 308, 318, 328, and 338 K temperatures, and obtained rate constants and correlation coefficient are provided in Table 4.2 and 4.3.

Table 4.2: Kinetic Models Fitting of Experimental Data at Different Temperatures for Rifampicin Using CuO NPs

Temperature (K)	Pseudo-first order		Pseudo-second order	
	Rate constant (Min^{-1})	R^2	Rate constant (Min^{-1})	R^2
298	-0.00391	0.99382	0.01038	0.9917
308	-0.01424	0.99516	0.07749	0.98263
318	-0.01372	0.98761	0.07725	0.99477
328	-0.02072	0.96142	0.13196	0.99278
338	-0.01736	0.9655	0.11281	0.99406

The kinetics of degradation of rifampicin using green CuO NPs was observed to fit pseudo-second-order kinetics rather than pseudo-first-order kinetics because the R^2 (correlation coefficient) values were ≥ 0.98 for all temperature conditions compared to first-order R^2 values. It was observed that the rate constants increased with temperature,

which was indicative that the degradation of rifampicin using green CuO NPs was endothermic, which was in agreement with previous findings investigating the degradation of rifampicin (Wanakai *et al*., 2022). The first-order and second-order kinetic plots used to calculate R^2 values are given in Appendix II.

Van't Hoff's plot of lnk_{eq} against $\frac{1}{T}$, was used to determine the change in heat and entropy of the degradation reaction of rifampicin using green CuO NPs and results are presented in Figure 4.17 below.

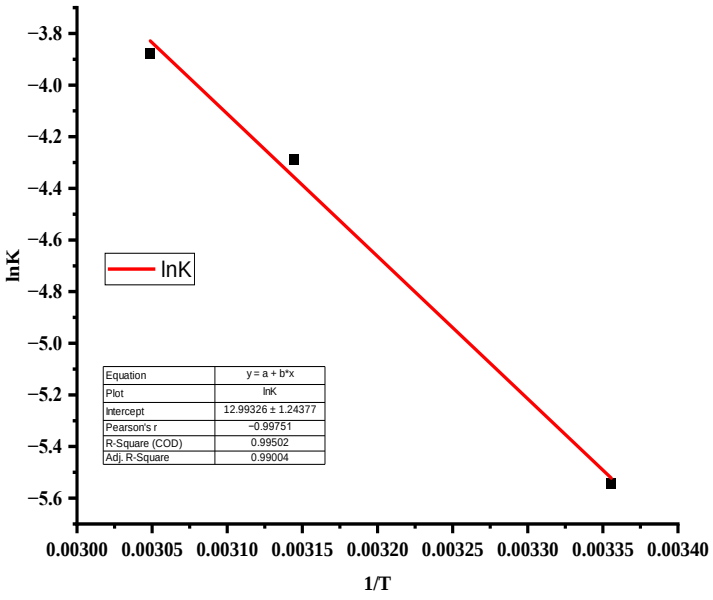

Figure 4.17: Van't Hoff Plot for Degradation of Rifampicin Using CuO NPs

From Figure 4.17, the change in heat was calculated from the slope, while the change in entropy was determined from the intercept values of Van't Hoff's plot. The change in heat and entropy were calculated to be 45.87 kJ mol^{-1} and 108.03 $JK^{-1,}$ respectively. The Van't Hoff's equation provides a relationship of change in equilibrium constant with a decrease in rifampicin concentration with increasing temperature. Notably, the degradation of rifampicin by green CuO NPs was higher at higher temperatures, implying the endothermic nature of the degradation reaction (Cai *et al*., 2019). It can be mentioned that

the entropy of an endothermic reaction decreases when the temperature increases, which is attributed to the formation of degradable products *(*Wanakai *et al*., 2022).

Figure 4.18 presents the Arrhenius plot of lnk against 1/T used to determine the activation energy of the degradation process of rifampicin using green CuO NPs.

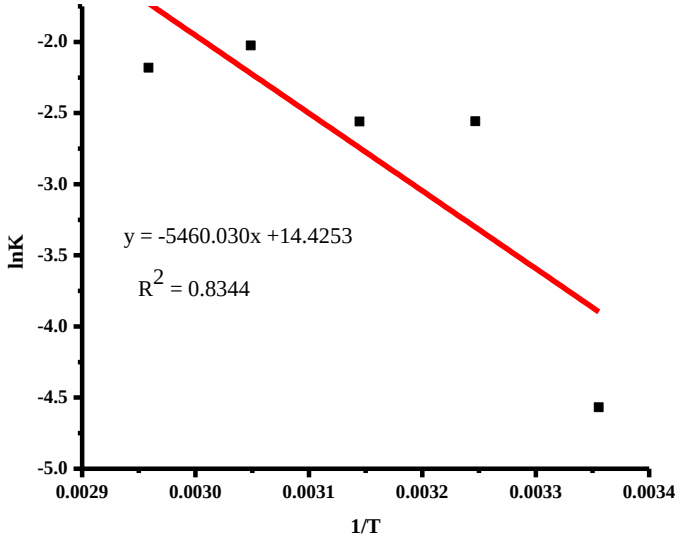

Figure 4.18: Arrhenius Plot of lnk against 1/T to Obtain Activation Energy of the Degradation Reaction of Rifampicin

From Figure 4.18, the activation energy (E_a) was calculated by following the pseudo-second-order kinetic model established for the degradation of rifampicin antibiotic using green CuO NPs and found to be 454 kJ mol^{-1}.

Table 4.3: Kinetic Models Fitting Experimental Data at Different Temperatures for Rifampicin Using ZnO NPs

Temperature (K)	Pseudo-first order		Pseudo-second order	
	Rate constant (Min^{-1})	R^2	Rate constant (Min^{-1})	R^2
298	-0.00582	-0.98484	0.01286	0.98255
308	-0.007	-0.9915	0.01574	0.98785
318	-0.007	-0.99675	0.01434	0.99625
328	-0.007	-0.99277	0.0175	0.98318
338	-0.008	-0.97919	0.0202	0.96278

The degradation of rifampicin using green ZnO NPs was found to follow pseudo-first-order kinetic model as most R^2 values were greater for pseudo-first-order kinetic model compared to R^2 values for the second-order-kinetic model. The kinetic plots are provided in Appendix III. The thermodynamics parameters, change in heat and entropy of the degradation reaction was determined using Van't Hoff's plot of lnKeq V 1/T and results presented in Figure 4.19.

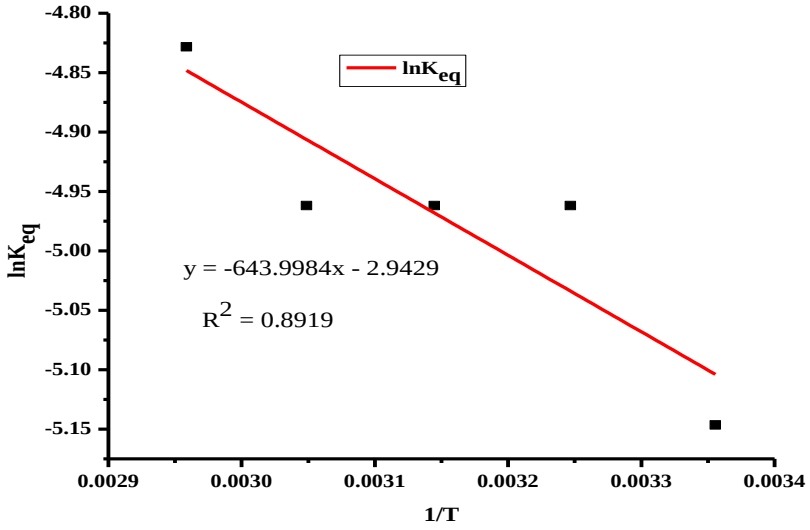

Figure 4.19: Van't Hoff Plot for Degradation of Rifampicin Using ZnO NPs

From Figure 4.19, the change in heat was calculated to be 5.35 kJ mol^{-1} while the change in entropy was found to be 24.46 J K^{-1}. These thermodynamic parameter values show that

the degradation of rifampicin using green ZnO NPs was an endothermic process, implying that the degradation was temperature-dependent (Cai *et al*., 2019).

4.3.1.7 Optimal Conditions for Degradation of Rifampicin

Optimal conditions that resulted in the highest degradation percentage in each of the varied parameters were combined, and the degradation of rifampicin was monitored. This study's optimal conditions were 10 mg/L rifampicin solution, temperature at 65℃, and 50 mg of green CuO NPs and ZnO NPs. The optimal studies were conducted at pH 8 for CuO NPs and pH 12 for ZnO NPs and absorption intensity of rifampicin at λ = 480 nm monitored and change in spectra presented in Figure 4.20 below.

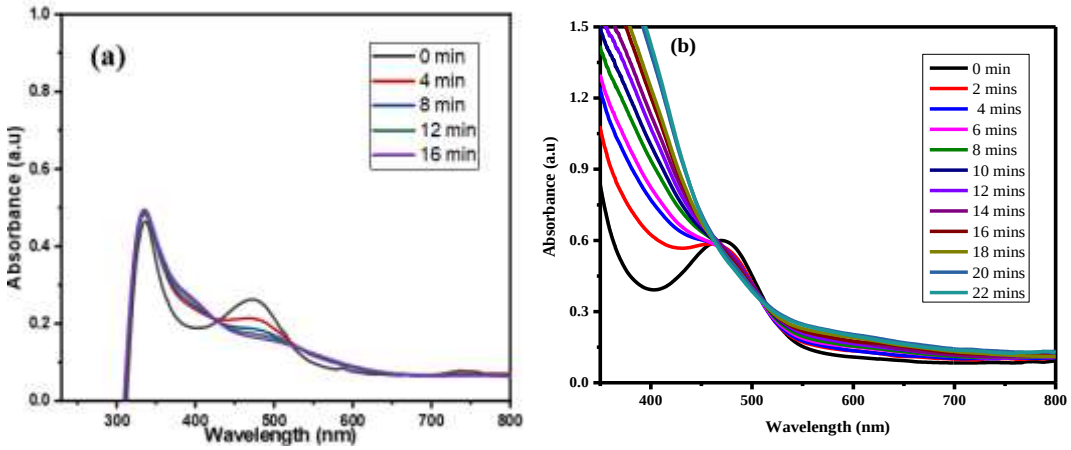

Figure 4.20: Degradation of Rifampicin at Optimal Conditions for (a) CuO NPs and (b) ZnO NPs

From Figure 4.20, the degradation of rifampicin was recorded to be completed as the absorption peak of rifampicin at λ = 480 nm flattened. The percentage degradation of rifampicin at optimal conditions was calculated and found to be 98.37%, achieved within 16 minutes under CuO NPs while it was 78.45% for ZnO NPs achieved within 22 minutes. This indicated that the combined optimal conditions of green CuO NPs and ZnO NPs amount, rifampicin concentration, reaction time, pH, and temperature to were able to achieve completion destruction of rifampicin molecules within a short period (16 and 22 minutes respectively) than when each parameter was used independently. Therefore, it

can be concluded that at these optimal conditions, more active sites are available on the surface of green CuO NPs and ZnO NPs to degrade the rifampicin molecules with high kinetic energy and generation of reactive radicals is maintained higher activating the surface of nanoparticles and thus, the resultant increase in degradation efficiency (Wanakai *et al*., 2022).

4.3.1.8 Functional Group Analysis of CuO NPs and ZnO NPs after Degradation Studies

After degradation studies of rifampicin using green CuO NPs and ZnO NPs, the nanoparticles were analyzed using an FTIR spectrophotometer to observe any possible changes in the frequencies of the functional groups before and after degradation, and the results are depicted in Figure 4.21.

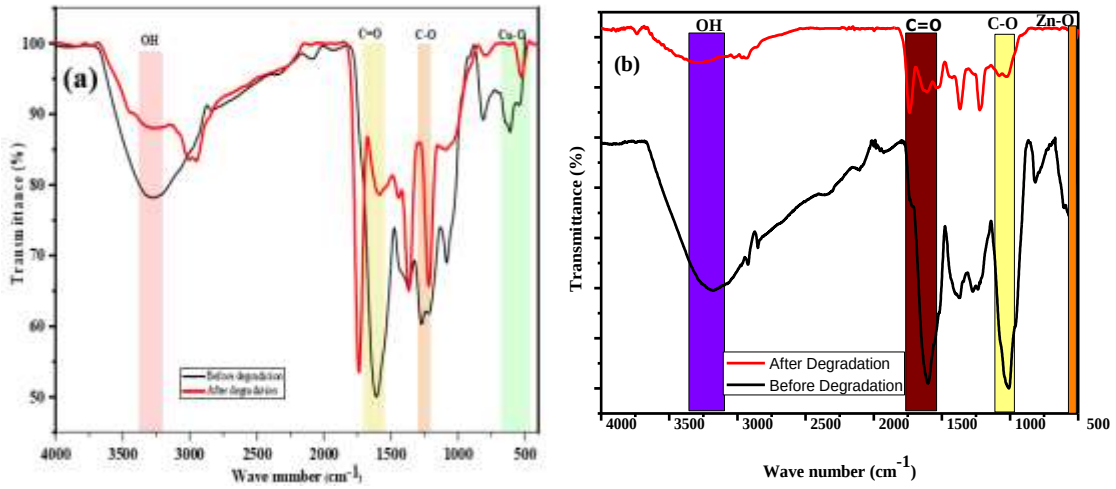

Figure 4.21: FTIR Spectra of (a) CuO NPs and (b) ZnO NPs before and after Degradation of Rifampicin

Slight changes were observed in the FTIR spectra of green CuO NPs after its use in the degradation of rifampicin antibiotic (Figure 4.21 (a)). Shifts in the wavenumber of the functional groups were observed after the green CuO NPs interacted with rifampicin. The broadband typical of an OH group shifted from 3270 cm^{-1} to two peaks at 3288 cm^{-1} and

2949 cm^{-1} after degradation, slightly narrower than before degradation studies. The band typical of C=O groups shifted from 1609 cm^{-1} before degradation to 1737 cm^{-1} after degradation. The shift of the C-O was observed from 1271 cm^{-1} before degradation to 1209 cm^{-1} after degradation studies. Related observations were also recorded for the IR spectra of ZnO NPs, as shown in Figure 4.21 (b). There were shifts in the frequencies of the functional groups present in the IR spectrum of green ZnO NPs after the degradation of the rifampicin antibiotic (Figure 4.21 (b)). Before degradation ZnO NPs had peaks at 3173 cm^{-1}, 2923 cm^{-1}, 1591 cm^{-1}, 1375 cm^{-1}, 1259 cm^{-1}, 1001 cm^{-1}, 809 cm^{-1}, and 543 cm^{-1}. However, variation in the wavenumbers occurred after degradation at 3187 cm^{-1}, 1606 cm^{-1}, 1363 cm^{-1}, 1219 cm^{-1}, 1009 cm^{-1}, and 522 cm^{-1}. The transitions were attributed to the adsorption of rifampicin on the surface of CuO NPs, which altered the frequencies. The peaks assigned to the Cu-O functional group slightly shifted from two peaks at 590 cm^{-1} and 522 cm^{-1} to a single peak after degradation at 528 cm^{-1}. The intensity of the peaks after degradation of rifampicin also reduced compared to the peaks before the degradation process. These changes in the peaks of CuO NPs and ZnO NPs before and after degradation studies of rifampicin demonstrate that their degradative ability in removing antibiotics did not lose the functionality of the CuO NPs (Xu *et al*., 2020).

4.3.1.9 Reusability Potential of CuO NPs and ZnO NPs

The reusability ability of green CuO NPs and ZnO NPs in the degradation of rifampicin solution was investigated in four cycles, each maintained for 90 minutes. The degradation was studied using 10 mg/L rifampicin solution and 20 mg green CuO NPs and ZnO NPs spiked with 1 mL H_2O_2. Figure 4.22 below presents the change in the degradation percentage of green CuO NPs and ZnO NPs in four recycling cycles.

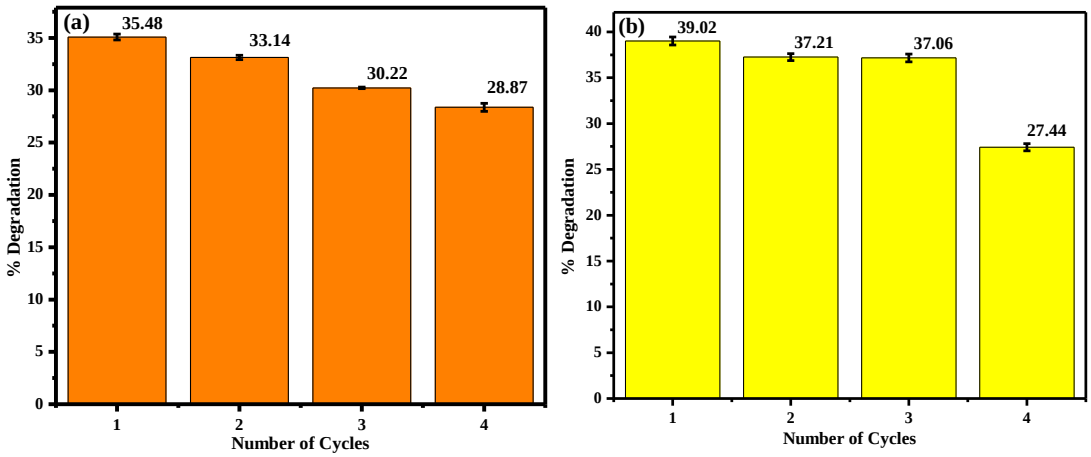

Figure 4.22: Reuse Ability of (a) CuO NPs and (b) ZnO NPs in Degradation of Rifampicin

It was recorded that the degradation percentage of green CuO NPs on rifampicin antibiotic decreased from 35.48% (first cycle) to 28.87% (fourth cycle) (Figure 4.22 (a)). A similar trend was also observed using ZnO NPs, in which in the first cycle, the degradation percentage was 39.02% and decreased to 27.42% in the fourth cycle (Figure 4.22 (b)). Several reasons can be attributed to the decline in degradation efficiency with the reuse of green CuO NPs and ZnO NPs. One of the probable reasons is that the adsorption of rifampicin antibiotic solution onto the active sites of the nanoparticles deactivates the catalytic properties of green CuO NPs and ZnO NPs (Faisal *et al*., 2022; Zhou *et al*., 2018). Another probable reason for the decline in degradation efficiency after each reuse cycle is that the nanoparticles can lose their catalytic potential during separation and drying processes (Chowdhury *et al*., 2020; Kaushal *et al*., 2023). The reusability property findings obtained in this study are consistent with previous study findings (Chowdhury *et al*., 2020; Kaushal *et al*., 2023).

4.3.2 Degradation Studies of Methylene Blue Dye

The degradation of MB dye was monitored using a UV-Vis spectrophotometer by measuring the change in absorbance of the dye alone; the dye spiked with H_2O_2, dye

sprinkled with 10 mg of CuO NPs and ZnO NPs, and dye spiked with H_2O_2 and sprinkled with 10 mg of CuO NPs and ZnO NPs at a constant time of 150 minutes, and the change in absorption intensity of MB at 664 nm were depicted in Figure 4.23.

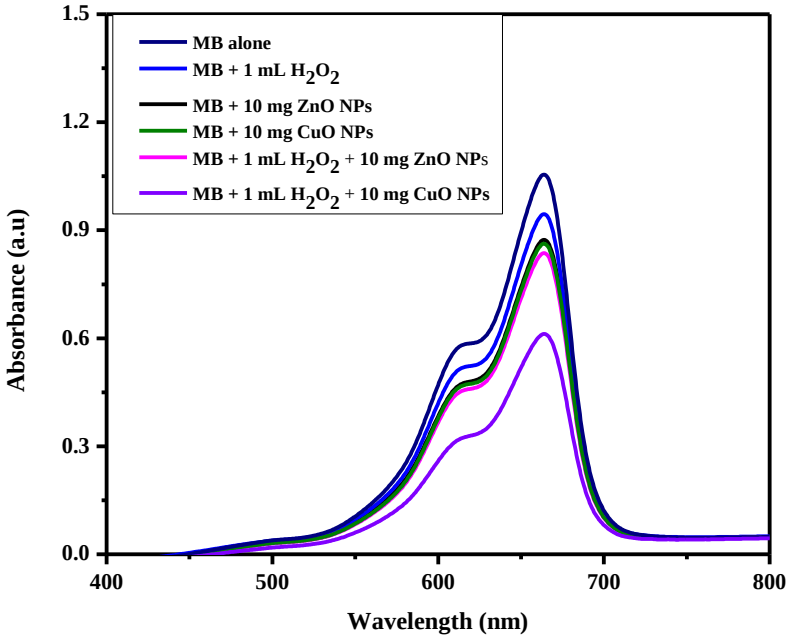

Figure 4.23: Monitoring Degradation of MB Using CuO NPs and ZnO NPs

From Figure 4.23, there were no observable changes in the absorption intensity of 5 mg/L MB dye after it was left standing for 150 minutes. This showed that MB dye is stable, and its degradation does not occur in the absence of the catalytic agent. Figure 4.23 also depicts a slight change in absorption intensity of 5 mg/L MB dye after it was reacted with 1 mL H_2O_2 and left for the same duration. Remarkable reduction of absorption intensity of MB was also recorded when the dye was sprinkled with 10 mg of CuO NPs and ZnO NPs for the same duration as shown in Figure 4.23. A significant decrease in absorption intensity was observed when the same concentration of MB dye was reacted with 1 mL H_2O_2 and 10 mg of green CuO NPs and ZnO NPs for the same time (Figure 4.23). This observation indicated that green CuO NPs and ZnO NPs had catalytic properties desired in the degradation of MB dye (Kgatle *et al*., 2021; Riapanitra *et al.*, 2022).

The degradation studies of MB dye were conducted by varying parameters such as the amount of the green CuO NPs and ZnO NPs, concentration of the MB dye solution, pH, reaction time, and temperature and degradation percentage calculated using equation 2.1 (Goyal *et al*., 2022; Kgatle *et al*., 2021; Reza *et al*., 2017).

4.3.2.1 Effect of CuO NPs and ZnO NPs Amount on Percentage Degradation

The effect of green CuO NPs and ZnO NPs amount was investigated by varying the amount from 10 mg, 20 mg, 30 mg, 40 mg, to 50 mg using 5 mg/L MB dye solution and 1 mL H_2O_2. The percentage degradation was calculated after 2.5 hours, and the results are represented in Figure 4.24.

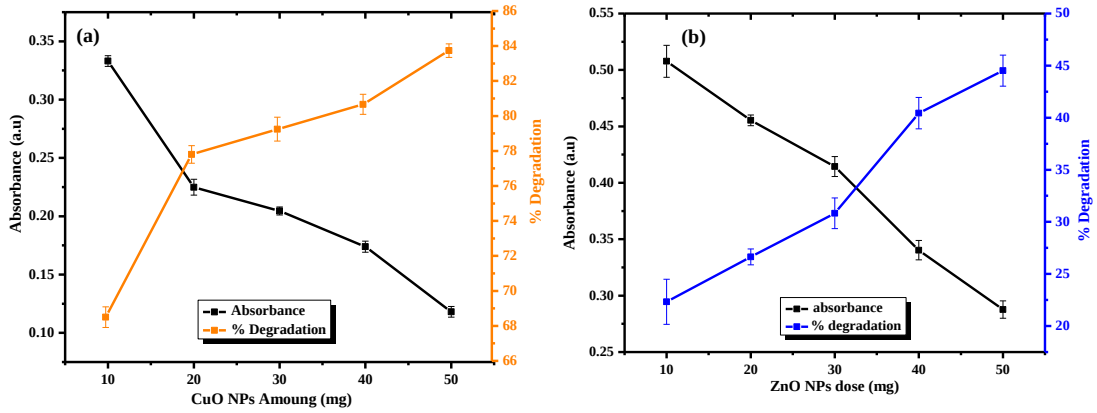

Figure 4.24: Effect of (a) CuO NPs and (b) ZnO NPs Amount on Degradation Percentage

The degradation percentage of MB dye using green CuO NPs increased from 68.49% to 83.73% as the amount of green CuO NPs was increased from 10 to 50 mg within 2.5 hours (Figure 4.24 (a)). In addition, by using ZnO NPs the degradation percentage of MB dye increased proportionally as the amount of the green ZnO NPs was increased from 10 mg (23.44%) to 50 mg (44.31%) (Figure 4.24 (b)). At higher amounts of green CuO NPs and ZnO NPs, the total surface area to volume ratio increases, making more active sites available for the interaction with the MB dye, enabling degradation process to occur (Aksu

Demirezen *et al*., 2019; Choudhary *et al*., 2023; Kutuzova *et al*., 2021; Vasiljevic *et al*., 2020). Furthermore, more radicals are generated at high amounts of green CuO NPs and ZnO NPs from the H_2O_2 used as a radical generator in the degradation process, which increases the catalytic properties of the nanoparticles against the MB dye when a larger amount of the nanoparticles is used and was consistent to previous study findings (El-Sayed *et al*., 2014; Kutuzova *et al*., 2021). The higher degradation of MB dye at a higher amount of green CuO NPs and ZnO NPs was also supported by the higher reduction of the absorbance of MB dye as observed using a UV-Vis spectrophotometer (Alkaykh *et al*., 2020).

4.3.2.2 Effect of MB Dye Concentration on Percentage Degradation

In studying the effect of MB dye concentration, the dye was prepared into 2.5 mg/L, 5 mg/L, 7.5 mg/L, 10 mg/L, and 12 mg/L concentrations. The degradation of the dye was then investigated using 10 mg green CuO NPs (a) and ZnO NPs (b) and 1 mL H_2O_2. The degradation percentage was calculated after 2.5 hours and the results are depicted in Figure 4.25.

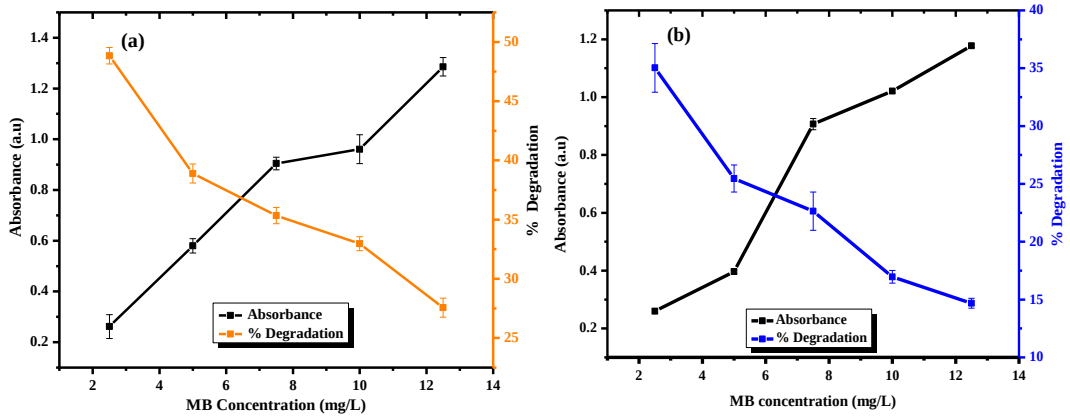

Figure 4.25: Effect of Concentration of MB Dye on Degradation Percentage

The percentage of degradation of MB dye decreased from 48.84% to 27.56% as the dye concentration was increased from 2.5 mg/L to 12 mg/L using CuO NPs (Figure 4.25 (a)). It was also observed that the degradation percentage of MB dye decreased from 33% to

14% as the concentration of MB dye solution increased from 2.5 mg/L to 12.5 mg/L respectively using ZnO NPs (Figure 4.25 (b)). The decrease in the degradation percentage of MB dye using green CuO NPs and ZnO NPs can be attributed to the saturation of the active sites of the nanoparticles by more molecules of the dyes (Alkaykh *et al*., 2020; El-Sayed *et al*., 2014; Kutuzova *et al*., 2021; Salama *et al*., 2018). There is also a possibility that the degradation intermediates compete for the active sites of the nanoparticles with the actual MB dye molecules present in the reaction (Kutuzova *et al*., 2021). This hinders the degradation of the dyes at this higher concentration than when the dye solution is less concentrated.

4.3.2.3 Effect of pH on Percentage Degradation

The pH of MB solution was varied from 2, 4, 5, 8, 9, and 12 and the degradation studied using 10 mg of green CuO NPs (a) and ZnO NPs (b), 5 mg/L MB dye solution, and 1 mL H_2O_2 and degradation percentage calculated after 2.5 hours and results depicted in Figure 4.26.

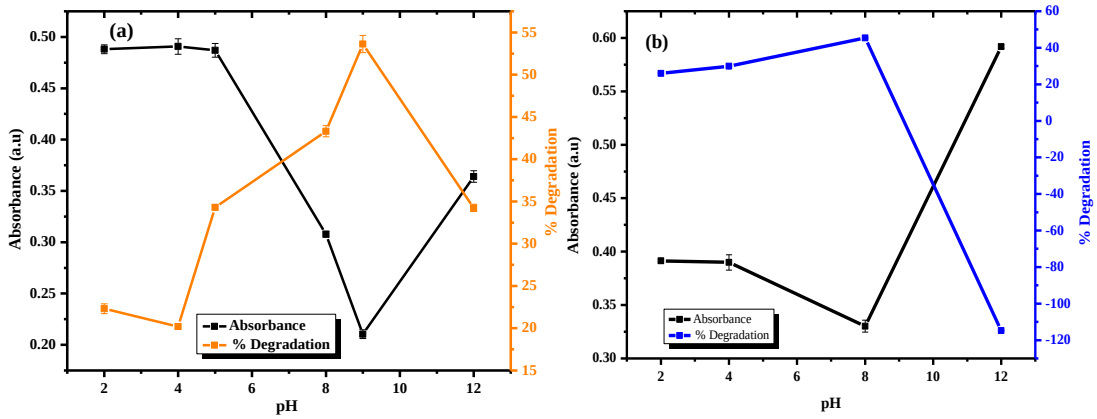

Figure 4.26: Effect of pH on Degradation Percentage

As shown in Figure 4.26 (a) using CuO NPs, at pH 2 and 4, the acidic conditions, the degradation percentage was 21.97% and 19.14% respectively. At pH 5, the degradation efficiency was 33.61%, while at basic conditions pH 8, 9, and 12, the degradation

percentages were 44.39%, 54.74%, and 33.51%, respectively. In addition, degradation using ZnO NPs showed that at acidic conditions, pH 2 and 4, the degradation percentage of MB dye was 26.04% and 29.92%, respectively (Figure 4.26 (b)). Moreover, at pH 8 and 12, the degradation efficiency was 45.50% and 114.80%, respectively (Figure 4.26 (b)). The changes in degradation efficiency of the MB using green CuO NPs and ZnO NPs at varying pH were attributed to H^+ in acidic conditions and OH^- in basic conditions, which plays a role in the generation of reactive radicals involved in the degradation process (Aksu Demirezen *et al*., 2019; Choudhary *et al*., 2023; Salama *et al*., 2018; Usman *et al*., 2020; Wanakai *et al*., 2022). The variation of pH resulted in a variation in the degradation efficiency of MB by green CuO NPs and ZnO NPs, demonstrating that the degradation process was pH-dependent, consistent with previous findings (Cai *et al*., 2019).

4.3.2.4 Effect of Reaction Time on Percentage Degradation

The effect of interaction time on the degradation percentage of CuO NPs and ZnO NPs against MB dye was studied using 10 mg of green CuO NPs and ZnO NPs, 5 mg/L MB dye solution, and 1 mL H_2O_2, and the change in absorbance intensity was measured after 30 minutes interval. The results were represented in Figure 4.27.

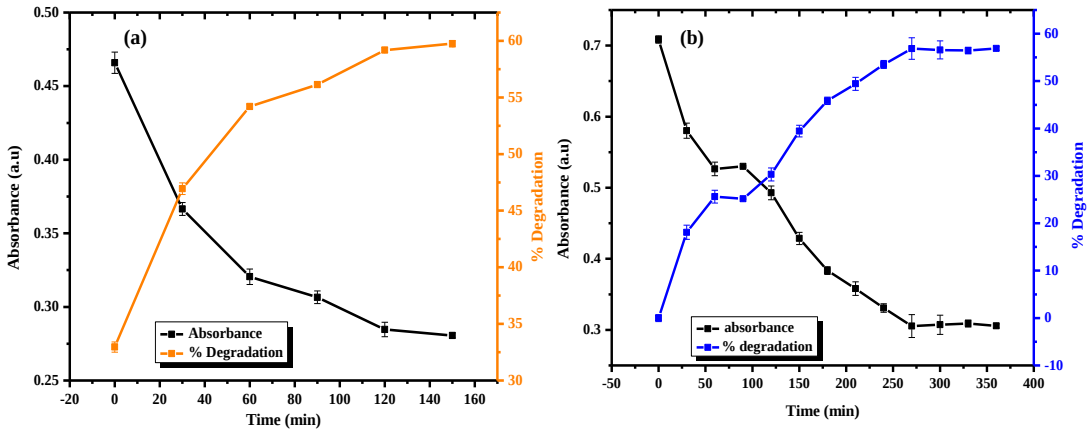

Figure 4.27: Effect of Interaction Time on Degradation Percentage of MB Dye

From Figure 4.27 (a), the percentage of degradation of MB using green CuO NPs was observed to increase as the contact time between reactants was increased. After 30 minutes, the degradation percentage was 32.18%, and it increased to 59.58% after 150 minutes. It was also observed that the percentage of degradation of MB dye by the green ZnO NPs increased from 9% at 30 minutes to 58% after 360 minutes (Figure 4.27 (b)). The increase in degradation percentage with reaction time is attributed to maximum contact between the reactants. The results obtained in this study agreed with previous studies (Faisal *et al.*, 2022; Faisal *et al.*, 2021).

4.3.2.5 Effect of Temperature on Percentage Degradation

The influence of temperature in the degradation of MB dye using green CuO NPs and ZnO NPs was investigated at 25℃, 35℃, 45℃, 55℃, and 65℃ using 5 mg/L MB dye solution, 10 mg of green CuO NPs and ZnO NPs, and 1 mL H_2O_2. The degradation percentage was calculated after 2.5 hours, and the result are depicted in Figure 4.28.

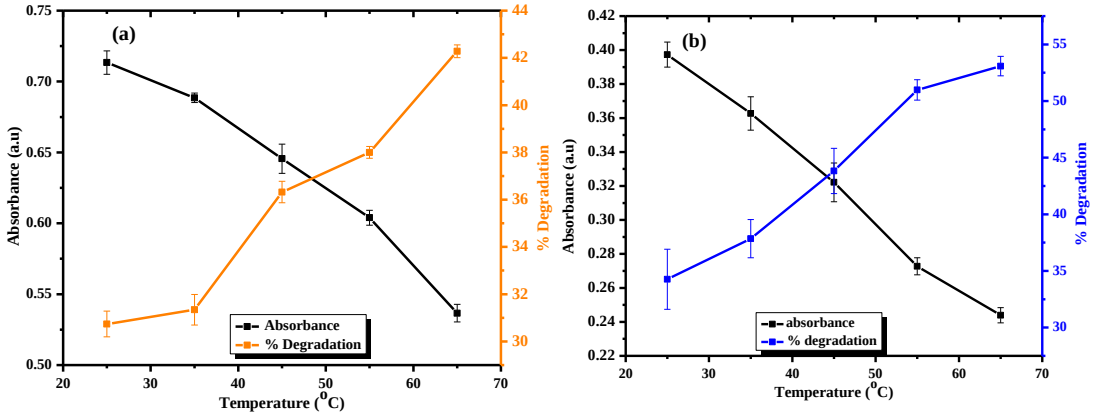

Figure 4.28: Effect of Temperature on Degradation Percentage

As shown in Figure 4.28 (a), the degradation percentage of MB dye using green CuO NPs increased from 30.46% to 42.99% within 2.5 hours as the temperature increased from 25℃ to 65℃. Under ZnO NPs, the percentage of degradation of MB dye of 53.78% was obtained at 65℃ (Figure 4.28 (b)). The increase in percentage degradation as the temperature increased was attributed to the kinetic properties of MB dye molecules due

to Brownian motion, making the degradation process of MB occur faster (Goyal *et al*., 2022; Wanakai *et al*., 2022; Xu *et al*., 2020). The absorption intensity of the MB dye solution also decreased as the temperature increased, indicating the dye molecules' destruction by the nanoparticles. Therefore, the MB dye molecules possess enough energy at higher temperatures for the reaction and degradation (Salama *et al*., 2018).

4.3.2.6 Kinetics of Degradation of MB Dye Using CuO NPs and ZnO NPs

Table 4.4 below presents the kinetic data of degradation of MB dye using green CuO NPs experimentally fitted assuming pseudo-first-order and pseudo-second-order kinetic models using equations 2.1 and 2.2, respectively, at 298, 308, 318, 328, and 338 K temperatures. The kinetics plots are provided in Appendix IV.

Table 4.4: Kinetic Data for Degradation of MB Dye Using CuO NPs at Different Temperatures

Temperature (K)	Pseudo-first order		Pseudo-second order	
	Rate constant (Min^{-1})	R^2	Rate constant (Min^{-1})	R^2
298	-0.002	-0.92278	0.00262	0.90449
308	-0.00281	-0.98148	0.00333	0.97764
318	-0.0029	-0.97641	0.00355	0.96487
328	-0.0033	-0.99061	0.00391	0.97356
338	-0.0036	-0.98899	0.00512	0.97312

From the kinetic information provided in Table 4.4, the degradation of MB dye by green CuO NPs was experimentally observed to fit the pseudo-first-order kinetic model since correlation coefficient values (R^2) were greater than the R^2 obtained assuming pseud-second order kinetic data. The change in heat and entropy of the reaction were then investigated using Van't Hoff's plot (Figure 4.29).

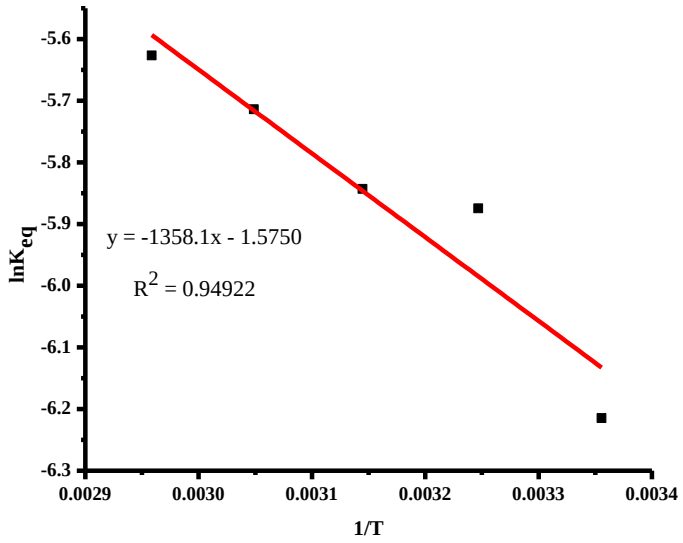

Figure 4.29: Van't Hoff Plot of lnKeq v 1/T for Degradation of MB Using CuO NPs

From Figure 4.29, the change in heat and entropy of the degradation reaction were calculated from the slope and intercept and found to be respectively 11.29 kJ mol^{-1} and 13.09 J K^{-1}. The values indicated that the degradation reaction was an endothermic process and thus the degradation reaction was highly dependent on temperature (Cai *et al*., 2019). Table 4.5 provides rate constant and correlation coefficient values of degradation of MB dye using green ZnO NPs assuming pseudo-first-order and pseudo-second-order kinetics obtained at 298, 308, 318, 328, and 338 K temperatures. Appendix V illustrates the kinetic plots for first-order and second-order kinetic models.

Table 4.5: Kinetic Models Fitting Experimental Data at Different Temperatures for MB and ZnO NPs

Temperature (K)	Pseudo-first order		Pseudo-second order	
	Rate constant (Min^{-1})	R^2	Rate constant (Min^{-1})	R^2
298	-0.00271	-0.98203	0.00552	0.97305
308	-0.00339	0.97307	0.0074	0.95715
318	-0.00385	-0.99156	0.00886	0.98896
328	-0.00483	-0.99318	0.01238	0.98201
338	-0.00529	-0.99532	0.0154	0.99618

From Table 4.5, the kinetic data was experimentally determined to fit the pseudo-first-order rather than the pseudo-second-order kinetic model because most R^2 (correlation coefficient) values were higher compared to the R^2 of the pseudo-second-order kinetic model. The kinetic plots are provided in Appendix V. In this regard, the degradation of MB was highly dependent on temperature. The increase in temperature increases the reacting molecules' Brownian motion, resulting in the highest degradation efficiency (Goyal *et al*., 2022; Salama *et al*., 2018).

The change in heat and entropy of the reaction was obtained by Van't Hoff's plot of $lnK\ v\ \frac{1}{T}$, as shown in Figure 4.30.

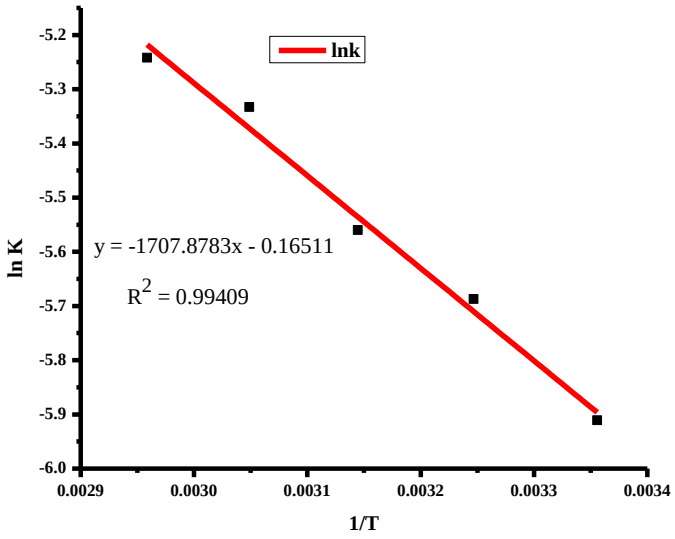

Figure 4.30: Van't Hoff's Plot of Degradation of MB Dye

From Figure 4.30, the change in heat and entropy of the degradation reaction of MB using green ZnO NPs was determined to be 14.199 kJ mol^{-1}, and the change in entropy was calculated to be 1.37264 J K^{-1}, respectively. It was also observed that the degradation of MB dye was an endothermic reaction, which implied an increase in temperature led to a resultant increase in the degradation rate of MB dye. At higher temperatures, the reaction's entropy enhanced system disorder, providing room for breakdown of MB dye molecules (Bhatti *et al*., 2020).

4.3.2.7 Optimal Conditions for Degradation of MB Dye

The degradation of MB dye using CuO NPs and ZnO NPs was studied at optimal conditions obtained for each parameter by reacting 2.5 mg/L MB dye with 50 mg green CuO NPs and ZnO NPs, pH 9 and at 65°C. The change in absorption intensity of MB dye was monitored using UV-Vis 1800 spectrophotometer and the results are presented in Figure 4.31.

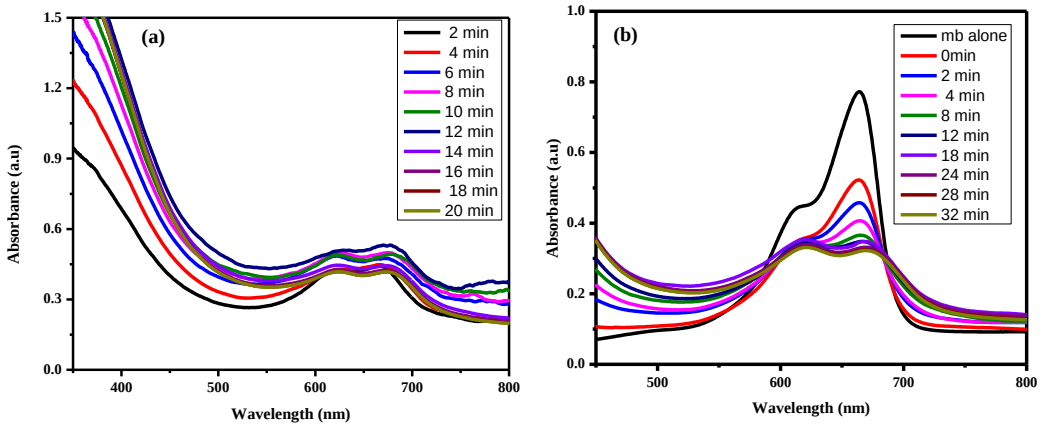

Figure 4.31: Degradation of MB Using (a) CuO NPs and (b) ZnO NPs at Optimal Conditions

As shown in Figure 4.31 (a) the absorption intensity was observed to reduce when the degradation was performed when the parameters were at their optimal conditions under CuO NPs degradation. However, it was observed that as the degradation proceeded with time, the absorption intensity increased and then reduced as reaction time was at 20 minutes. For ZnO NPs there was a significant decrease in the absorption intensity of MB dye within 32 minutes at the optimal conditions described in this study (Figure 4.31 (b)). After the degradation, the degradation efficiency was calculated to be 54.74% and 59.69% for CuO NPs and ZnO NPs respectively. These observations revealed the formation of degradation products probably with high absorption intensity occur before the products were degraded further to formation of products with lower absorption intensity (Kgatle *et al*., 2021; Riapanitra *et al.*, 2022).

4.3.2.8 Functional Group Analysis of CuO NPs and ZnO NPs after Degradation Studies

After the degradation study of MB with CuO NPs and ZnO NPs was performed, the IR spectra of green CuO NPs and ZnO NPs were recorded using FTIR spectrophotometer and compared with the spectra before degradation. The results are illustrated in Figure 4.32 below.

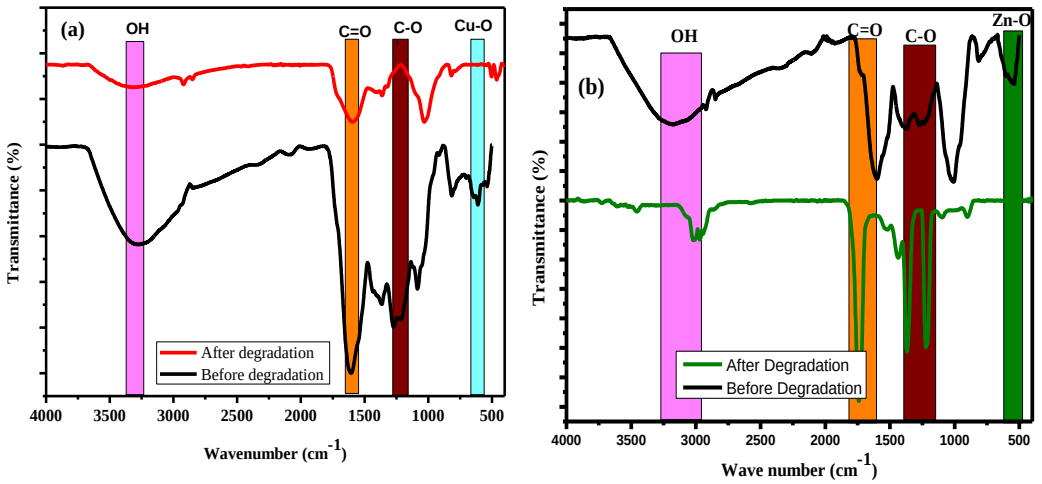

Figure 4.32: IR Spectra of (a) CuO NPs and (b) ZnO NPs before and after MB Degradation

From the FTIR spectra (Figure 4.32), it was observed that there were slight changes in wavenumbers of the functional groups in the IR spectra before degradation and after degradation. The IR spectra show CuO NPs (Figure 4.32 (a)) had peaks at 3284, 1600, 1368, 1278, 1084, 820, 522, and 590 cm^{-1} before degradation. The wavenumber shifted to 3293, 1590, 1365, 1010, 803, 474, and 457 cm^{-1} after the degradation of MB dye by the CuO NPs. The intensity of the peaks of CuO NPs decreased after the degradation of MB dye. Similarly, the frequencies of functional groups in the IR spectrum of green ZnO NPs (Figure 4.32 (b)) before degradation were observed at 3173 cm^{-1}, 2923 cm^{-1}, 1591 cm^{-1}, 1375 cm^{-1}, 1259 cm^{-1}, 1001 cm^{-1}, 809 cm^{-1}, and 543 cm^{-1}. The peak at 3173 cm^{-1} was attributed to the O-H group of phenols, 2923 cm^{-1} due to the C-H band, while the bands at 1375 cm^{-1} and 1259 cm^{-1} were characteristic of C-N. The peak at 1001 cm^{-1} and 809 cm^{-1} was attributed to C=C bending vibration. The peak at 543 cm^{-1} was characteristic of Zn-O stretching vibration (Alamdari *et al*., 2020; Choudhary *et al*., 2023). The shifts in the IR spectrum of ZnO NPs after degradation studies with MB dye were observed at 3023 cm^{-1}, 2958 cm^{-1}, 1734 cm^{-1}, 1447 cm^{-1}, 1364 cm^{-1}, 1215 cm^{-1}, 1095 cm^{-1}, 891 cm^{-1}, and 521 cm^{-1}. The peaks at 3023 cm^{-1} were due to O-H of phenols, the band at 2958 cm^{-1} due to C-H band, 1734 cm^{-1} attributable to C=O, 1445 cm^{-1} band attributable to C-H bending,

the bands at 1364 cm^{-1} and 1215 cm^{-1}attributable to C-N stretching band. The peaks at 1095 cm^{-1} and 891 cm^{-1} are due to C-O and C=C bending bands, respectively. The characteristic peak at 521 cm^{-1} is associated with Zn-O vibration bands. These changes in the functional groups' position and intensity indicated the interaction between the nanoparticles and the MB dye during the degradation process (Ainane *et al*., 2014; Massoudinejad *et al*., 2019).

4.3.2.9 Reusability Potential of CuO NPs and ZnO NPs

The reusability potential of the nanoparticles was studied in four cycles. In each cycle, the degradation conditions were maintained at 20 mg green CuO NPs and ZnO NPs, 5 mg/L MB dye solution, 1 mL H_2O_2, and a reaction time of 2.5 hours per cycle. The degradation percentage of MB after each cycle was calculated and the results are represented in Figure 4.33 below.

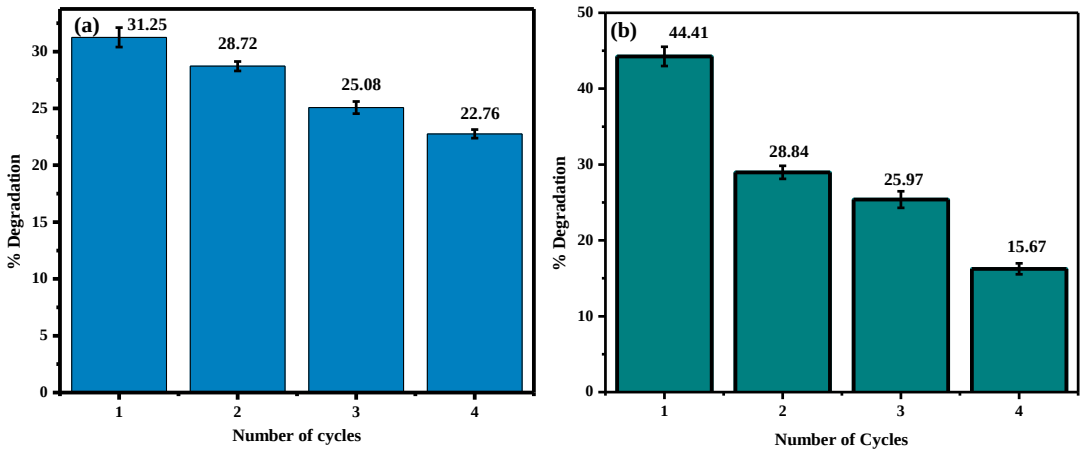

Figure 4.33: Reuse Ability of (a) CuO NPs and (b) ZnO NPs in Degradation of MB Dye

From Figure 4.33 it was noticeable that the percentage of degradation decreased as the number of cycles increased from one to four. In the first cycle, the degradation percentage of MB dye was 31.23% and decreased to 22.76% after the fourth cycle using CuO NPs (Figure 4.33 (a)). For ZnO NPs the degradation percentage declined from 44.41% to 15.67 for the same cycle numbers (Figure 4.33 (b)). The decrease in degradation efficiency of

the green CuO NPs and ZnO NPs with the number of cycles can be attributed to the loss of catalytic properties of the nanoparticles, which occurs during the decantation and drying processes (Ainane *et al*., 2014; Chowdhury *et al*., 2020).

CHAPTER FIVE

CONCLUSION AND RECOMMENDATIONS

5.1 Conclusion

In this study, copper oxide and zinc oxide nanoparticles were synthesized from aqueous extract of *P. hysterophorus.* The synthesized CuO NPs and ZnO NPs were then used in the degradation of rifampicin antibiotic and methylene blue dye at different degradation conditions. The following conclusions can be drawn from the study;

i. Aqueous extract of *P. hysterophorus* whole plant contain secondary metabolites (flavonoids, tannins, alkaloids, saponins, and terpenoids), which act as reducing, stabilizing, and capping agents. These electron-rich metabolites were able to form green ZnO NPs and CuO NPs from their respective metal salts.
ii. The formation of green ZnO NPs and CuO NPs was confirmed by various characterization techniques, including; UV-Vis spectroscopy, FTIR, SEM, TEM, XRD, and DLS. The UV-Vis spectroscopy showed the SPR band associated with ZnO NPs and CuO NPs occurred at 340 and 337 nm respectively. The FTIR spectrophotometer showed bonding of zinc and copper ions with secondary metabolites while SEM and TEM techniques revealed the nearly spherical morphology of these nanoparticles. These characterization techniques showed that the formed ZnO NPs and CuO NPs were in the nanometer scale range.
iii. The green ZnO NPs and CuO NPs degraded the rifampicin antibiotic and MB dye. The degradation percentage depended on parameters such as the amount of the nanoparticles, the concentration of MB or rifampicin, pH, reaction time, and temperature. The highest degradation percentage of rifampicin was achieved using 50 mg of green CuO NPs (>99%) while for MB dye percentage degradation (>58%) was achieved using 10 mg of green ZnO NPs within 360 minutes.

iv. The degradation percentage of rifampicin antibiotic and MB dye was enhanced when the parameters tested in (iii) above were combined with highest degradation percentage occurring within short time (minutes).

v. The green ZnO NPs and CuO NPs showed potential for reuse in the degradation of rifampicin and MB dye in multiple cycles. This indicated that CuO NPs and ZnO NPs showed stability for multiple uses.

5.2 Recommendations

i. There is a need to establish actual phytochemicals involved in the synthesis process, since the synthesis is from a mixture of secondary metabolites.

ii. Future studies could be done to identify the actual degradation products from the degradation of rifampicin and methylene blue dye using green copper oxide and zinc oxide nanoparticles by employing LC-MS/MS.

iii. Studies should be done to explore the probable toxicity and ecotoxicity of degradation products from the degradation processes of rifampicin and methylene blue dye using green zinc oxide and copper oxide nanoparticles.

iv. Studies should be conducted to explore the possibility of using green zinc oxide and copper oxide nanoparticles to remove other water contaminants, such as pathogens, heavy metals, and pesticides.

v. An investigation on the encapsulation of zinc oxide and copper oxide nanoparticles with polymeric adsorbents and their effect on the degradation efficiency of pollutants should be explored in future studies.

REFERENCES

Abdullah, Rahman, A. ur, Faisal, S., Almostafa, M. M., Younis, N. S., & Yahya, G. (2023). Multifunctional Spirogyra-hyalina-mediated barium oxide nanoparticles (BaONPs): *Synthesis and applications. Molecules, 28*(17). https://doi.org/10.3390/molecules28176364

Ahmadi, S., & Adaobi Igwegbe, C. (2021). Kinetic studies on penicillin g removal from aqueous environments by cupric oxide nanoparticles. *Archives of Hygiene Sciences, 10*(1), 86–96. https://doi.org/10.52547/archhygsci.10.1.86

Ahsan, A., Farooq, M. A., Bajwa, A. A., & Parveen, A. (2020). Green synthesis of silver nanoparticles using Parthenium hysterophorus: Optimization, characterization and in vitro therapeutic evaluation. *Molecules, 25*(15), 3324. https://doi.org/10.3390/molecules25153324

Ainane, T., Khammour, F., Talbi, M., & Elkouali, M. (2014). A novel bio-adsorbent of mint waste for dyes remediation in aqueous environments: Study and modeling of isotherms for removal of methylene blue. *Oriental Journal of Chemistry, 30*(3), 1183–1189. https://doi.org/10.13005/ojc/300332

Ajala, O. A., Akinnawo, S. O., Bamisaye, A., Adedipe, D. T., Adesina, M. O., Okon-Akan, O. A., Adebusuyi, T. A., Ojedokun, A. T., Adegoke, K. A., & Bello, O. S. (2023). Adsorptive removal of antibiotic pollutants from wastewater using biomass/biochar-based adsorbents. *RSC Advances, 13*(7), 4678–4712. https://doi.org/10.1039/d2ra06436g

Akintelu, S. A., Folorunso, A. S., Folorunso, F. A., & Oyebamiji, A. K. (2020). Green synthesis of copper oxide nanoparticles for biomedical application and environmental remediation. *Heliyon, 6*(7). https://doi.org/10.1016/j.heliyon.2020.e04508

Aksu Demirezen, D., Yıldız, Y. Ş., & Demirezen Yılmaz, D. (2019). Amoxicillin degradation using green synthesized iron oxide nanoparticles: Kinetics and mechanism analysis. Environmental Nanotechnology, *Monitoring and Management, 11,* 100219. https://doi.org/10.1016/j.enmm.2019.100219

Alamdari, S., Ghamsari, M. S., Lee, C., Han, W., Park, H., Tafreshi, M. J., & Afarideh, H. (2020). Preparation and characterization of zinc oxide nanoparticles using leaf extract of Sambucus ebulus Sanaz. *Applied Sciences, 10*(3620), 1–19. doi:10.3390/app10103620

Alhalili, Z. (2022). Green synthesis of copper oxide nanoparticles CuO NPs from Eucalyptus Globoulus leaf extract: Adsorption and design of experiments. *Arabian Journal of Chemistry, 15*(5), 103739. https://doi.org/10.1016/j.arabjc.2022.103739

Alkaykh, S., Mbarek, A., & Ali-Shattle, E. E. (2020). Photocatalytic degradation of methylene blue dye in aqueous solution by MnTiO3 nanoparticles under sunlight irradiation. *Heliyon, 6*(4), e03663. https://doi.org/10.1016/j.heliyon.2020.e03663

Almatroudi, A. (2020). Silver nanoparticles: Synthesis, characterisation and biomedical applications. *Open Life Sciences, 15*(1), 819–839. https://doi.org/10.1515/biol-2020-0094

Altikatoglu, M., Attar, A., Erci, F., Cristache, C. M., & Isildak, I. (2017). Green synthesis of copper oxide nanoparticles using Ocimum basilicum extract and their antibacterial activity. *Fresenius Environmental Bulletin, 25*(12), 7832–7837.

Amin, F., Fozia, Khattak, B., Alotaibi, A., Qasim, M., Ahmad, I., Ullah, R., Bourhia, M., Gul, A., Zahoor, S., & Ahmad, R. (2021). Green synthesis of copper oxide nanoparticles using Aerva javanica leaf extract and their characterization and investigation of in vitro antimicrobial potential and cytotoxic activities. *Evidence-Based Complementary and Alternative Medicine, 2021*(Mic). https://doi.org/ 10.1155/2021/5589703

Amjad, R., Mubeen, B., Ali, S. S., Imam, S. S., Alshehri, S., Ghoneim, M. M., Alzarea, S. I., Rasool, R., Ullah, I., Nadeem, M. S., & Kazmi, I. (2021). Green synthesis and characterization of copper nanoparticles using Fortunella margarita leaves. *Polymers*, *13*(24), 1–12. https://doi.org/10.3390/polym13244364

Anastopoulos, I., Hosseini-Bandegharaei, A., Fu, J., Mitropoulos, A. C., & Kyzas, G. Z. (2017). Use of nanoparticles for dye adsorption: Review. *Journal of Dispersion Science and Technology*, *39*(6), 836–847. https://doi.org/10.1080/01932691.2017.1398661

Andualem, W. W., Sabir, F. K., Mohammed, E. T., Belay, H. H., & Gonfa, B. A. (2020). Synthesis of copper oxide nanoparticles using plant leaf extract of Catha edulis and its antibacterial activity. *Journal of Nanotechnology, 2020.* https://doi.org/10.1155/2020/2932434

Anjum, M., Miandad, R., Waqas, M., Gehany, F., & Barakat, M. A. (2019). Remediation of wastewater using various nano-materials. *Arabian Journal of Chemistry*, *12*(8), 4897–4919. https://doi.org/10.1016/j.arabjc.2016.10.004

Ardila-Leal, L. D., Poutou-Piñales, R. A., Pedroza-Rodríguez, A. M., Quevedo-Hidalgo, B. E., Capela, I., Kamali, M., & Zuorro, A. (2021). A brief history of colour, the environmental impact of synthetic dyes and removal by using laccases. M*olecules*, *26*(13), 3813. https://doi.org/10.3390/molecules26133813

Asamoah, R. B., Yaya, A., Mensah, B., Nbalayim, P., Apalangya, V., Bensah, Y. D., Damoah, L. N. W., Agyei-Tuffour, B., Dodoo-Arhin, D., & Annan, E. (2020). Synthesis and characterization of zinc and copper oxide nanoparticles and their antibacteria activity. *Results in Materials*, *7*(April), 100099. https://doi.org/10.1016/j.rinma.2020.100099

Ashwini, J., Aswathy, T. R., Rahul, A. B., Thara, G. M., & Nair, A. S. (2021). Synthesis and characterization of zinc oxide nanoparticles using Acacia caesia bark extract and

its photocatalytic and antimicrobial activities. Catalysts, 11(12), 1507. https://doi.org/10.3390/catal11121507

Bai, X., Chen, W., Wang, B., Sun, T., Wu, B., & Wang, Y. (2022). Photocatalytic degradation of some typical antibiotics: Recent advances and future outlooks. *International Journal of Molecular Sciences, 23*(15). https://doi.org/10.3390/ijms23158130

Bao, Y., He, J., Song, K., Guo, J., Zhou, X., & Liu, S. (2021). Plant-extract-mediated synthesis of metal nanoparticles. *Journal of Chemistry*, *2021*. https://doi.org/10.1155/2021/6562687

Bashar, H. M. K., Juraimi, A. S., Ahmad-hamdani, M. S., Uddin, K., Asib, N., Anwar, P., Rahaman, F., Karim, S. M. R., Haque, M. A., Berahim, Z., Amelia, N., Mustapha, N., & Hossain, A. (2022). Leaf extract of Parthenium hysterophorus L . and their weed species. *Plants*, *11*(3209).

Basnet, P., Samanta, D., Inakhunbi Chanu, T., Mukherjee, J., & Chatterjee, S. (2019). Assessment of synthesis approaches for tuning the photocatalytic property of ZnO nanoparticles. *SN Applied Sciences*, *6*(1), 1–13. https://doi.org/10.1007/S42452-019-0642-x

Bayda, S., Adeel, M., Tuccinardi, T., Cordani, M., & Rizzolio, F. (2020). The history of nanoscience and nanotechnology: From chemical-physical applications to nanomedicine. *Molecules*, *25*(1), 1–15. https://doi.org/10.3390/molecules25010112

Berradi, M., Hsissou, R., Khudhair, M., Assouag, M., Cherkaoui, O., El Bachiri, A., & El Harfi, A. (2019). Textile finishing dyes and their impact on aquatic environs. *Heliyon, 5*(11), e02711. https://doi.org/10.1016/j.heliyon.2019.e02711

Bezuneh, T. T. (2015). Phytochemistry and antimicrobial activity of Parthenium hysterophorus L.: A Review. *Science Journal of Analytical Chemistry, 3*(3), 30.

https://doi.org/10.11648/j.sjac.20150303.11

Bhatia, D., Sharma, N. R., Kanwar, R., & Singh, J. (2018). Physicochemical assessment of industrial textile effluents of Punjab (India). *Applied Water Science, 8*(3), 1–12. https://doi.org/10.1007/S13201-018-0728-4

Bhatnagar, S., Kobori, T., Ganesh, D., Ogawa, K., & Aoyagi, H. (2019). Biosynthesis of silver nanoparticles mediated by extracellular pigment from talaromyces purpurogenus and their biomedical applications. *Nanomaterials, 9*(7), 1–27. https://doi.org/10.3390/nano9071042

Bhatti, H. N., Iram, Z., Iqbal, M., Nisar, J., & Khan, M. I. (2020). Facile synthesis of zero valent iron and photocatalytic application for the degradation of dyes. *Materials Research Express, 7*(1). https://doi.org/10.1088/2053-1591/ab66a0

Cai, W., Weng, X., & Chen, Z. (2019). Highly efficient removal of antibiotic rifampicin from aqueous solution using green synthesis of recyclable nano-Fe3O4. *Environmental Pollution, 247*, 839–846. https://doi.org/10.1016/j.envpol.2019.01.108

Carvalho, I. T., & Santos, L. (2016). Antibiotics in the aquatic environments: A review of the European scenario. *Environment International, 94*, 736–757.https://doi.org/10.1016/j.envint.2016.06.025

Carvalho, P. M., Felício, M. R., Santos, N. C., Gonçalves, S., & Domingues, M. M. (2018). Application of light scattering techniques to nanoparticle characterization and development. *Frontiers in Chemistry, 6*(June), 1–17. https://doi.org/10.3389/fchem.2018.00237

Chand Mali, S., Raj, S., & Trivedi, R. (2019). Biosynthesis of copper oxide nanoparticles using Enicostemma axillare (Lam.) leaf extract. *Biochemistry and Biophysics Reports, 20*(November), 100699. https://doi.org/10.1016/j.bbrep.2019.100699

Chaudhary, A., Kumar, N., Kumar, R., & Salar, R. K. (2019). Antimicrobial activity of zinc oxide nanoparticles synthesized from Aloe vera peel extract. *SN Applied Sciences, 1*(1). https://doi.org/10.1007/s42452-018-0144-2

Choudhary, N., Yadav, V. K., Ali, H., Ali, D., Almutairi, B. O., Cavalu, S., & Patel, A. (2023). Remediation of methylene blue dye from wastewater by using zinc oxide nanoparticles loaded on nanoclay. *Water, 15*(7), 1427. https://doi.org/10.3390/w15071427

Chowdhury, R., Khan, A., & Rashid, M. H. (2020). Green synthesis of CuO nanoparticles using: Lantana camara flower extract and their potential catalytic activity towards the aza-Michael reaction. *RSC Advances, 10*(24), 14374–14385. https://doi.org/10.1039/d0ra01479f

Crisan, M. C., Teodora, M., & Lucian, M. (2022). Copper Nanoparticles : Synthesis and characterization, physiology, toxicity and antimicrobial applications. *Applied Sciences, 12*(1), 141. https://doi.org/10.3390/app12010141

Criveanu, A., Dumitrache, F., Fleaca, C., Gavrila-Florescu, L., Lungu, I., Morjan, I. P., Socoliuc, V., & Prodan, G. (2023). Chitosan-coated iron oxide nanoparticles obtained by laser pyrolysis. *Applied Surface Science Advances, 15*(January), 100405. https://doi.org/10.1016/j.apsadv.2023.100405

Danish, M. S. S., Estrella, L. L., Alemaida, I. M. A., Lisin, A., Moiseev, N., Ahmadi, M., Nazari, M., Wali, M., Zaheb, H., & Senjyu, T. (2021). Photocatalytic applications of metal oxides for sustainable environmental eemediation. *Metals, 11*(1), 80. https://doi.org/10.3390/met11010080

Datta, A., Patra, C., Bharadwaj, H., Kaur, S., Dimri, N., & Khajuria, R. (2017). Green synthesis of zinc oxide nanoparticles using Parthenium hysterophorus leaf extract and evaluation of their antibacterial properties. *Journal of Biotechnology & Biomaterials, 07*(03). https://doi.org/10.4172/2155-952x.1000271

De Ilurdoz, M. S., Sadhwani, J. J., & Reboso, J. V. (2022). Antibiotic removal processes from water & wastewater for the protection of the aquatic environment - a review. *Journal of Water Process Engineering, 45*, 102474. https://doi.org/10.1016/j.jwpe.2021.102474

Derakhshan, Z., Mokhtari, M., Babaei, F., Ahmadi, R. M., Ehrampoush, M. H., & Faramarzian, M. (2016). Removal methods of antibiotic compounds from aqueous environments- A Review. *Journal of Environmental Health and Sustainable Development, 1*(1), 43–62.

Dhand, C., Dwivedi, N., Loh, X. J., Jie Ying, A. N., Verma, N. K., Beuerman, R. W., Lakshminarayanan, R., & Ramakrishna, S. (2015). Methods and strategies for the synthesis of diverse nanoparticles and their applications: A comprehensive overview. *RSC Advances, 5*(127), 105003–105037. https://doi.org/10.1039/c5ra19388e

El-Ramady, H., Abdalla, N., Sári, D., Ferroudj, A., Muthu, A., Prokisch, J., Fawzy, Z. F., Brevik, E. C., & Solberg, S. Ø. (2023). Nanofarming: Promising solutions for the future of the global agricultural industry. *Agronomy, 13*(6), 1600. https://doi.org/10.3390/agronomy13061600

El-Sayed, G., Jahin, H., Ibrahim, S., El-Sayed, G. O., Dessouki, H. A., Jahin, H. S., & Ibrahiem, S. S. (2014). Photocatalytic degradation of metronidazole in aqueous solutions by copper oxide nanoparticles. *Journal of Basic and Environmental Sciences, 1*(October 2020), 102–110. http://dx.doi.org/10.21608/jbes.2014.369577

Eniola, J. O., Kumar, R., & Barakat, M. A. (2019). Adsorptive removal of antibiotics from water over natural and modified adsorbents. *Environmental Science and Pollution Research, 26*(34), 34775–34788. https://doi.org/10.1007/S11356-019-06641-6

Fagier, M. A. (2021). Plant-mediated biosynthesis and photocatalysis activities of zinc oxide nanoparticles: A prospect towards dyes mineralization. *Journal of Nanotechnology, 2021*(1), 6629180. https://doi.org/10.1155/2021/6629180

Faisal, S., Al-Radadi, N. S., Jan, H., Abdullah, Shah, S. A., Shah, S., Rizwan, M., Afsheen, Z., Hussain, Z., Uddin, M. N., Idrees, M., & Bibi, N. (2021). Curcuma longa mediated synthesis of copper oxide, nickel oxide and Cu-Ni bimetallic hybrid nanoparticles: Characterization and evaluation for antimicrobial, anti-parasitic and cytotoxic potentials. *Coatings, 11*(7), 1–22. https://doi.org/10.3390/coatings 11070849

Faisal, S., Jan, H., Abdullah, Alam, I., Rizwan, M., Hussain, Z., Sultana, K., Ali, Z., & Uddin, M. N. (2022). In vivo analgesic, anti-inflammatory, and anti-diabetic screening of Bacopa monnieri-synthesized copper oxide nanoparticles. *ACS Omega, 7*(5), 4071–4082. https://doi.org/10.1021/acsomega.1c05410

Faisal, S., Jan, H., Shah, S. A., Shah, S., Khan, A., Akbar, M. T., Rizwan, M., Jan, F., Wajidullah, Akhtar, N., Khattak, A., & Syed, S. (2021). Green synthesis of zinc oxide (ZnO) nanoparticles using aqueous fruit extracts of Myristica fragrans: Their characterizations, biological and environmental applications. *ACS Omega, 6*(14), 9709–9722. https://doi.org/10.1021/acsomega.1c00310

Faisal, S., Ullah, R., Alotaibi, A., Zafar, S., Rizwan, M., & Tariq, M. H. (2023). Biofabrication of silver nanoparticles employing biomolecules of Paraclostridium benzoelyticum strain: Its characterization and their in-vitro antibacterial, anti-aging, anti-cancer and other biomedical applications. *Microscopy Research and Technique, 86(*7), 846–861. https://doi.org/10.1002/jemt.24362

Fayiga, A. O., Ipinmoroti, M. O., & Chirenje, T. (2018). Environmental pollution in Africa. Environment, *Development and Sustainability, 20*(1), 41–73. https://doi.org/ 10.1007/s10668-016-9894-4

Gebre, S. H., & Sendeku, M. G. (2019). New frontiers in the biosynthesis of metal oxide nanoparticles and their environmental applications: an overview. *SN Applied Sciences, 1*(8). https://doi.org/10.1007/s42452-019-0931-4

Goyal, N., Rastogi, D., Jassal, M., & Agrawal, A. K. (2022). Kinetic studies of photocatalytic degradation of an Azo dye by titania nanoparticles. *Research Journal of Textile and Apparel, 26*(4), 500–514. https://doi.org/10.1108/rjta-03-2021-0033

Gudikandula, K., & Charya Maringanti, S. (2016). Synthesis of silver nanoparticles by chemical and biological methods and their antimicrobial properties. *Journal of Experimental Science, 11*(9), 714–721. https://doi.org/10.1080/17458080.2016.1139196

Hamad, M. T. M. H., & El-Sesy, M. E. (2023). Adsorptive removal of levofloxacin and antibiotic resistance genes from hospital wastewater by nano-zero-valent iron and nano-copper using kinetic studies and response surface methodology. *Bioresources and Bioprocessing, 10*(1), 1–29. https://doi.org/10.1186/s40643-022-00616-1

Hameed, H., Waheed, A., Sharif, M. S., Saleem, M., Afreen, A., Tariq, M., Kamal, A., Al-onazi, W. A., Al Farraj, D. A., Ahmad, S., & Mahmoud, R. M. (2023). Green synthesis of zinc oxide (ZnO) nanoparticles from green algae and their assessment in various biological applications. *Micromachines, 14*(5). https://doi.org/10.3390/mi14050928

Hanna, N., Tamhankar, A. J., & Stålsby Lundborg, C. (2023). Antibiotic concentrations and antibiotic resistance in aquatic environments of the WHO Western Pacific and South-East Asia regions: a systematic review and probabilistic environmental hazard assessment. *The Lancet Planetary Health, 7*(1), e45–e54. https://doi.org/10.1016/S2542-5196(22)00254-6

Ho, Y. C., Chua, S. C., & Chong, F. K. (2019). *Coagulation-flocculation technology in water and wastewater treatment. Handbook of Research on Resource Management for Pollution and Waste Treatment*, pp. 432–457. https://doi.org/10.4018/978-1-7998-0369-0.ch018

Hu, E., Shang, S., Chiu, K.-L., Novillo, F. J. B., & Álvarez, P. M. (2019). Removal of

reactive dyes in textile effluents by catalytic ozonation pursuing on-site effluent recycling. *Molecules, 24*(15), 2755. https://doi.org/10.3390/molecules24152755

Huang, A., Yan, M., Lin, J., Xu, L., Gong, H., & Gong, H. (2021). A Review of processes for removing antibiotics from breeding wastewater. *International Journal of Environmental Research and Public Health, 18*(9). https://doi.org/10.3390/ijerph18094909

Huang, S., Yu, J., Li, C., Zhu, Q., Zhang, Y., Lichtfouse, E., & Marmier, N. (2022). The effect review of various biological, physical and chemical methods on the removal of antibiotics. *Water* (Switzerland), *14*(19), 1–27. https://doi.org/10.3390/w14193138

Ijaz, F., Shahid, S., Khan, S. A., Ahmad, W., & Zaman, S. (2017). Green synthesis of copper oxide nanoparticles using Abutilon indicum leaf extract: Antimicrobial, antioxidant and photocatalytic dye degradation activitie. *Tropical Journal of Pharmaceutical Research, 16*(4), 743–753. https://doi.org/10.4314/tjpr.v16i4.2

Ijaz, I., Gilani, E., Nazir, A., & Bukhari, A. (2020). Detail review on chemical, physical and green synthesis, classification, characterizations and applications of nanoparticles. *Green Chemistry Letters and Reviews, 13*(3), 59–81. https://doi.org/10.1080/17518253.2020.1802517

Iqbal, J., Abbasi, B. A., Yaseen, T., Zahra, S. A., Shahbaz, A., Shah, S. A., Uddin, S., Ma, X., Raouf, B., Kanwal, S., Amin, W., Mahmood, T., El-Serehy, H. A., & Ahmad, P. (2021). Green synthesis of zinc oxide nanoparticles using Elaeagnus angustifolia L. leaf extracts and their multiple in vitro biological applications. *Scientific Reports, 11*(1), 1–13. https://doi.org/10.1038/s41598-021-99839-z

Iravani, S., Korbekandi, H., Mirmohammadi, S. V., & Zolfaghari, B. (2014). Synthesis of silver nanoparticles: chemical, physical and biological methods. *Research in Pharmaceutical Sciences, 9*(6), 385.

Ismail, M., Akhtar, K., Khan, M. I., Kamal, T., Khan, M. A., M. Asiri, A., Seo, J., & Khan, S. B. (2019). Pollution, toxicity and carcinogenicity of organic dyes and their catalytic bio-remediation. *Current Pharmaceutical Design, 25*(34), 3645–3663. https://doi.org/10.2174/1381612825666191021142026

Jadoun, S., Arif, R., Jangid, N. K., & Meena, R. K. (2020). Green synthesis of nanoparticles using plant extracts: a review. *Environmental Chemistry Letters, 19*(1), 355–374. https://doi.org/10.1007/S10311-020-01074-x

Jain, D., Shivani, Bhojiya, A. A., Singh, H., Daima, H. K., Singh, M., Mohanty, S. R., Stephen, B. J., & Singh, A. (2020). Microbial fabrication of zinc oxide nanoparticles and evaluation of their antimicrobial and photocatalytic properties. *Frontiers in Chemistry, 8*(September), 1–11. https://doi.org/10.3389/fchem.2020.00778

Jan, H., Shah, M., Andleeb, A., Faisal, S., Khattak, A., Rizwan, M., Drouet, S., Hano, C., & Abbasi, B. H. (2021). Plant-based synthesis of zinc oxide nanoparticles (ZnO-NPs) using aqueous leaf extract of Aquilegia pubiflora: Their antiproliferative activity against HepG2 cells inducing reactive oxygen species and other in vitro properties. *Oxidative Medicine and Cellular Longevity, 2021*. https://doi.org/10.1155/2021/4786227

Jayachandran, A., T.R., A., & Nair, A. S. (2021). Green synthesis and characterization of zinc oxide nanoparticles using Cayratia pedata leaf extract. *Biochemistry and Biophysics Reports, 26*(March), 100995. https://doi.org/10.1016/j.bbrep.2021.100995

Jiang, J., Pi, J., & Cai, J. (2018). The Advancing of Zinc Oxide Nanoparticles for Biomedical Applications. *Bioinorganic Chemistry and Applications, 2018*(1), 1062562. https://doi.org/10.1155/2018/1062562

Kairigo, P., Ngumba, E., Sundberg, L. R., Gachanja, A., & Tuhkanen, T. (2020). Occurrence of antibiotics and risk of antibiotic resistance evolution in selected

Kenyan wastewaters, surface waters and sediments. Science of the Total Environment, 720. https://doi.org/10.1016/j.scitotenv.2020.137580

Kamaz, M., Wickramasinghe, S. R., Eswaranandam, S., Zhang, W., Jones, S. M., Watts, M. J., & Qian, X. (2019). Investigation into micropollutant removal from wastewaters by a membrane bioreactor. *International Journal of Environmental Research and Public Health, 16*(8). https://doi.org/10.3390/ijerph16081363

Kansal, S. K., Kundu, P., Sood, S., Lamba, R., Umar, A., & Mehta, S. K. (2014). Photocatalytic degradation of the antibiotic levofloxacin using highly crystalline TiO2 nanoparticles. *New Journal of Chemistry, 38*(7), 3220–3226. https://doi.org/ 10.1039/c3nj01619f

Kapanga, P. M., Nyakairu, G. W. A., Nkanga, C. I., Lusamba, S. N., Tshimanga, R. M., & Shehu, Z. (2024). A review of dye effluents polluting African surface water: sources, impacts, physicochemical properties, and treatment methods. *Discover Water*, *4*(1). https://doi.org/10.1007/s43832-024-00129-2

Katheresan, V., Kansedo, J., & Lau, S. Y. (2018). Efficiency of various recent wastewater dye removal methods: A review. *Journal of Environmental Chemical Engineering, 6*(4), 4676–4697. https://doi.org/10.1016/j.jece.2018.06.060

Kaur, L., Malhi, D. S., Cooper, R., Kaur, M., Sohal, H. S., Mutreja, V., & Sharma, A. (2021). Comprehensive review on ethnobotanical uses, phytochemistry, biological potential and toxicology of Parthenium hysterophorus L.: A journey from noxious weed to a therapeutic medicinal plant. *Journal of Ethnopharmacology*, *281*, 114525. https://doi.org/10.1016/j.jep.2021.114525

Kaushal, S., Kumar, A., Bains, H., & Singh, P. P. (2023). Photocatalytic degradation of tetracycline antibiotic and organic dyes using biogenic synthesized CuO/Fe2O3 nanocomposite: pathways and mechanism insights. *Environmental Science and Pollution Research, 30*(13), 37092–37104. https://doi.org/10.1007/s11356-022-

24848-y

Keat, C. L., Aziz, A., Eid, A. M., & Elmarzugi, N. A. (2015). Biosynthesis of nanoparticles and silver nanoparticles. *Bioresources and Bioprocessing, 2*(1), 1–11. https://doi.org/10.1186/s40643-015-0076-2

Kgatle, M., Sikhwivhilu, K., Ndlovu, G., & Moloto, N. (2021). Degradation kinetics of methyl orange dye in water using trimetallic Fe/Cu/Ag nanoparticles. *Catalysts, 11*, 428. https://doi.org/10.3390/catal11040428

Khan, I., Khan, I., Usman, M., Imran, M., & Saeed, K. (2020). Nanoclay-mediated photocatalytic activity enhancement of copper oxide nanoparticles for enhanced methyl orange photodegradation. *Journal of Materials Science: Materials in Electronics, 31*(11), 8971–8985. https://doi.org/10.1007/S10854-020-03431-6

Khan, M. I., Shah, S., Faisal, S., Gul, S., Khan, S., Abdullah, Shah, S. A., & Shah, W. A. (2022). Monotheca buxifolia driven synthesis of zinc oxide nano material its characterization and biomedical applications. *Micromachines, 13*(5), 1–16. https://doi.org/10.3390/mi13050668

Khan, M., Ware, P., & Shimpi, N. (2021). Synthesis of ZnO nanoparticles using peels of Passiflora foetida and study of its activity as an efficient catalyst for the degradation of hazardous organic dye. *SN Applied Sciences, 3*(5), 1–17. https://doi.org/10.1007/s42452-021-04436-4

Khashan, K. S., Sulaiman, G. M., & Abdulameer, F. A. (2015). Synthesis and antibacterial activity of CuO nanoparticles suspension induced by laser ablation in liquid. *Arabian Journal for Science and Engineering*, *41*(1), 301–310. https://doi.org/10.1007/S13369-015-1733-7

Khoshnamvand, N., Kord Mostafapour, F., Mohammadi, A., & Faraji, M. (2018). Response surface methodology (RSM) modeling to improve removal of

ciprofloxacin from aqueous solutions in photocatalytic process using copper oxide nanoparticles (CuO/ UV). *Amb Express, 8*, 1-9. https://doi.org/10.1186/s13568-018-0579-2

Kokkinos, P., Mantzavinos, D., & Venieri, D. (2020). Current trends in the application of nanomaterials for the removal of emerging micropollutants and pathogens from water. *Molecules, 25*(9). https://doi.org/10.3390/molecules25092016

Kolahalam, L. A., Prasad, K. R. S., Krishna, P. M., Supraja, N., & Shanmugan, S. (2022). The exploration of bio-inspired copper oxide nanoparticles: synthesis, characterization and in-vitro biological investigations. *Heliyon, 8(*6), e09726. https://doi.org/10.1016/j.heliyon.2022.e09726

Kulis-Kapuscinska, A., Kwoka, M., Borysiewicz, M. A., Wojciechowski, T., Licciardello, N., Sgarzi, M., & Cuniberti, G. (2023). Photocatalytic degradation of methylene blue at nanostructured ZnO thin films. *Nanotechnology, 34*(15). https://doi.org/10.1088/1361-6528/aca910

Kulkarni, P., Olson, N. D., Raspanti, G. A., Goldstein, R. E. R., Gibbs, S. G., Sapkota, A., & Sapkota, A. R. (2017). Antibiotic concentrations decrease during wastewater treatment but persist at low levels in reclaimed water. *International Journal of Environmental Research and Public Health, 14*(6), 1–13. https://doi.org/10.3390/ijerph14060668

Kumar, A. (2017). A Review on the factors affecting the photocatalytic degradation of hazardous materials. *Material Science & Engineering International Journal, 1*(3), 106–114. https://doi.org/10.15406/mseij.2017.01.00018

Kumari, P., Alam, M., & Siddiqi, W. A. (2019). Usage of nanoparticles as adsorbents for waste water treatment: An emerging trend. *Sustainable Materials and Technologies, 22.* https://doi.org/10.1016/j.susmat.2019.e00128

Kutuzova, A., Dontsova, T., & Kwapinski, W. (2021). Application of TiO2-based photocatalysts to antibiotics degradation: Cases of sulfamethoxazole, trimethoprim and ciprofloxacin. *Catalysts*, *11*(6). https://doi.org/10.3390/catal11060728

Lellis, B., Fávaro-Polonio, C. Z., Pamphile, J. A., & Polonio, J. C. (2019). Effects of textile dyes on health and the environment and bioremediation potential of living organisms. *Biotechnology Research and Innovation*, *3*(2), 275-290. https://doi.org/ 10.1016/j.biori.2019.09.001

Letchumanan, D., Sok, S. P. M., Ibrahim, S., Nagoor, N. H., & Arshad, N. M. (2021). Plant-based biosynthesis of copper/copper oxide nanoparticles: An update on their applications in biomedicine, mechanisms, and toxicity. *Biomolecules*, *11*(4). https://doi.org/10.3390/biom11040564

Lvshan Zhou, Xiaogang Guo, C. L. and W. W. (2018). Electro - photocatalytic degradation of amoxicillin using calcium titanate. *Open Chemistry*, *16*(1), 949–955. https://doi.org/10.1515/chem-2018-0108

Madivoli, E., Kareru, P., Gachanja, A., Mugo, S., Murigi, M., Kairigo, P., Kipyegon, C., Mutembei, J., & Njonge, F. (2016). Adsorption of selected heavy metals on modified nano cellulose. *International Research Journal of Pure and Applied Chemistry*, *12*(3), 1–9. https://doi.org/10.9734/irjpac/2016/28548

Madivoli, E. S., Kareru, P. G., & Fromm, K. (2022). Versatility of Cellulose Stimuli Responsive Membranes in the Detection of Dimethylamine. https://doi.org/10.5281 /zenodo.7392545

Madivoli, E. S., Kareru, P. G., Makhanu, D. S., Wandera, K. S., Maina, E. G., Wanakai, S. I., & Kimani, P. K. (2020). Synthesis of spherical titanium dioxide microspheres and its application to degrade rifampicin. *Environmental Nanotechnology, Monitoring and Management*, *14*, 100327. https://doi.org/10.1016/ j.enmm. 2020.100327

Magwira, C. A., Aneck-Hahn, N., & Taylor, M. B. (2019). Fate, occurrence and potential adverse effects of antimicrobials used for treatment of tuberculosis in the aquatic environment in South Africa. *Environmental Pollution, 254*, 112990. https://doi.org/10.1016/j.envpol.2019.112990

Malakootian, M., Nasiri, A., Majid, &, Gharaghani, A., & Gharaghani, M. A. (2020). Photocatalytic degradation of ciprofloxacin antibiotic by TiO2 nanoparticles immobilized on a glass plate. *Chemical Engineering Communications, 207*(1), 56–72. https://doi.org/10.1080/00986445.2019.1573168

Mali, S. C., Dhaka, A., Githala, C. K., & Trivedi, R. (2020). Green synthesis of copper nanoparticles using Celastrus paniculatus Willd. leaf extract and their photocatalytic and antifungal properties. *Biotechnology Reports, 27*, e00518. https://doi.org/10.1016/j.btre.2020.e00518

Manisalidis, I., Stavropoulou, E., Stavropoulos, A., & Bezirtzoglou, E. (2020). Environmental and health impacts of air pollution: A review. *Frontiers in Public Health, 8*, 14. https://doi.org/10.3389/fpubh.2020.00014/bibtex

Marimuthu, K., Kalaivani, M., Krishnakumari, G., & Ragina Banu, C. (2015). Phytoanalysis of Parthenium hysterophorus L root, stem. *Research Journal of Pharmacy and Technology, 8*(12), 1685–1690. https://doi.org/10.5958/0974-360X.2015.00304.2

Marimuthu, K., & Ravi, D. (2014). Phytochemical analysis of Parthenium hysterophorus L. leaf. *World J. Pharm. Res, 3*, 1066-1074.

Marslin, G., Siram, K., Maqbool, Q., Selvakesavan, R. K., Kruszka, D., Kachlicki, P., & Franklin, G. (2018). Secondary metabolites in the green synthesis of metallic nanoparticles. *Materials, 11*(6), 1–25. https://doi.org/10.3390/ma11060940

Maruthupandy, M., Zuo, Y., Chen, J.-S., Song, J.-M., Niu, H.-L., Mao, C.-J., Zhang, S.-

Y., Shen, Y.-H., Maruthupandy, M., Zuo, Y., Chen, J.-S., Song, J.-M., Niu, H.-L., Mao, C.-J., Zhang, S.-Y., & Shen, Y.-H. (2017). Synthesis of metal oxide nanoparticles (CuO and ZnO NPs) via biological template and their optical sensor applications. *Applied Surface Science, 397*, 167–174. https://doi.org/10.1016/j.apsusc.2016.11.118

Massoudinejad, M., Sadani, M., Gholami, Z., Rahmati, Z., Javaheri, M., Keramati, H., Sarafraz, M., Avazpour, M., & Shiri, S. (2019). Optimization and modeling of photocatalytic degradation of direct Blue 71 from contaminated water by TiO2 nanoparticles: Response surface methodology approach (RSM). *Iranian Journal of Catalysis, 9*(2), 121–132.

Mekewi, M. A., Darwish, A. S., Amin, M. S., Eshaq, G., & Bourazan, H. A. (2016). Copper nanoparticles supported onto montmorillonite clays as efficient catalyst for methylene blue dye degradation. *Egyptian Journal of Petroleum, 25*(2), 269–279. https://doi.org/10.1016/j.ejpe.2015.06.011

Menon, S., Agarwal, H., & Shanmugam, V. K. (2021). Catalytical degradation of industrial dyes using biosynthesized selenium nanoparticles and evaluating its antimicrobial activities. *Sustainable Environment Research, 31*(1), 1–12. https://doi.org/10.1186/s42834-020-00072-6

MOH. (2025). Kenya showcases breakthroughs in TB diagnosis and treatment at TICAD9 side event. Ministry of Health, Kenya. https://www.health.go.ke/kenya-showcases-breakthroughs-tb-diagnosis-and-treatment-ticad9-side-event

Mohan, S., Vellakkat, M., Aravind, A., & Reka, U. (2020). Hydrothermal synthesis and characterization of Zinc Oxide nanoparticles of various shapes under different reaction conditions. *Nano Express, 1*(3). https://doi.org/10.1088/2632-959x/abc813

Motmainna, M., Juraimi, A. S., Uddin, M. K., Asib, N. B., Islam, A. K. M. M., & Hasan, M. (2021). Bioherbicidal Properties of Parthenium hysterophorus, Cleome

rutidosperma and Borreria alata extracts on selected crop and weed species. *Agronomy*, *11*(4), 643. https://doi.org/10.3390/agronomy11040643

Mtetwa, H. N., Amoah, I. D., Kumari, S., Bux, F., & Reddy, P. (2024). Optimisation of analytical methods for tuberculosis drug detection in wastewater: A multinational study. *Heliyon*, *10*(10), e30720. https://doi.org/10.1016/j.heliyon.2024.e30720

Musza, K., Szabados, M., Ádám, A. A., Kónya, Z., Kukovecz, Á., Sipos, P., & Pálinkó, I. (2018). Ball milling of copper powder under dry and surfactant-assisted conditions—on the way towards Cu/Cu 2 O nanocatalyst . *Journal of Nanoscience and Nanotechnology*, *19*(1), 389–394. https://doi.org/10.1166/jnn.2019.15784

Muthukumar, H., Palanirajan, S. K., Shanmugam, M. K., Arivalagan, P., & Gummadi, S. N. (2022). Photocatalytic degradation of caffeine and E. coli inactivation using silver oxide nanoparticles obtained by a facile green co-reduction method. *Clean Technologies and Environmental Policy*, *24*(4), 1087–1098. https://doi.org/10.1007/s10098-021-02135-7

Nabilah Mohd Noor, N., Hazirah Kamaruzaman, N., Al-Gheethi, A., Maya Saphira Radin Mohamed, R., & Hossain, M. S. (2022). Degradation of antibiotics in aquaculture wastewater by bio-nanoparticles: A critical review. *Ain Shams Engineering Journal*, *14*(7), 101981. https://doi.org/10.1016/j.asej.2022.101981

Naddaf, M. (2023). The World Faces a Water Crisis, and 4 Powerful Charts Show How. https://www.scientificamerican.com/article/the-world-faces-a-water-crisis-and-4-powerful-charts-show-how/

Nam, S. W., Yoon, Y., Chae, S., Kang, J. H., & Zoh, K. D. (2017). Removal of selected micropollutants during conventional and advanced water treatment processes. *Environmental Engineering Science*, *34*(10), 752–761. https://doi.org/10.1089/ees.2016.0447

Narasaiah, P., Mandal, B. K., & Sarada, N. C. (2017). Biosynthesis of copper oxide nanoparticles from Drypetes sepiaria leaf extract and their catalytic activity to dye degradation. *IOP Conference Series: Materials Science and Engineering, 263*(2). https://doi.org/10.1088/1757-899x/263/2/022012

Naseer, M., Aslam, U., Khalid, B., & Chen, B. (2020). Green route to synthesize zinc oxide nanoparticles using leaf extracts of Cassia fistula and Melia azadarach and their antibacterial potential. *Scientific Reports, 10*(1), 1–10. https://doi.org/10.1038/s41598-020-65949-3

Nasrollahi, N., Vatanpour, V., & Khataee, A. (2022). Removal of antibiotics from wastewaters by membrane technology: Limitations, successes, and future improvements. *Science of The Total Environment, 838*, 156010. https://doi.org/10.1016/j.scitotenv.2022.156010

Nayeri, D., & Mousavi, S. A. (2020). Dye removal from water and wastewater by nanosized metal oxides - modified activated carbon: a review on recent researches. *Journal of Environmental Health Science and Engineering, 18*(2), 1671. https://doi.org/10.1007/s40201-020-00566-w

Ngumba, E., Gachanja, A., Nyirenda, J., Maldonado, J., & Tuhkanen, T. (2020). Occurrence of antibiotics and antiretroviral drugs in source-separated urine, groundwater, surface water and wastewater in the peri-urban area of Chunga in Lusaka, Zambia. *Water SA, 46*(2 April), 278–284. https://doi.org/10.17159/wsa/2020.v46.i2.8243

Ngumba, E., Gachanja, A., & Tuhkanen, T. (2016). Occurrence of selected antibiotics and antiretroviral drugs in Nairobi river basin, Kenya. *Science of the Total Environment, 539*, 206–213. https://doi.org/10.1016/j.scitotenv.2015.08.139

Ongaji. (2023). Climate Change to Take Centre Stage at Africa Health Agenda *International Conference (AHAIC)* in March 2023. March, 3–4.

https://ahaic.org/climate-change-to-take-centre-stage-at-africa-health-agenda-international-conference-ahaic-in-march-2023/

Pal, G., Rai, P., & Pandey, A. (2019). Green synthesis of nanoparticles: A greener approach for a cleaner future. *Green Synthesis, Characterization and Applications of Nanoparticles, Elsevier*, 1–26. https://doi.org/10.1016/B978-0-08-102579-6.00001-0

Parveen, K., Banse, V., & Ledwani, L. (2016). Green synthesis of nanoparticles: Their advantages and disadvantages. *AIP Conference Proceedings*, 1724. https://doi.org/10.1063/1.4945168

Pati, U. K., & Chowdhury, A. (2015). Study of Parthenium hysterophorus L. extracts (first clean-up fractions) on seed germination behaviour in search of bioactive fractions for preparation of bioherbicide formulations. *International Letters of Natural Sciences, 49*, 69–80. https://doi.org/10.18052/www.scipress.com.ilns.49.69

Patil, A. P., Ahire, S. A., & Hiray, S. N. kishor. (2021). Enhanced photocatlytic activity of two dimensional graphitic C3N4@Co3O4 core shell nanocomposite for discriminatory organic transformation under Hg-vapor reactor. *Material Science Research India*, *18*(2), 190–205. https://doi.org/10.13005/msri/180207

Piaskowski, K., Świderska-Dąbrowska, R., & Zarzycki, P. K. (2018). Dye removal from water and wastewater using various physical, chemical, and biological processes. *Journal of AOAC International, 101*(5), 1371–1384. https://doi.org/10.5740/jaoacint.18-0051

Polianciuc, S. I., Gurzău, A. E., Kiss, B., Ștefan, M. G., & Loghin, F. (2020). Antibiotics in the environment: causes and consequences. *Medicine and Pharmacy Reports, 93*(3), 231–240. https://doi.org/10.15386/mpr-1742

Rahimi, H.-R., & Doostmohammadi, M. (2019). Nanoparticle Synthesis, Applications,

and Toxicity. *Applications of Nanobiotechnology*. https://doi.org/10.5772/intechopen.87973

Raj, V. J., Ghosh, R., Girigoswami, A., & Girigoswami, K. (2022). Application of zinc oxide nanoflowers in environmental and biomedical science. *BBA Advances, 2*. https://doi.org/10.1016/j.bbadva.2022.100051

Rangel, W. M., Boca Santa, R. A. A., & Riella, H. G. (2020). A facile method for synthesis of nanostructured copper (II) oxide by coprecipitation. *Journal of Materials Research and Technology*, *9*(1), 994–1004. https://doi.org/10.1016/j.jmrt.2019.11.039

Raval, N., Maheshwari, R., Kalyane, D., Youngren-Ortiz, S. R., Chougule, M. B., & Tekade, R. K. (2019). Importance of physicochemical characterization of nanoparticles in pharmaceutical product development. *Basic Fundamentals of Drug Delivery*, 369–400. https://doi.org/10.1016/b978-0-12-817909-3.00010-8

Renuga, D., Jeyasundari, J., Shakthi Athithan, A. S., & Brightson Arul Jacob, Y. (2020). Synthesis and characterization of copper oxide nanoparticles using Brassica oleracea var. italic extract for its antifungal application. *Materials Research Express, 7*(4). https://doi.org/10.1088/2053-1591/ab7b94

Reza, K. M., Kurny, A., & Gulshan, F. (2017). Parameters affecting the photocatalytic degradation of dyes using TiO2: a review. *Applied Water Science, 7*(4), 1569–1578. https://doi.org/10.1007/s13201-015-0367-y

Riapanitra, A., Riyani, K., & Setyaningtyas, T. (2022). Photocatalytic and Kinetics Study of Copper Oxide on the Degradation of Methylene Blue Dye. *Proceedings of the Soedirman International Conference on Mathematics and Applied Sciences (SICOMAS 2021)*, 5(Sicomas 2021), 3–7. https://doi.org/10.2991/apr.k.220503.001

Rogowska, J., Cieszynska-Semenowicz, M., Ratajczyk, W., & Wolska, L. (2020).

Micropollutants in treated wastewater. *Ambio, 49*(2), 487–503. https://doi.org/10.1007/S13280-019-01219-5/tables/2

Roy, A., Sharma, A., Yadav, S., Jule, L. T., & Krishnaraj, R. (2021). Nanomaterials for Remediation of Environmental Pollutants. *Bioinorganic Chemistry and Applications, 2021*. https://doi.org/10.1155/2021/1764647

Saeed, M., Usman, M., & Haq, A. ul. (2018). Catalytic Degradation of Organic Dyes in Aqueous Medium. Photochemistry and Photophysics - Fundamentals to Applications. https://doi.org/10.5772/intechopen.75008

Saini, A., Aggarwal, N. K., Sharma, A., Kaur, M., & Yadav, A. (2014). Utility potential of Parthenium hysterophorus for its strategic management. *Advances in Agriculture, 2014*. https://doi.org/10.1155/2014/381859

Saini, R. D. (2018). Synthetic textile dyes: Constitution, dying process and environmental impacts. *Asian Journal of Research in Chemistry, 11*(1), 206. https://doi.org/10.5958/0974-4150.2018.00040.8

Salama, A., Mohamed, A., Aboamera, N. M., Osman, T. A., & Khattab, A. (2018). Photocatalytic degradation of organic dyes using composite nanofibers under UV irradiation. *Applied Nanoscience (Switzerland), 8*(1–2), 155–161. https://doi.org/10.1007/s13204-018-0660-9

Salvador, M., Gutiérrez, G., Noriega, S., Moyano, A., Blanco-López, M. C., & Matos, M. (2021). Microemulsion synthesis of superparamagnetic nanoparticles for bioapplications. *International Journal of Molecular Sciences, 22*(1), 1–17. https://doi. org/10.3390/ijms22010427

Shafey, A. M. El. (2020). Green synthesis of metal and metal oxide nanoparticles from plant leaf extracts and their applications: A review. *Green Processing and Synthesis, 9(*1), 304–339. https://doi.org/10.1515/gps-2020-0031

Shreya Modi, Virendra Kumar Yadav, Abdelfattah Amari, Abeer Yousef Alyami, Amel Gacem, H. N. H. andMadhusudan H. F. 7. (2023). Photocatalytic degradation of methylene blue dye from wastewater by using doped zinc oxide nanoparticles. *Water* (*Switzerland*), 15(7). https://doi.org/10.3390/w15071427

Singh, J., Dutta, T., Kim, K. H., Rawat, M., Samddar, P., & Kumar, P. (2018). 'Green' synthesis of metals and their oxide nanoparticles: applications for environmental remediation. *Journal of Nanobiotechnology, 16*(1), 1–24. https://doi.org/10.1186/S12951-018-0408-4

Singh, J., Kumar, V., Kim, K. H., & Rawat, M. (2019). Biogenic synthesis of copper oxide nanoparticles using plant extract and its prodigious potential for photocatalytic degradation of dyes. *Environmental Research, 177*. https://doi.org/10.1016/j.envres.2019.108569

Singh, V., Yadav, S. S., Chauhan, V., Shukla, S., & Vishnolia, K. K. (2020). Applications of nanoparticles in various fields. D*iagnostic Applications of Health Intelligence and Surveillance Systems*, 221-236. https://doi.org/10.4018/978-1-7998-6527-8.ch011

Slama, H. Ben, Bouket, A. C., Pourhassan, Z., Alenezi, F. N., Silini, A., Cherif-Silini, H., Oszako, T., Luptakova, L., Golińska, P., & Belbahri, L. (2021). Diversity of synthetic dyes from textile industries, discharge impacts and treatment methods. *Applied Sciences (Switzerland), 11*(14), 1–21. https://doi.org/10.3390/app11146255

Sridevi, H., Bhat, M. R., Kumar, P. S., Kumar, N. M., & Selvaraj, R. (2023). Structural characterization of cuboidal α-Fe2O3 nanoparticles synthesized by a facile approach. *Applied Nanoscience (Switzerland), 13*(8), 5605–5613. https://doi.org/10.1007/s13204-023-02780-y

Umamaheswari, A., Prabu, S. L., John, S. A., & Puratchikody, A. (2021). Green synthesis of zinc oxide nanoparticles using leaf extracts of Raphanus sativus var. Longipinnatus and evaluation of their anticancer property in A549 cell lines.

Biotechnology Reports, 29, e00595. https://doi.org/10.1016/j.btre.2021.e00595

UNESCO. (2023). Imminent risk of a global water crisis, warns the UN World Water Development Report 2023. UNESCO. https://www.unesco.org/en/articles/imminent-risk-global-water-crisis-warns-un-world-water-development-report-2023

Usman, M. R., Prasasti, A., Islamiah, S., Firdaus, A. N., Marita, A. W., Fajriyah, S., & Yanti, E. F. (2020). Ceftriaxone degradation by titanium dioxide (TiO2) nanoparticles: Toxicity and degradation mechanism. *Jurnal Kimia Valensi*, *6*(1), 82–89. https://doi.org/10.15408/jkv.v6i1.12475

Vasiljevic, Z. Z., Dojcinovic, M. P., Vujancevic, J. D., Jankovic-Castvan, I., Ognjanovic, M., Tadic, N. B., Stojadinovic, S., Brankovic, G. O., & Nikolic, M. V. (2020). Photocatalytic degradation of methylene blue under natural sunlight using iron titanate nanoparticles prepared by a modified sol-gel method: Methylene blue degradation with Fe2TiO5. *Royal Society Open Science*, *7*(9). https://doi.org/10.1098/rsos.200708

Venkatesan, S., Suresh, S., Ramu, P., Arumugam, J., Thambidurai, S., & Pugazhenthiran, N. (2022). Methylene blue dye degradation potential of zinc oxide nanoparticles bioreduced using Solanum trilobatum leaf extract. *Results in Chemistry*, *4*(September), 100637. https://doi.org/10.1016/j.rechem.2022.100637

Wabuyele, E., Lusweti, A., Bisikwa, J., Kyenune, G., Clark, K., Lotter, W. D., McConnachie, A. J., & Wondi, M. (2015). A roadside survey of the invasive weed Parthenium hysterophorus (Asteraceae) in East Africa . *Journal of East African Natural History*, *103*(1), 49–57. https://doi.org/10.2982/028.103.0105

Wanakai, I. S., Kareru, G. P., Sujee, M. D., Madivoli, S. E., Gachui, M. E., & Kairigo, K. P. (2022). Kinetics of rifampicin antibiotic degradation using green synthesized iron oxide nanoparticles. *Chemistry Africa*, November. https://doi.org/10.1007/s42250-022-00543-w

Wanakai, S. I., Kareru, P. G., Makhanu, D. S., Madivoli, E. S., Maina, E. G., & Nyabola, A. O. (2019). Catalytic degradation of methylene blue by iron nanoparticles synthesized using Galinsoga parviflora, Conyza bonariensis and Bidens pilosa leaf extracts. *SN Applied Sciences, 1*(10), 1–10. https://doi.org/10.1007/s42452-019-1203-z

Wang, Q., Mei, S., Manivel, P., Ma, H., & Chen, X. (2022). Zinc oxide nanoparticles synthesized using coffee leaf extract assisted with ultrasound as nanocarriers for mangiferin. *Current Research in Food Science, 5*(May), 868–877. https://doi.org/10.1016/j.crfs.2022.05.002

Wang, S., Yu, H., & Cheng, X. (2014). Degradation of typical indoor air pollutants using Fe-doped TiO2 thin film under daylight illumination. *Journal of Chemistry, 20*14. https://doi.org/10.1155/2014/829892

World Health Organization (2023). Antimicrobial resistance. World Health Organization.

Wilkinson, J. L., Boxall, A. B. A., Kolpin, D. W., Leung, K. M. Y., Lai, R. W. S., Wong, D., Ntchantcho, R., Pizarro, J., Mart, J., Echeverr, S., Garric, J., Chaumot, A., Gibba, P., Kunchulia, I., Seidensticker, S., Lyberatos, G., Morales-salda, J. M., & Kang, H. (2022). Pharmaceutical pollution of the world's rivers. *Proceedings of the National Academy of Sciences.* 119(8), 1–10. https://doi.org/10.1073/pnas.2113947119

Wu, F., Zhou, Z., & Hicks, A. L. (2019). Life cycle impact of titanium dioxide nanoparticle synthesis through physical, chemical, and biological routes. *Environmental Science and Technology, 53*(8), 4078–4087. https://doi.org/10.1021/acs.est.8b06800

Xu, Q., Owens, G., & Chen, Z. (2020). Adsorption and catalytic reduction of rifampicin in wastewaters using hybrid rGO@Fe/Pd nanoparticles. *Journal of Cleaner Production, 264*, 121617. https://doi.org/10.1016/j.jclepro.2020.121617

Yadav, S. K. (2016). Synthesis and characterization of copper nanoparticles, using combination of two different sizes of balls in wet ball milling. *International Journal of Emerging Trends in Science and Technology*, *April*. https://doi.org/10.18535/ijetst/v3i04.07

Yang, M., Li, J., Gu, P., & Fan, X. (2021). The application of nanoparticles in cancer immunotherapy: Targeting tumor microenvironment. *Bioactive Materials*, *6*(7), 1973–1987. https://doi.org/10.1016/j.bioactmat.2020.12.010

Zainuri, N. Z., Hairom, N. H. H., Sidik, Di. A. B., Misdan, N., Yusof, N., & Mohammad, A. W. (2018). Reusability performance of zinc oxide nanoparticles for photocatalytic degradation of POME. *E3S Web of Conferences*, 34, 1–9. https://doi.org/10.1051/e3sconf/20183402013

Zikalala, N. E., Azizi, S., Zikalala, S. A., Kamika, I., Maaza, M., Zinatizadeh, A. A., Mokrani, T., & Kaviyarasu, K. (2022). An evaluation of the biocatalyst for the synthesis and application of zinc oxide nanoparticles for water remediation—A review. *Catalysts*, *12*(11). https://doi.org/10.3390/catal12111442

APPENDICES

Appendix I: *P. hysterophorus* JKUAT Botany Herbarium Specimen Voucher Number

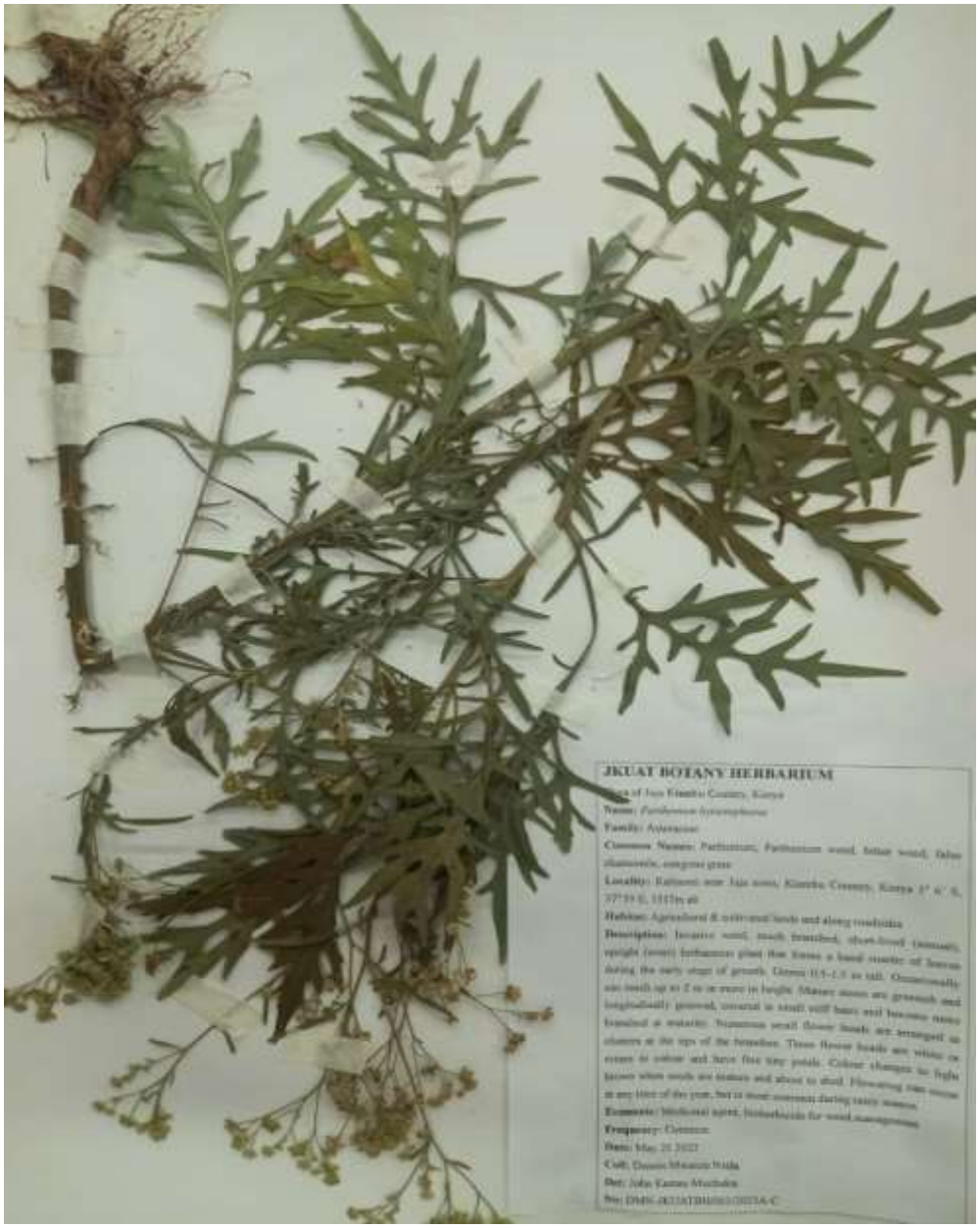

Appendix II: Kinetic Model Plots for Degradation of Rifampicin and CuO NPs

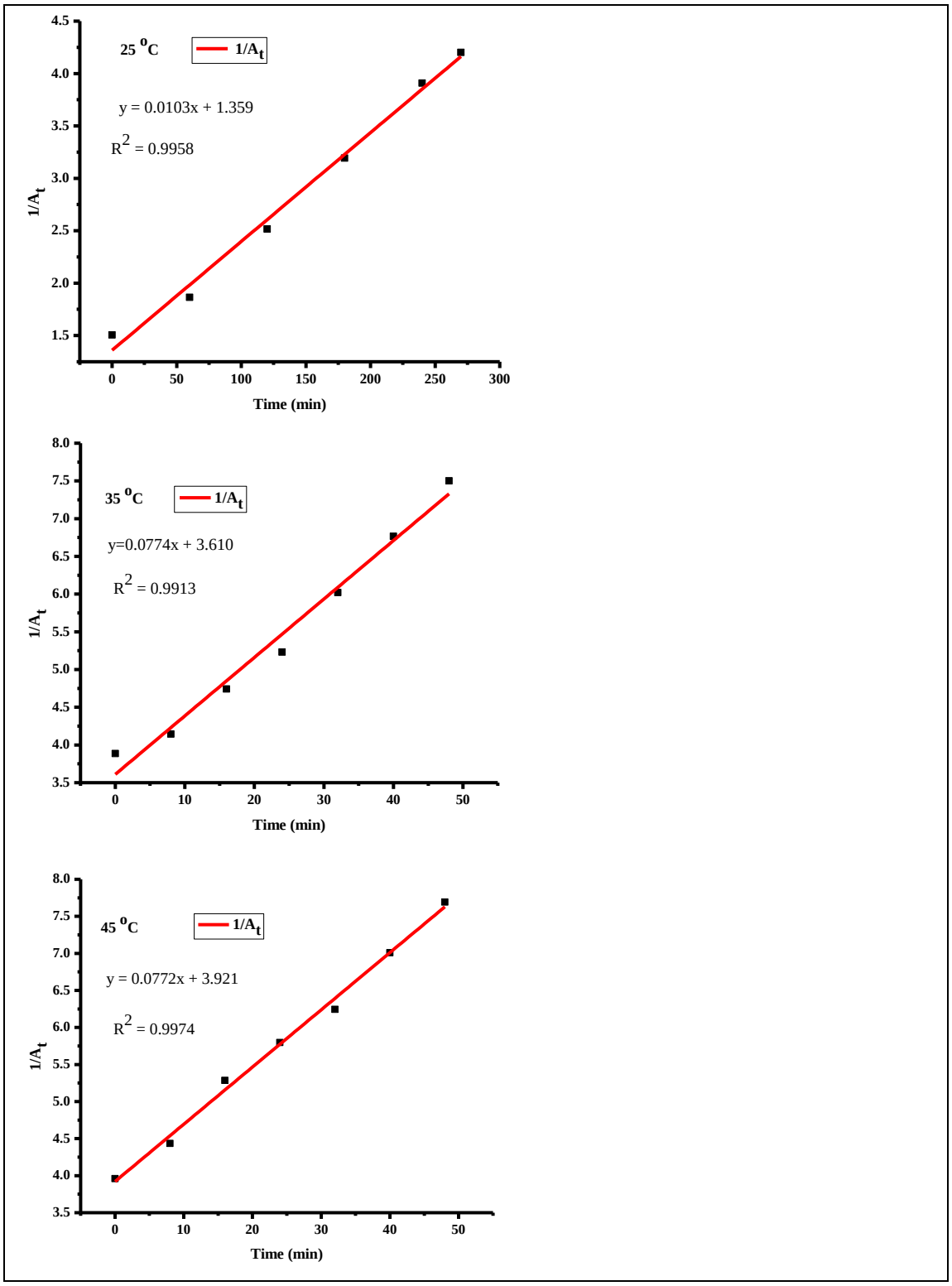

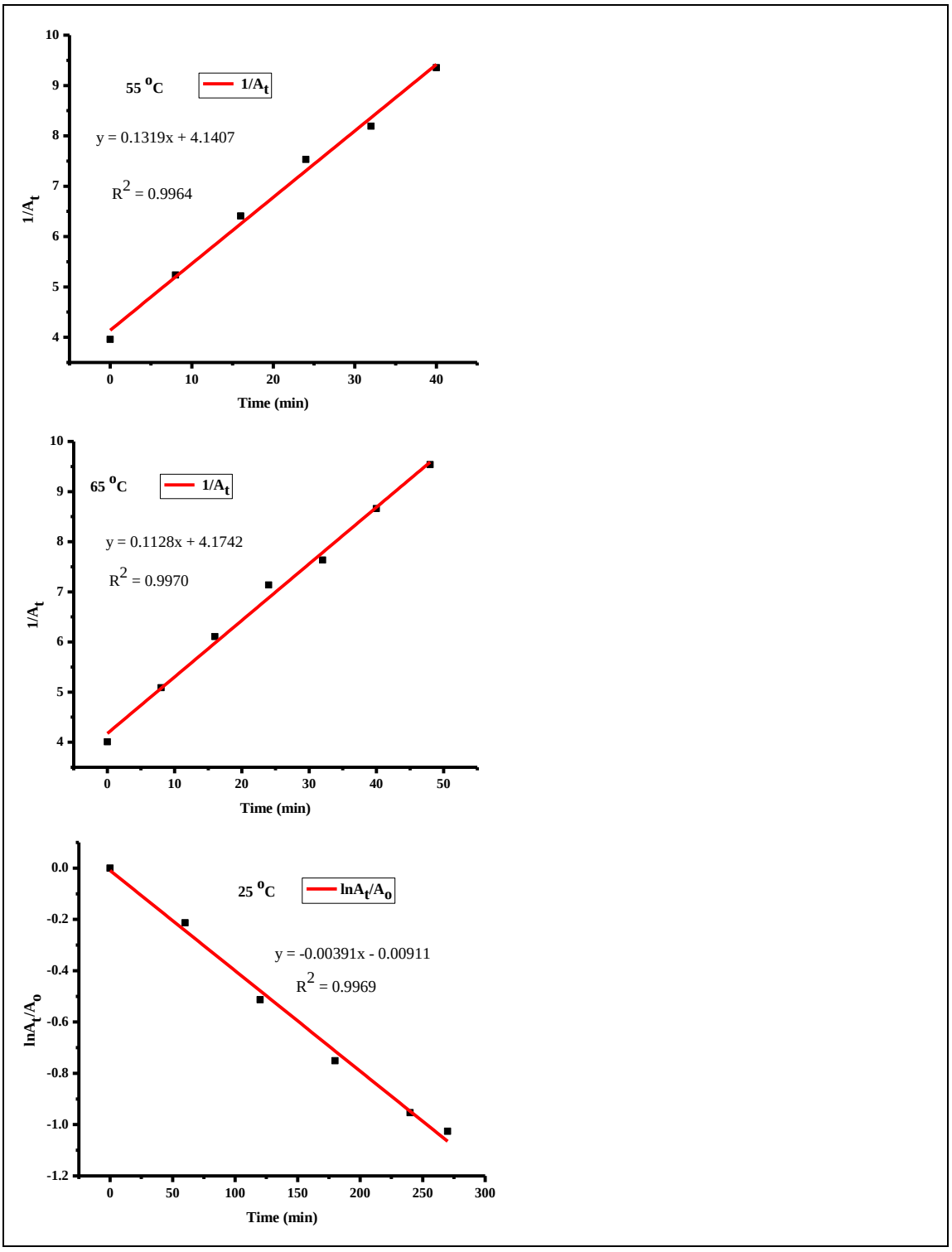
55 °C
1/A_t
y = 0.1319x + 4.1407
R2 = 0.9964
1/A_t
Time (min)
65 °C
1/A_t
y = 0.1128x + 4.1742
R2 = 0.9970
1/A_t
Time (min)
25 °C
lnA_t/A_0
y = -0.00391x - 0.00911
R2 = 0.9969
lnA_t/A_0
Time (min)

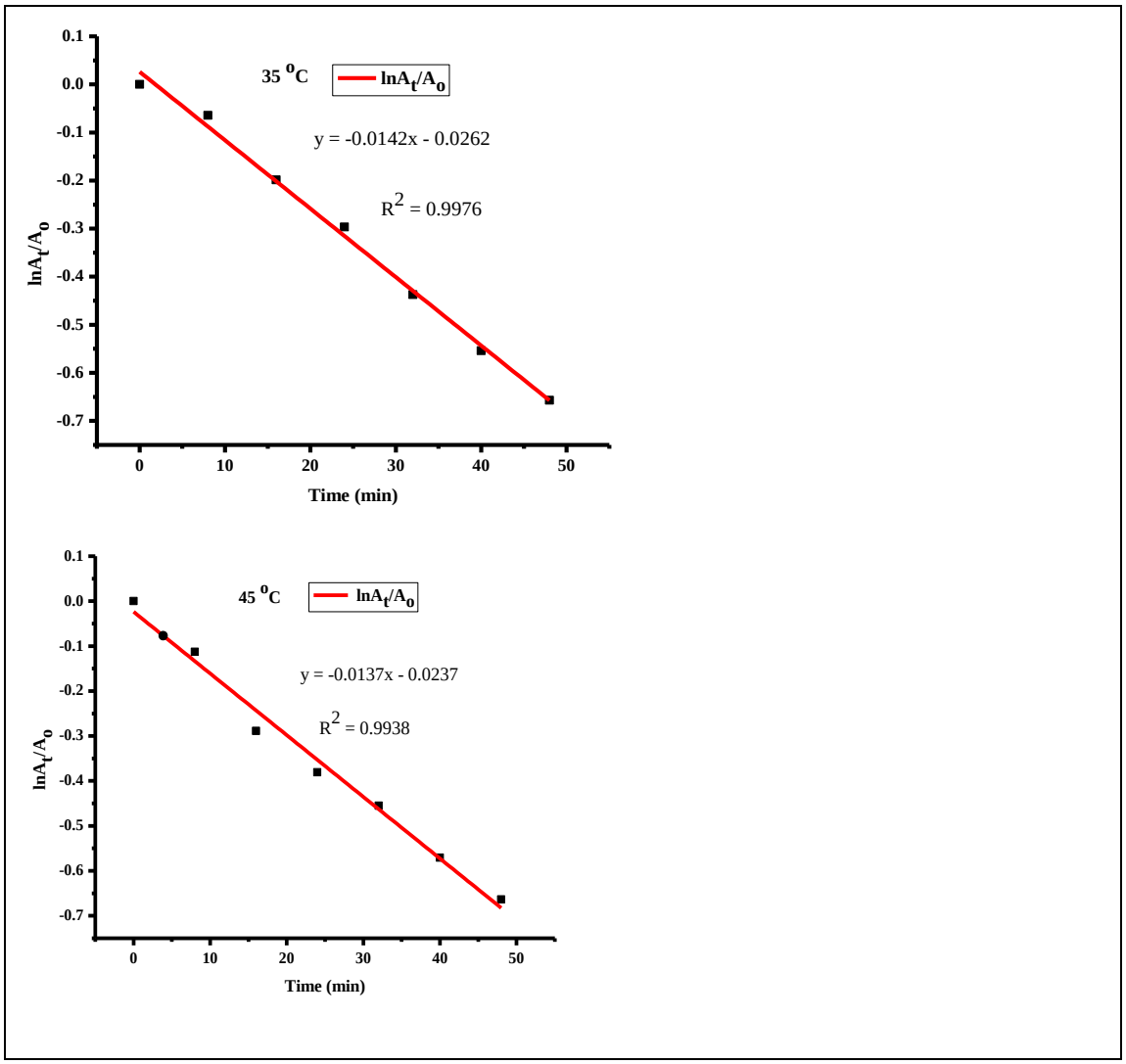
35 °C
lnA$_t$/A$_o$
y = -0.0142x - 0.0262
R^2 = 0.9976
lnA$_t$/A$_o$
Time (min)
45 °C
lnA$_t$/A$_o$
y = -0.0137x - 0.0237
R^2 = 0.9938
lnA$_t$/A$_o$
Time (min)

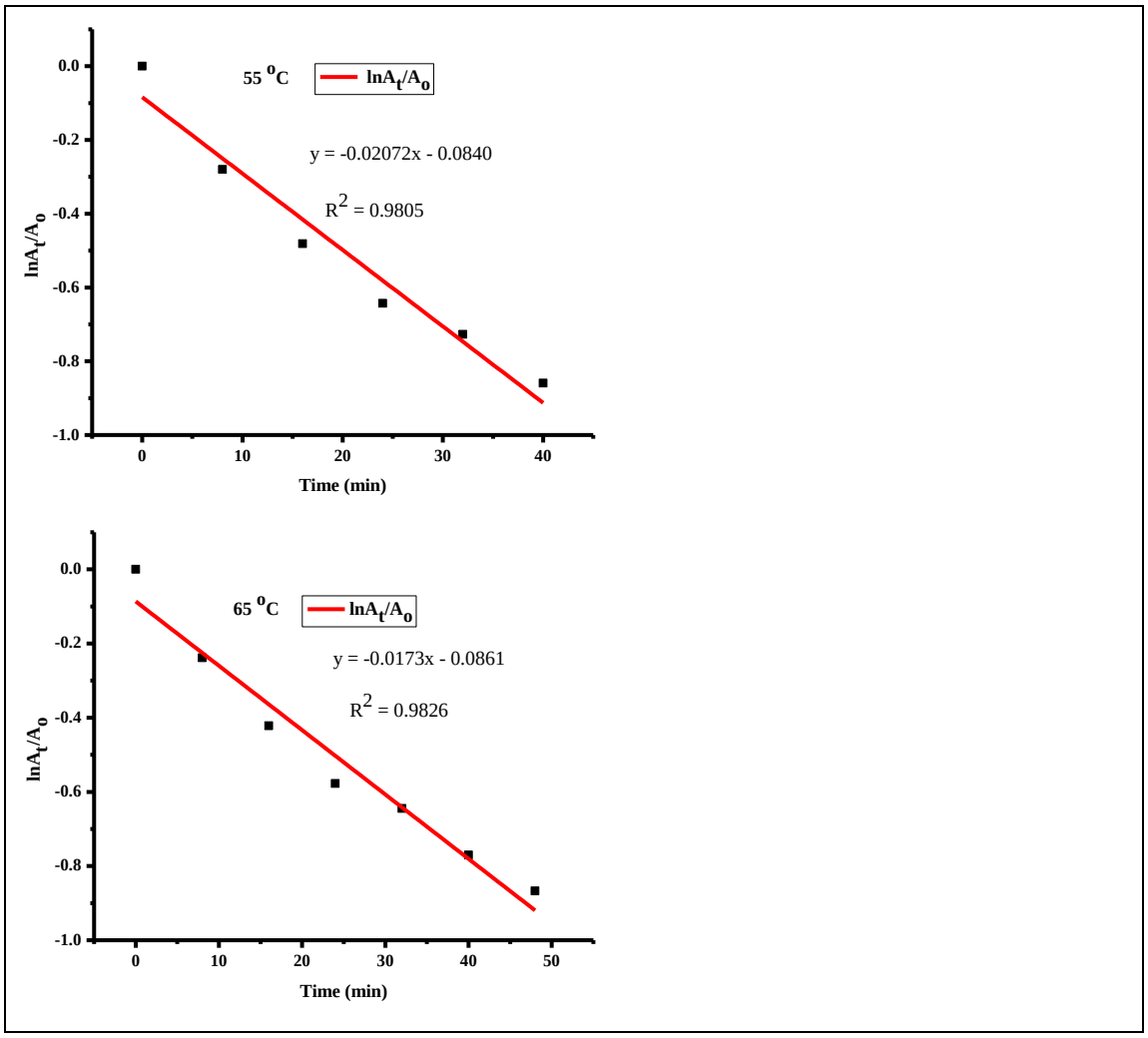
55 °C
lnA$_t$/A$_o$
y = -0.02072x - 0.0840
R^2 = 0.9805
lnA$_t$/A$_o$
Time (min)
65 °C
lnA$_t$/A$_o$
y = -0.0173x - 0.0861
R^2 = 0.9826
lnA$_t$/A$_o$
Time (min)

Appendix III: Kinetic Model Plots for Degradation of Rifampicin Using ZnO NPs

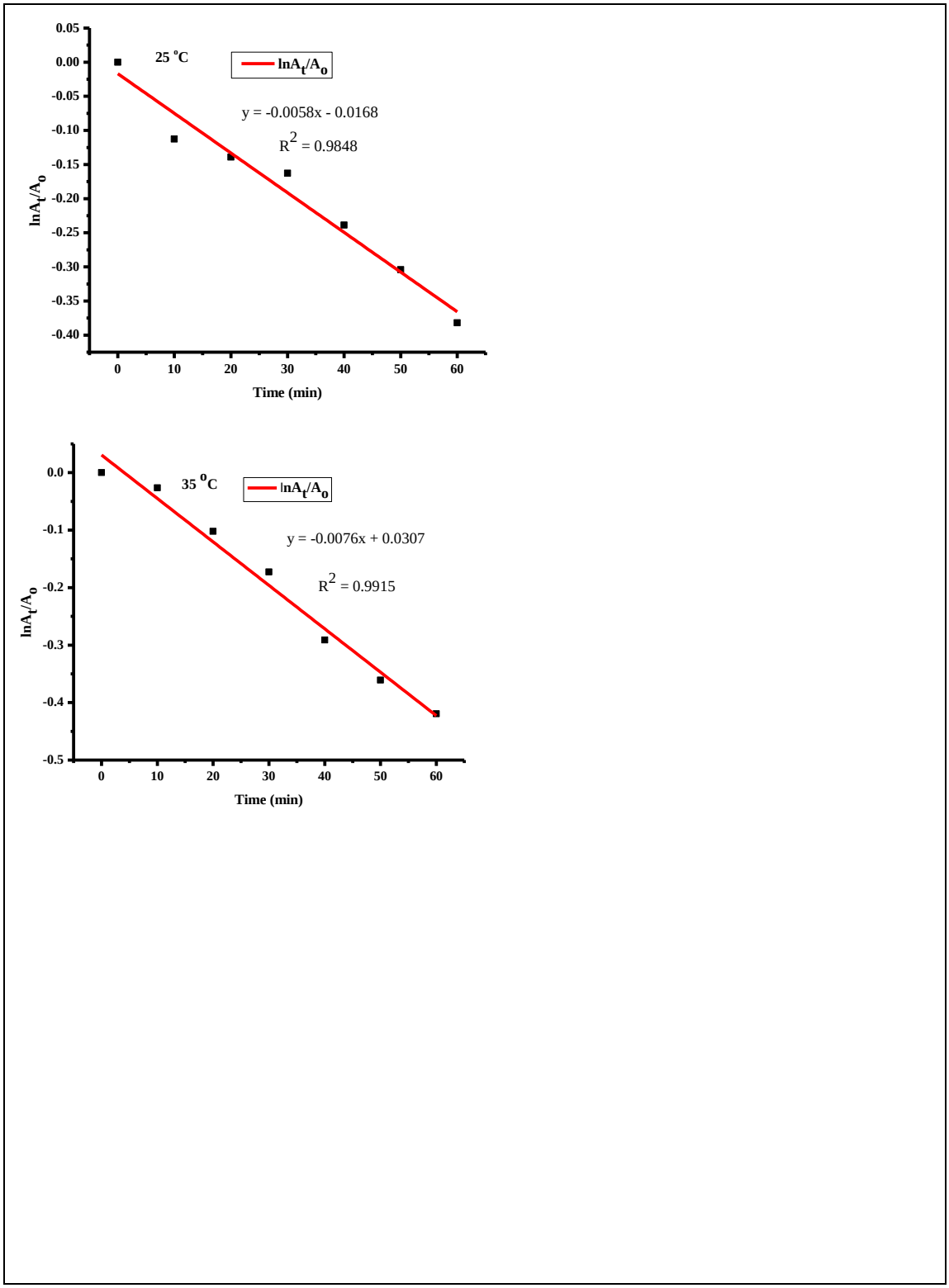

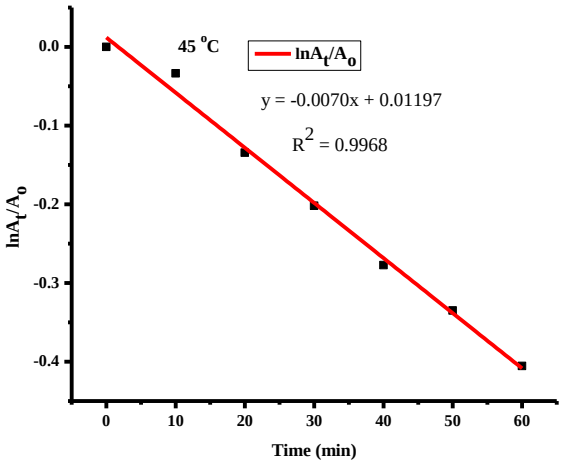
45 °C
lnA$_t$/A$_o$
y = -0.0070x + 0.01197
R^2 = 0.9968
lnA$_t$/A$_o$
Time (min)
0.0
-0.1
-0.2
-0.3
-0.4
0
10
20
30
40
50
60

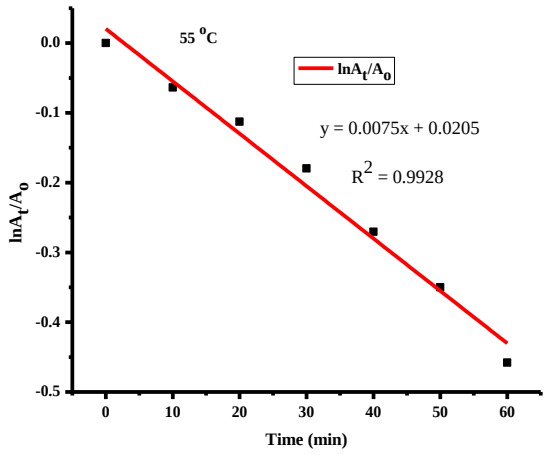
55 °C
lnA$_t$/A$_o$
y = 0.0075x + 0.0205
R^2 = 0.9928
lnA$_t$/A$_o$
Time (min)
0.0
-0.1
-0.2
-0.3
-0.4
-0.5
0
10
20
30
40
50
60

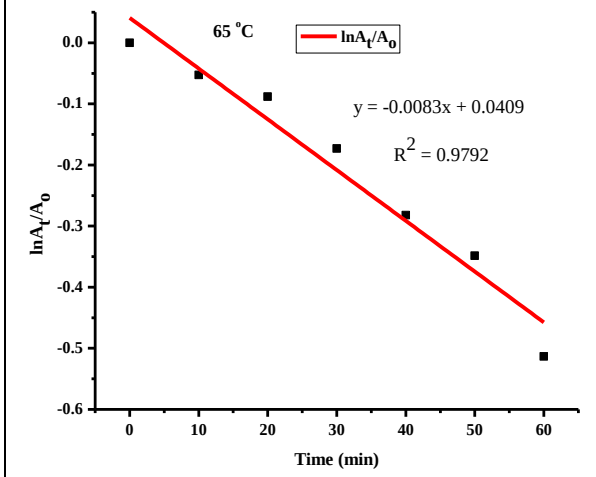
65 °C
lnA$_t$/A$_o$
y = -0.0083x + 0.0409
R^2 = 0.9792
lnA$_t$/A$_o$
Time (min)

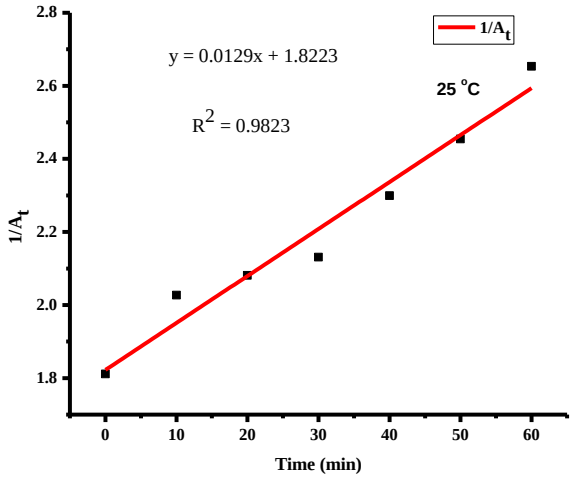
1/A$_t$
y = 0.0129x + 1.8223
25 °C
R^2 = 0.9823
1/A$_t$
Time (min)

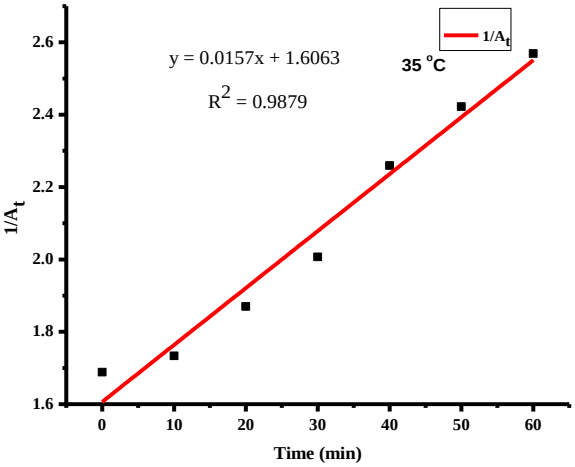
1/A$_t$
y = 0.0157x + 1.6063
35 °C
R^2 = 0.9879
1/A$_t$
Time (min)

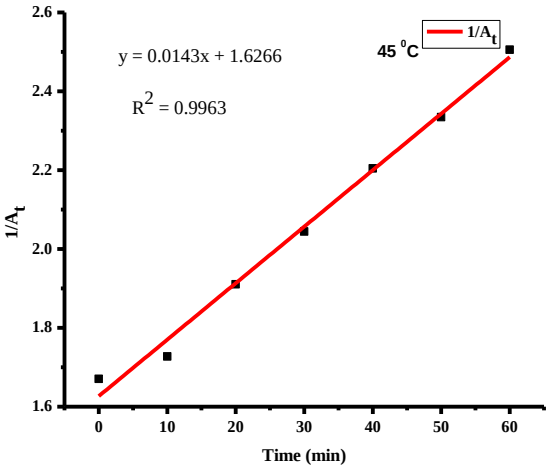
y = 0.0143x + 1.6266
R2 = 0.9963
45 °C
1/At
1/At
Time (min)

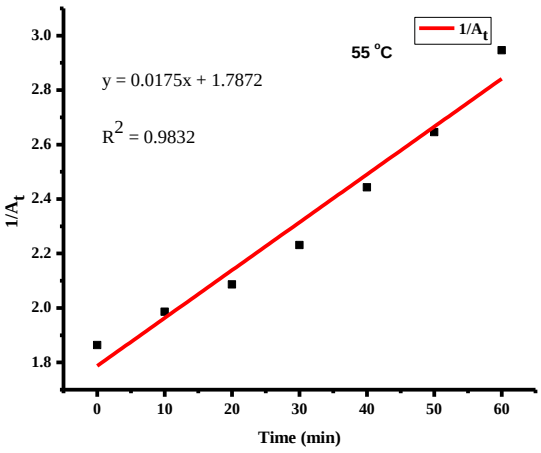
y = 0.0175x + 1.7872
R2 = 0.9832
55 °C
1/At
1/At
Time (min)

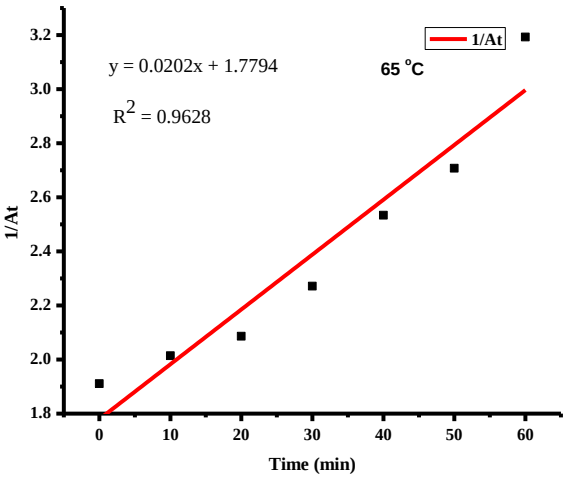
y = 0.0202x + 1.7794
R2 = 0.9628
65 °C
1/At
1/At
Time (min)

Appendix IV: Kinetic Model Plots for Degradation of MB and CuO NPs

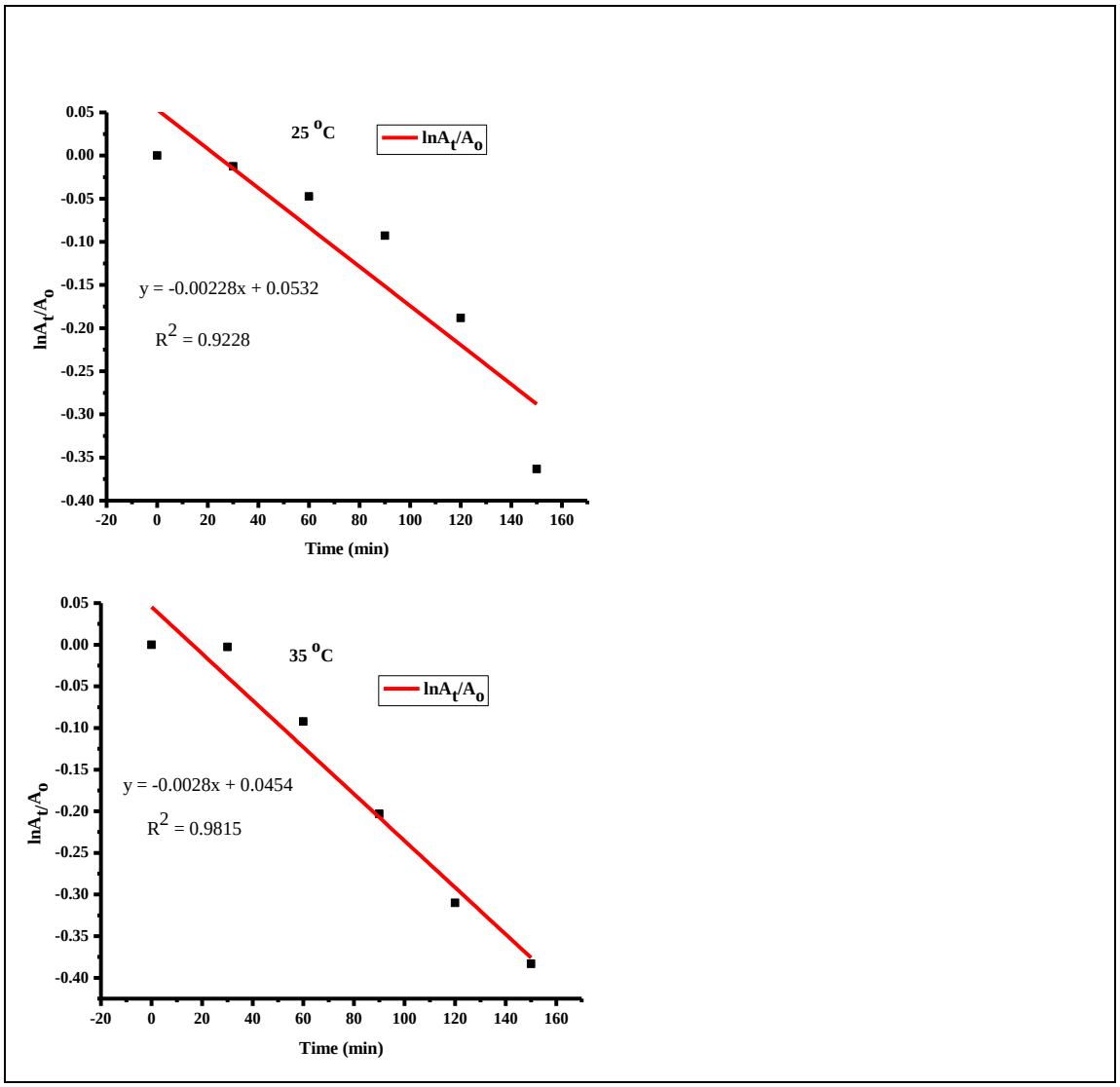

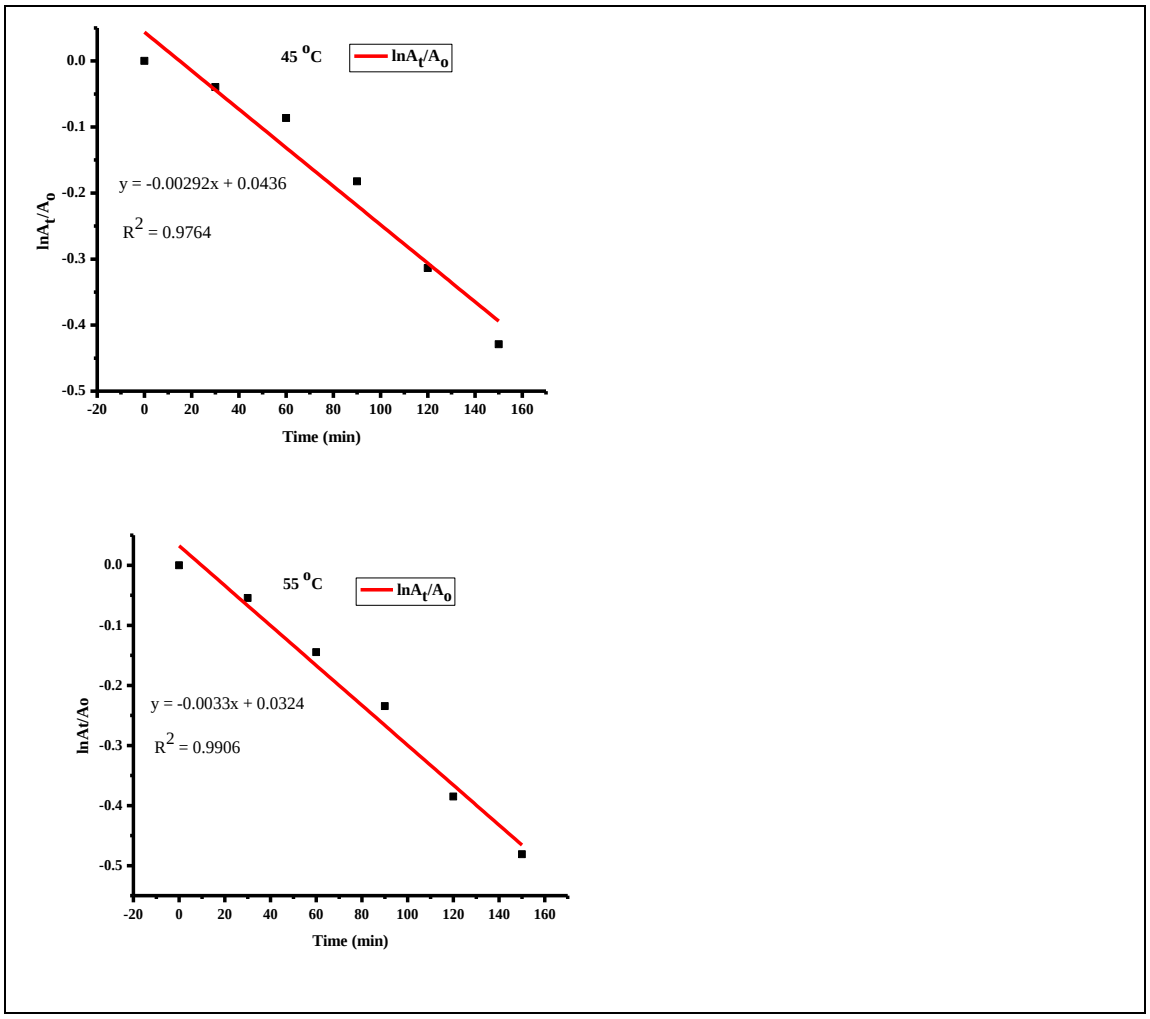
45 °C
lnAt/A0
y = -0.00292x + 0.0436
R2 = 0.9764
lnAt/Ao
Time (min)
55 °C
lnAt/A0
y = -0.0033x + 0.0324
R2 = 0.9906
lnAt/Ao
Time (min)

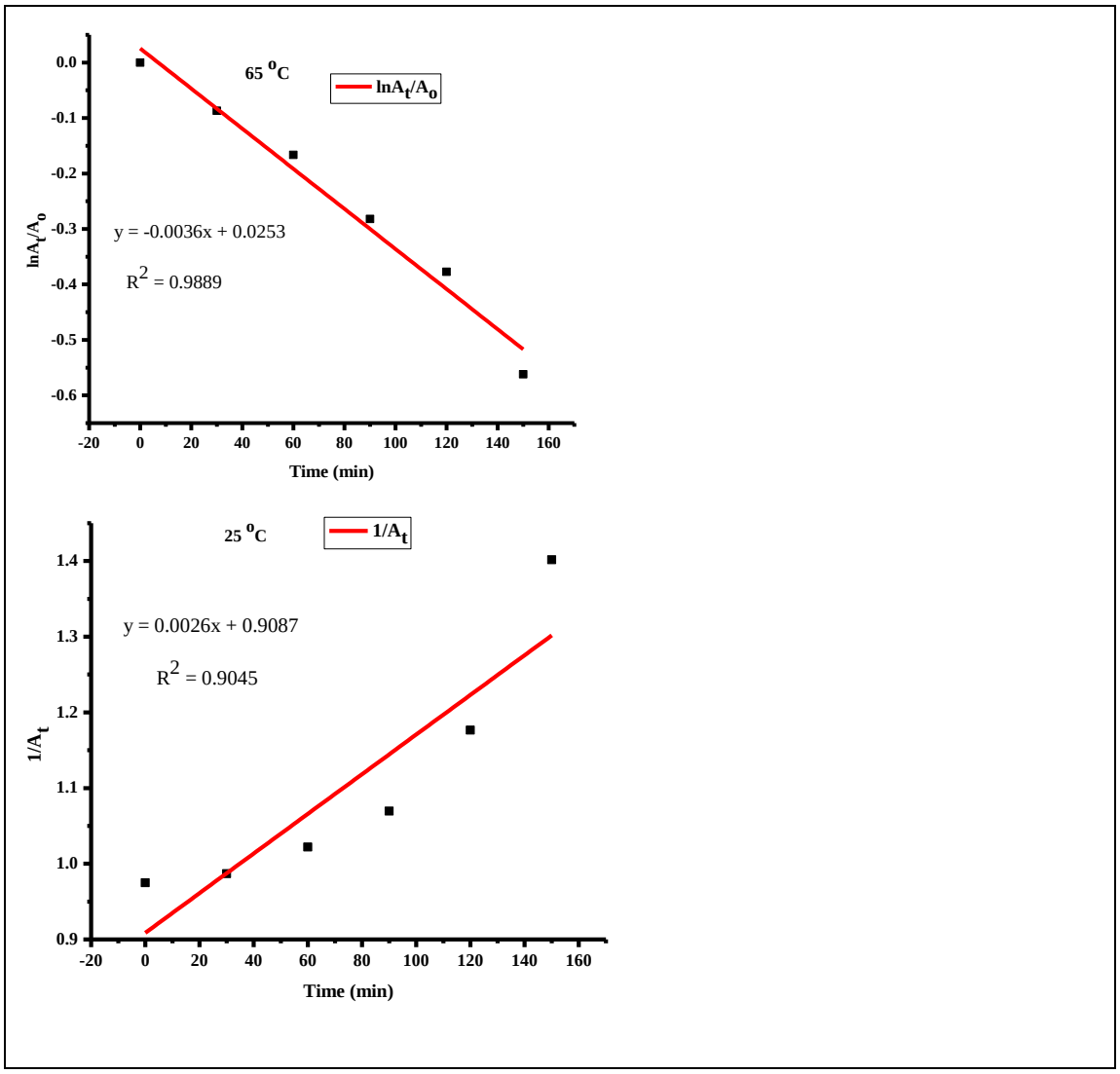
65 °C
lnA$_t$/A$_o$
y = -0.0036x + 0.0253
R^2 = 0.9889
lnA$_t$/A$_o$
Time (min)
25 °C
1/A$_t$
y = 0.0026x + 0.9087
R^2 = 0.9045
1/A$_t$
Time (min)

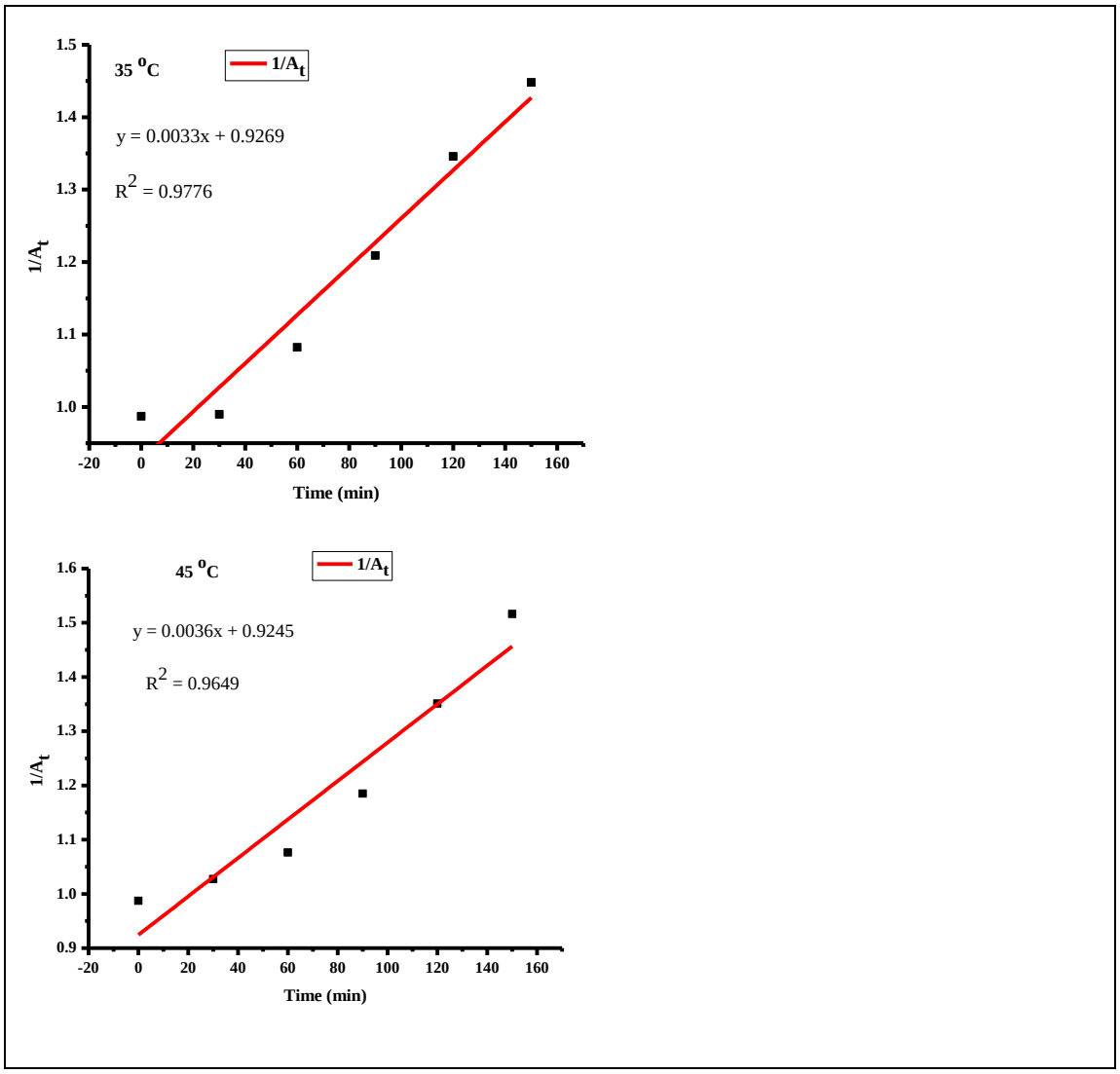
35 °C
1/At
y = 0.0033x + 0.9269
R2 = 0.9776
1/At
Time (min)
45 °C
1/At
y = 0.0036x + 0.9245
R2 = 0.9649
1/At
Time (min)

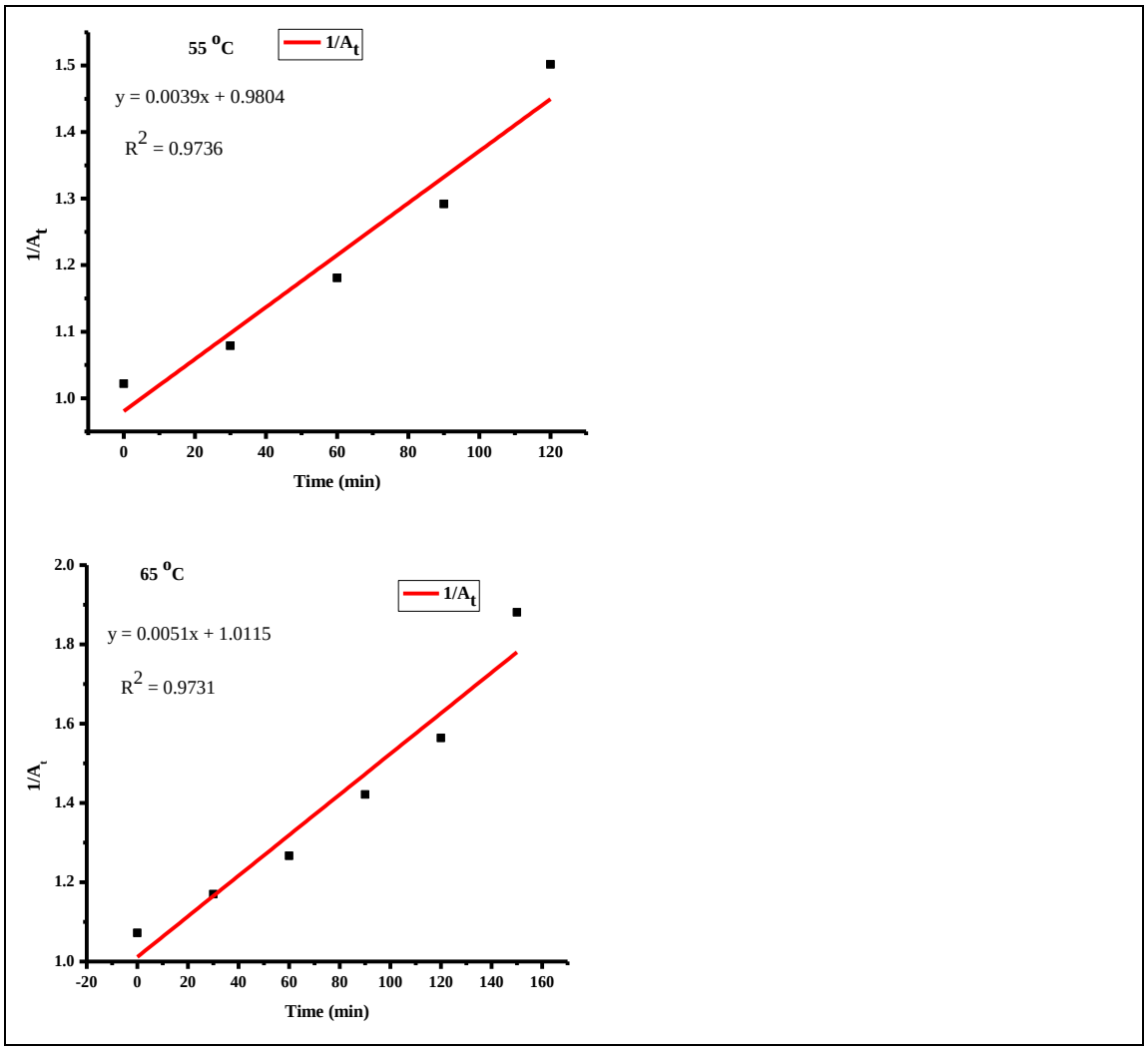
55 °C
1/At
y = 0.0039x + 0.9804
R2 = 0.9736
1/At
Time (min)
65 °C
1/At
y = 0.0051x + 1.0115
R2 = 0.9731
1/At
Time (min)

Appendix V: Kinetic Model Plots for Degradation of MB Using ZnO NPs

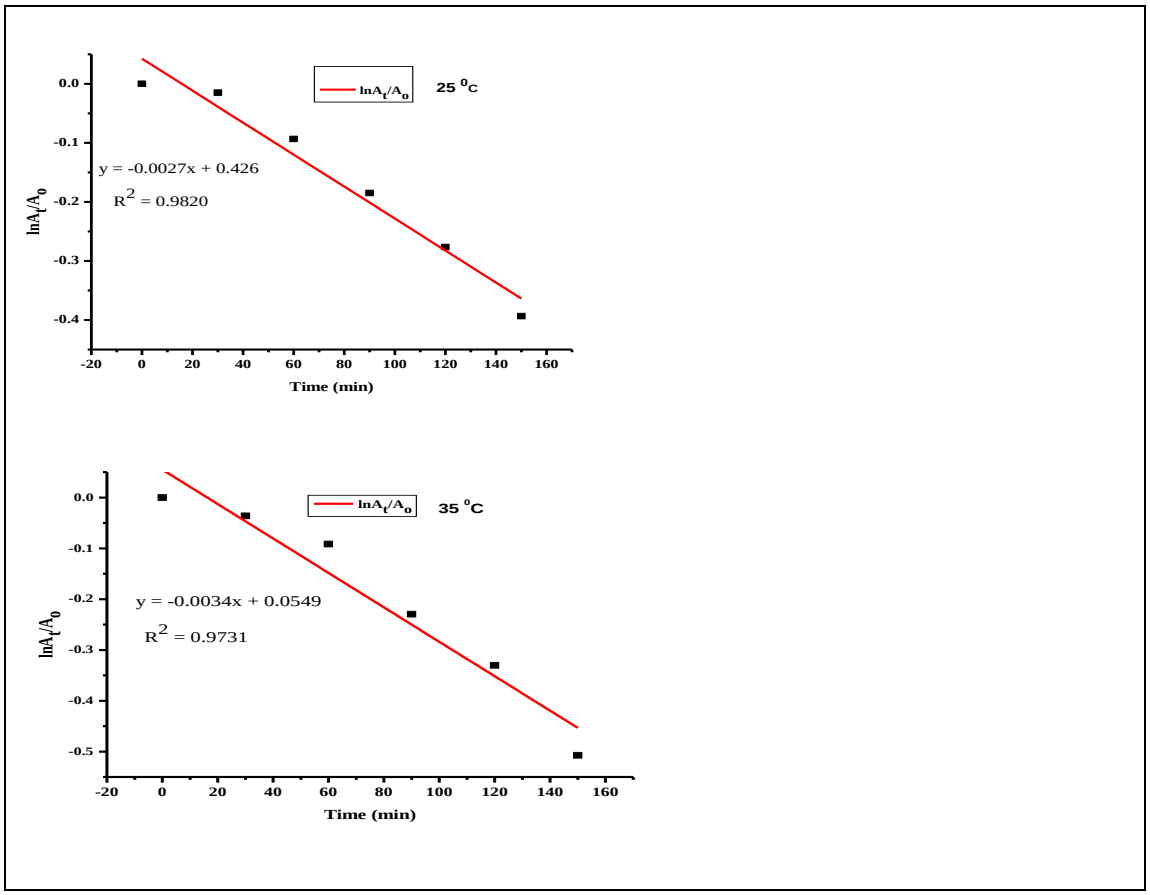

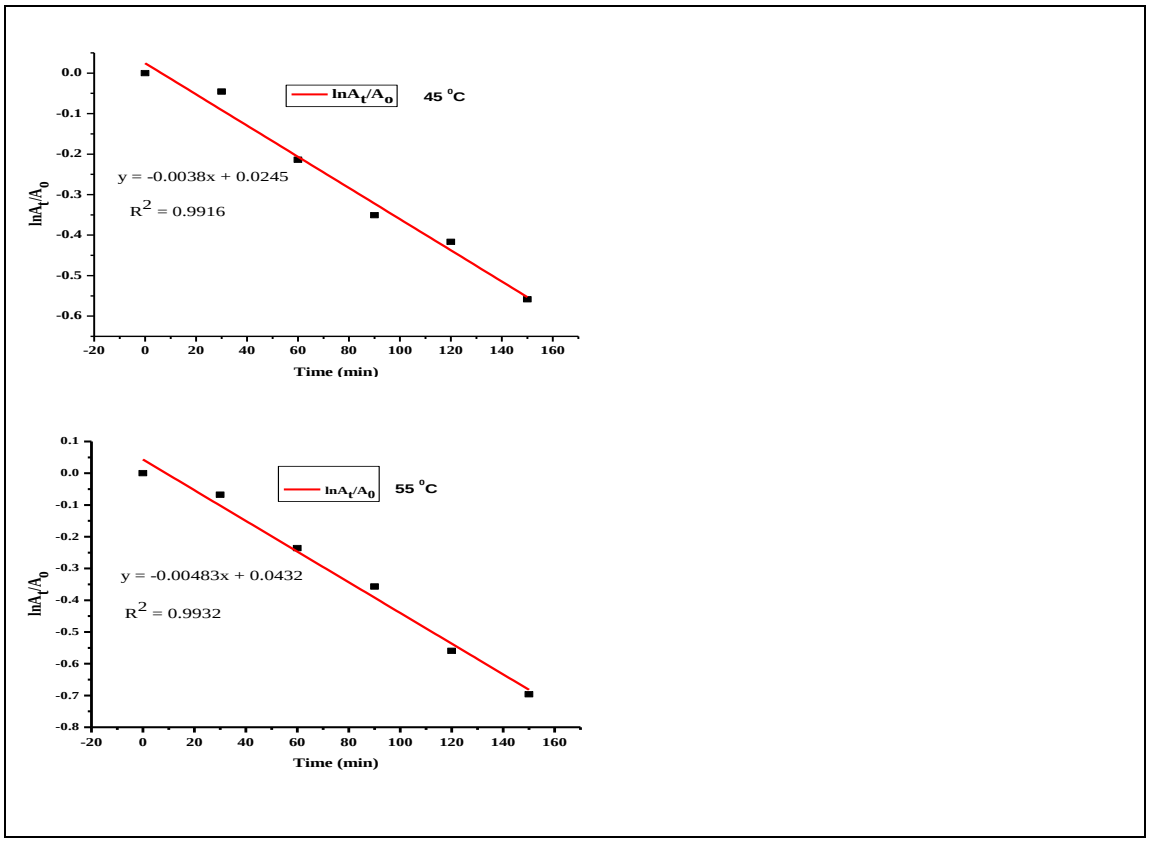
lnA$_t$/A$_o$
45 °C
y = -0.0038x + 0.0245
R^2 = 0.9916
lnA$_t$/A$_0$
Time (min)
lnA$_t$/A$_0$
55 °C
y = -0.00483x + 0.0432
R^2 = 0.9932
lnA$_t$/A$_0$
Time (min)

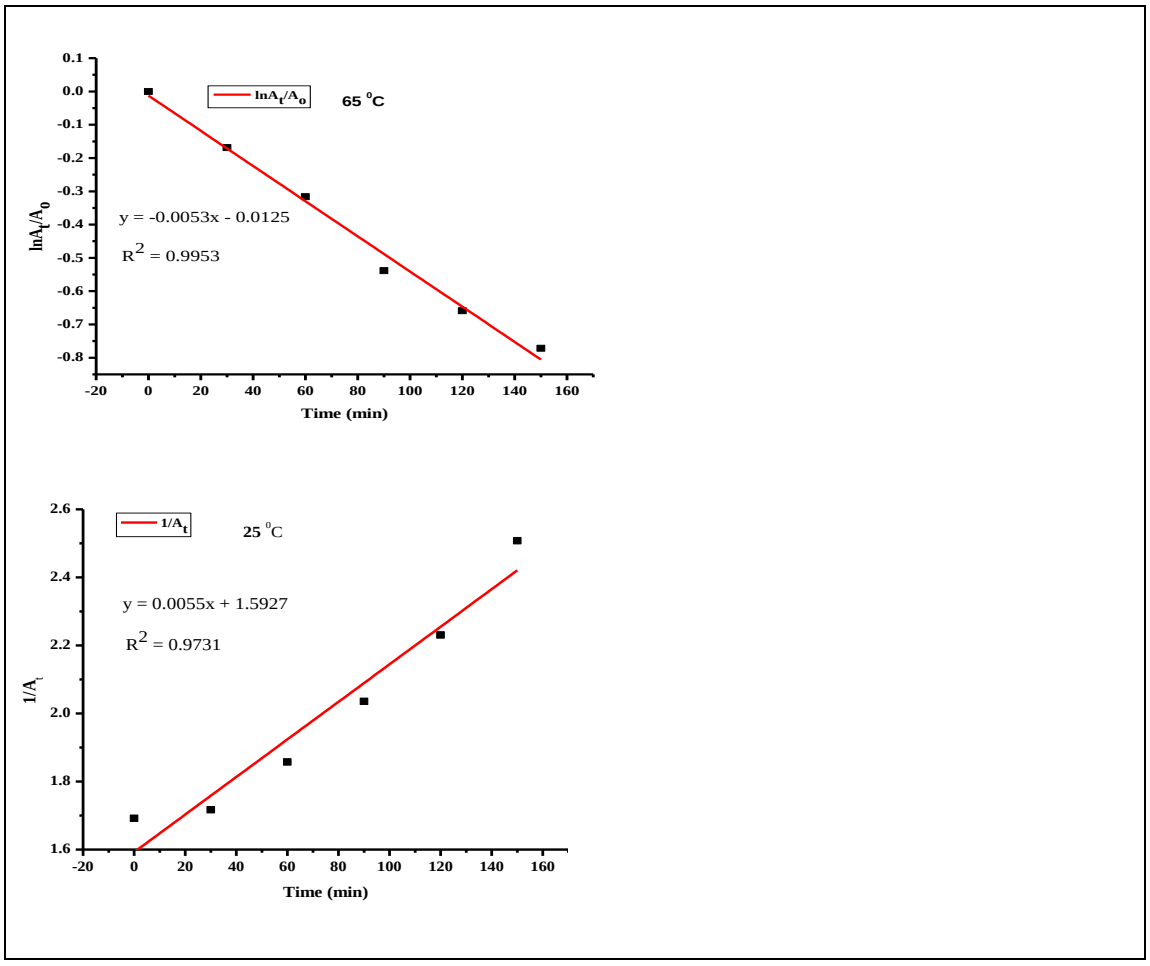
lnA$_t$/A$_o$
65 °C
y = -0.0053x - 0.0125
R^2 = 0.9953
lnA$_t$/A$_0$
Time (min)
1/A$_t$
25 °C
y = 0.0055x + 1.5927
R^2 = 0.9731
1/A$_t$
Time (min)

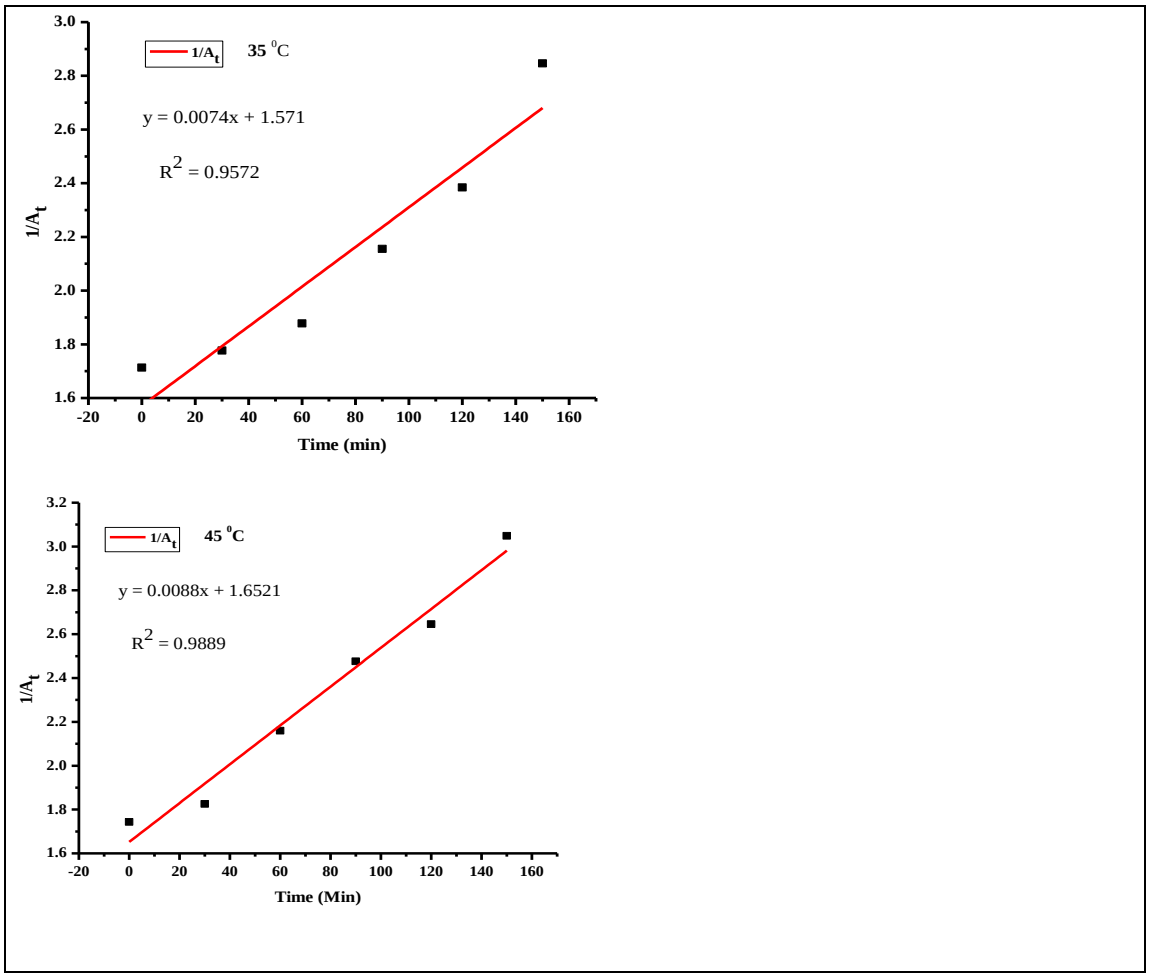
1/A$_t$
35 ^{0}C
y = 0.0074x + 1.571
R^2 = 0.9572
1/A$_t$
Time (min)
1/A$_t$
45 ^{0}C
y = 0.0088x + 1.6521
R^2 = 0.9889
1/A$_t$
Time (Min)

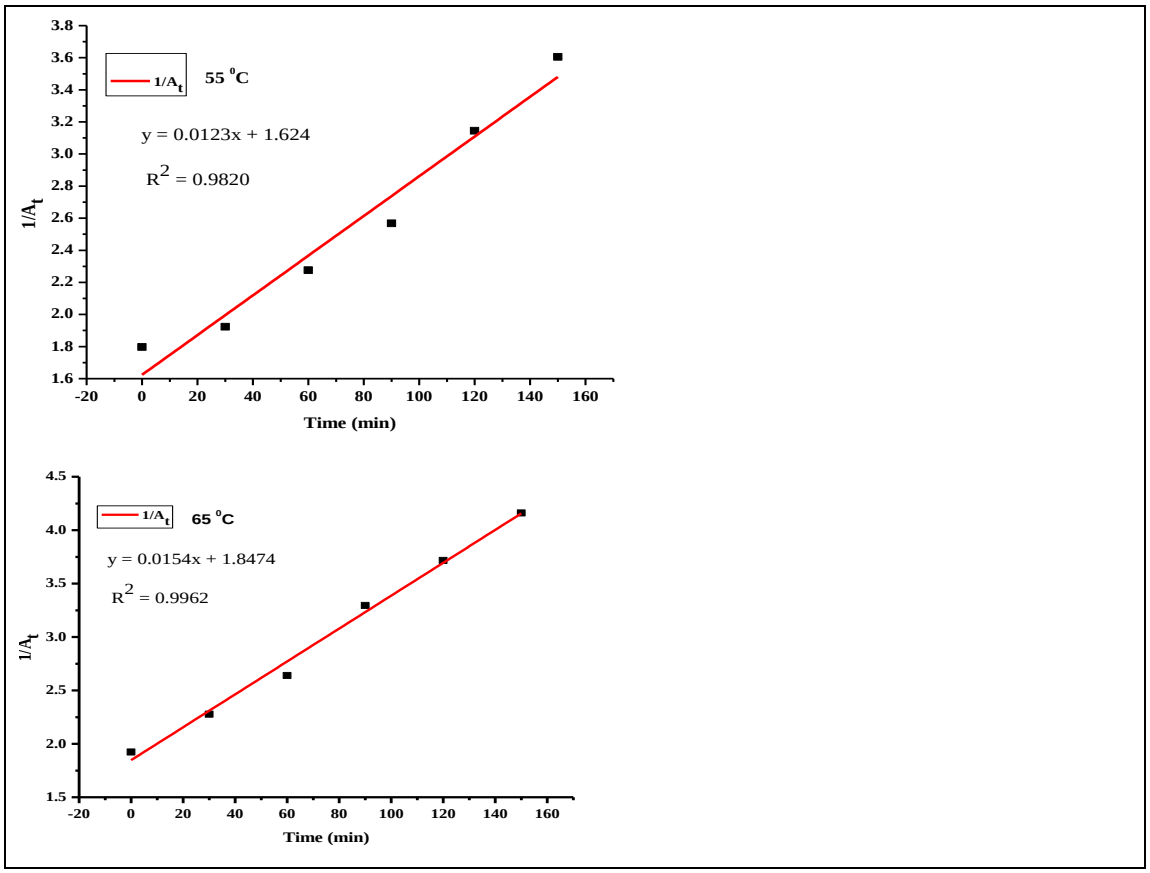
1/A_t
55 °C
y = 0.0123x + 1.624
R2 = 0.9820
1/At
Time (min)
1/A_t
65 °C
y = 0.0154x + 1.8474
R2 = 0.9962
1/At
Time (min)

Appendix VI: Publication I

www.nature.com/scientificreports

scientific reports

Check for updates

OPEN

Green synthesis of copper oxide nanoparticles and its efficiency in degradation of rifampicin antibiotic

Dennis Mwanza Nzilu[1✉], Edwin Shigwenya Madivoli[1], David Sujee Makhanu[2], Sammy Indire Wanakai[1], Gideon Kirui Kiprono[1] & Patrick Gachoki Kareru[1]

In recent ages, green nanotechnology has gained attraction in the synthesis of metallic nanoparticles due to their cost-effectiveness, simple preparation steps, and environmentally-friendly. In the present study, copper oxide nanoparticles (CuO NPs) were prepared using *Parthenium hysterophorus* whole plant aqueous extract as a reducing, stabilizing, and capping agent. The CuO NPs were characterized via UV–Vis Spectroscopy, Fourier Transform Infrared Spectroscopy (FTIR), powder X-Ray Diffraction (XRD), Scanning Electron Microscopy (SEM), Transmission Electron Microscopy (TEM), and Dynamic Light Scattering (DLS). The UV–Vis spectra of CuO NPs showed a surface plasmonic resonance band to occur at 340 nm. FTIR analysis revealed the presence of secondary metabolites on the surface of CuO NPs, with a characteristic Cu–O stretching band being identified at 522 cm^{-1}. Scanning electron micrographs and transmission electron micrographs showed that CuO NPs were nearly spherical, with an average particle of 59.99 nm obtained from the SEM micrograph. The monoclinic crystalline structure of CuO NPs was confirmed using XRD, and crystallite size calculated using the Scherrer-Debye equation was found to be 31.58 nm. DLS showed the presence of nanoparticle agglomeration, which revealed uniformity of the CuO NPs. Furthermore, the degradation ability of biosynthesized nanoparticles was investigated against rifampicin antibiotic. The results showed that the optimum degradation efficiency of rifampicin at 98.43% was obtained at 65°C temperature, 50 mg dosage of CuO NPs, 10 mg/L concentration of rifampicin solution, and rifampicin solution at pH 2 in 8 min. From this study, it can be concluded that CuO NPs synthesized from *Parthenium hysterophorus* aqueous extract are promising in the remediation of environmental pollution from antibiotics. In this light, the study reports that *Parthenium hysterophorus*-mediated green synthesis of CuO NPs can effectively address environmental pollution in cost-effective, eco-friendly, and sustainable ways.

Water shortage remains one of the global challenges affecting many of the world's population as it is documented that about 26% (2 billion people) lack access to safe drinking water per the UNESCO 2023 report[1]. The report further indicates that 2–3 billion people worldwide experience water shortage, with water scarcity projected to increase in the coming years. It is reported that about half of the global population is at risk of experiencing water scarcity[2]. A report published during Africa Health Agenda International Conference (AHAIC2023) revealed that climatic changes have worsened water scarcity challenges in Africa[3]. Climatic changes affect terrestrial water storage, further exacerbating water scarcity and leading to a global water crisis. Amidst the water shortage crisis, water pollution from active pharmaceutical compounds (APIs), such as antibiotics classified as emerging pollutants, continues to rise[4–6]. Pathways for antibiotics into the environment (soil or surface water) are infiltration from wastewater treatment plants and domestic discharge of human excretion[6–8]. These antibiotics exhibit detrimental effects on humans and water ecosystems, attributed to their higher concentrations above the predicted environmental concentration[8]. The existence of antibiotics in the environment propagates antimicrobial resistance[8–11], and their low concentrations are difficult to remove using conventional wastewater treatment plants[12]. The World Health Organization declared this resistance a public health crisis, threatening modalities to treat the increasing

[1]Chemistry Department, Jomo Kenyatta University of Agriculture and Technology, P.O. Box 62000, 00200 Nairobi, Kenya. [2]Department of Biological and Physical Sciences, Karatina University, P.O. Box 1957-10101, Karatina, Kenya. ✉email: dennisym21@gmail.com

Appendix VII: Publication II

Hindawi
Journal of Chemistry
Volume 2024, Article ID 1088430, 19 pages
https://doi.org/10.1155/2024/1088430

Research Article

Synthesis and Characterization of *Parthenium hysterophorus*-Mediated ZnO Nanoparticles for Methylene Blue Dye Degradation

Dennis Nzilu,[1] **Edwin Madivoli**,[1] **David Makhanu**,[2] **Sammy Wanakai**,[1] **Gideon Kirui**,[1] **Vincent Mwangi**,[1] **and Patrick Kareru**[1]

[1]*Chemistry Department, Jomo Kenyatta University of Agriculture and Technology, P.O. Box 62000-00200, Nairobi, Kenya*
[2]*Department of Biological & Physical Sciences, Karatina University, P.O. Box 1957-10101, Karatina, Kenya*

Correspondence should be addressed to Dennis Nzilu; dennisym21@gmail.com

Received 5 September 2023; Revised 14 November 2023; Accepted 26 December 2023; Published 3 January 2024

Academic Editor: Liviu Mitu

Copyright © 2024 Dennis Nzilu et al. This is an open access article distributed under the Creative Commons Attribution License, which permits unrestricted use, distribution, and reproduction in any medium, provided the original work is properly cited.

Herein, zinc oxide nanoparticles (ZnO NPs) were synthesized using *Parthenium hysterophorus* whole plant aqueous extract as reducing and capping agents. The synthesized ZnO NPs were characterized via UV-Vis spectroscopy, Fourier-transform infrared spectroscopy (FTIR), scanning electron microscopy (SEM), transmission electron microscopy (TEM), X-ray diffraction (XRD), and dynamic light scattering (DLS). An intrinsic optical absorbance of ZnO NPs occurred at 337 nm in the UV-Vis spectrum. The FTIR analysis revealed the presence of secondary metabolites responsible for reducing and stabilizing the nanoparticles. Furthermore, SEM and TEM images revealed that ZnO NPs were spherical with an average particle size of 38 nm. The XRD analysis revealed that ZnO NPs had a hexagonal wurtzite crystal structure with a crystallite size of 42.6 nm. The synthesized nanoparticles were investigated for degradation ability against methylene blue dye at varying conditions of ZnO NPs' dosage, methylene blue concentrations, pH, temperature, and interaction time. Degradation efficiency of 55.69% was obtained at optimal conditions using 50 mg of ZnO NPs, 5 mg/L of MB dye concentration, and pH 12 and at 65°C within 32 minutes. Due to their novel green synthesis route, *Parthenium hysterophorus*-mediated ZnO NPs are promising candidates for removing persistent organic dyes from aquatic environments.

1. Introduction

Aquatic pollution by industrial effluents and emissions from wastewater treatment plants is a serious threat facing humanity and the ecosystem [1, 2]. Among the industrial wastewater contaminating our water systems are organic dyes from textile, cosmetic, paper, plastic, and pharmaceutical factories [3–5]. These organic dyes endanger water quality, and some, such as methylene blue, are nonbiodegradable and toxic because of their mutagenic and carcinogenic properties, threatening human health [6].

Chemical, physical, and biological methods are conventional methods employed in wastewater treatment to remove contaminants, including dyes [5]. However, these methods have drawbacks in removing the contaminants at low concentrations. Recently, researchers have embraced green nanotechnology to develop materials in nanoscale size that can effectively remediate the pollutants before being discharged into the water system [7–11]. Chemical, biological, and physical methods are the primary methods employed in the synthesis of nanoparticles [11, 12]. Chemical and physical processes of synthesizing nanoparticles include coprecipitation, pyrolysis, thermal decomposition, sol-gel, solvothermal, laser ablation, and ball milling [13, 14]. However, both chemical and physical processes of synthesizing nanomaterials have drawbacks of using toxic chemicals and being time-consuming, energy inefficient, and cost-ineffective [14–16]. Researchers find biological methods for synthesizing nanomaterials more attractive because they are environmentally friendly and cost-effective [16, 17]. Biological methods involve the use of microorganisms and plants. However, the use of microorganisms is characterized to be labor-intensive and involves delicate procedures in microbe isolation, growth,